# 3D GEOSTATISTICAL MODELING OF FACIES AND PETROPHYSICAL PROPERTIES OF THE UPPER KHARTAM OUTCROP OF KHUFF FORMATION, CENTRAL SAUDI ARABIA

BY

ABDASEED KUBUR BOKHARI KUBUR

A Thesis Presented to the

DEANSHIP OF GRADUATE STUDIES

**KING FAHD UNIVERSITY OF PETROLEUM & MINERALS**

DHAHRAN, SAUDI ARABIA

In Partial Fulfillment of the

Requirements for the Degree of

# MASTER OF SCIENCE

**In**

GEOLOGY

MAY 2016

KING FAHD UNIVERSITY OF PETROLEUM & MINERALS

DHAHRAN- 31261, SAUDI ARABIA

**DEANSHIP OF GRADUATE STUDIES**

This thesis, written by **ABDASEED KUBUR BOKHARI KUBUR** under the direction his thesis advisor and approved by his thesis committee, has been presented and accepted by the Dean of Graduate Studies, in partial fulfillment of the requirements for the degree of **MASTER OF SCIENCE IN GEOLOGY.**

Dr. Mohammad Makkawi
(Advisor)

Dr. Abdulaziz M. Al-Shaibani
Department Chairman

Dr. Osman Mahmoud Abdullatif
(Co-Advisor)

Dr. Salam A. Zummo
Dean of Graduate Studies

Prof. Gabor Korvin
(Member)

31/5/16
Date

Dr. Abdulaziz Abdulraheem
(Member)

Dr. Lamidi Babalola
(Member)

# *Dedication*

*To my parents, brothers and sisters*

*To my grandfather and all of the family members*

*To my fiancée*

*To my colleagues at College of Petroleum Engineering and Geosciences*

*To Sudanese community at King Fahd University of Petroleum and Minerals*

# ACKNOWLEDGMENTS

I would like to acknowledge King Fahd of Petroleum and Minerals for giving opportunity to pursue my graduate study. College of petroleum engineering and geosciences is highly appreciated for offering courses and research opportunities. Also many thanks to my advisor Dr. Mohammed Makkawi, Dr. Osman Abdullatif, Prof. Gabor Korvin, Dr. Abdulazeez and Dr. LamidiBabalola for their supervision, invaluable comments andguidance during this work.

Also I would like to thank Dr. Hassan Eltom for his help and collaboration during this work. Acknowledgment extended to Mr. Assad Abdulraziq and Mr. Mutasim Osman for their valuable comments.

Also I would like to acknowledge funding and support of the Deanship of Scientific Research for this work provided by King AbdulazizCity for Science and Technology (KACST) through the Science & Technology Unit at the King Fahd University of Petroleum and Minerals (KFUPM) and project No. 10-OIL1379-04 as part of the National Science, Technology and Innovation Plan.

# TABLE OF CONTENTS

# LIST OF TABLES

# LIST OF FIGURES

# LIST OF ABBREVIATIONS

| | | |
|---|---|---|
| **SEM** | : | Scanning Electron Microscope |
| **XRD** | : | X-Ray Diffraction |
| **IK** | : | Indicator Kriging |
| **SIS** | : | Sequential Indicator Simulation |
| **TGS** | : | Truncated Gaussian Simulation |

# ABSTRACT

Full Name : ABDASEED KUBUR BOKHARI KUBUR

Thesis Title : [3D GEOSTATISTICAL MODELING OF FACIES AND PETROPHYSICAL PROPERTIES OF THE UPPER KHARTAM OUTCROP OF KHUFF FORMATION, CENTRAL SAUDI ARABIA]

Major Field : GEOLOGY

Date of Degree : 2015, NOVEMBER

Oolitic grainstones can contain significant hydrocarbon reserves. The heterogeneity in carbonate reservoir ascribes to the depositional and digenetic processes. Within the studied interval, facies were analyzed and grouped into four depositional sub-environment which stacked in five cycle sets (4th order sequences). The porosity and permeability were measured from core plug of outcrop samples. However, the measured porosity and permeability values showed patterns of distributions when statistically analyzed based on the rock typing and stratigraphic intervals.

Based on the outcrop observations, the 3D framework was constructed which comprises of five zones separated by six surfaces. In the context of depositional environment, these zones are; foreshoal and shoal (zones 1 and 2), shoal and backshoal (zones 3 and 4) and tidal flat deposits (zone 5). The sea level within these zones was relatively high, fluctuated and dropped within deposits of zones 1 and 2, zones 3 and 4 and zone 5, respectively. In the context of 3D modelling, lithofacies within each zone was populated separately by using different geostatistical algorithm. Based on the relative sea level, the dominated lithofacies and the presence or absence of marine fauna, the studied interval was subdivided into three broad intervals. These intervals are; lower (zones 1 and 2), middle (zones 3 and 4) and the upper interval (zone 5). The porosity evolution was investigated within each zone and incorporated within the 3D outcrop model. The results showed how the incorporation of the porosity scenarios within the 3D framework can provide a realistic

and to some extent the exact vertical stacking of reservoir units. This approach could be applied to predict and enhance the reservoir quality in the analogous oolitic reservoir.

# ملخص الرسالة

**الاسم الكامل: عبدالسيد كبر بخاري كبر**

**عنوان الرسالة:دراسة لعمل نماذج جيواحصائية ثلاثية الابعاد للسحنات الرسوبية والخواص البتروفيزيائية للجزء العلوي من عضو خرطم في مكشف تكوين الخف في وسط المملكة العربية السعودية**

**التخصص: جيولوجيا**

**تاريخ الدرجة العلمية: 2016**

صخور الكربونات الاوليتية تحتوي علي معظم الاحتياطي النفطي في العالم. وكما تتميز بتعدد انواع المسامية نتيجة للعمليات الرسوبية و اللاحقة. في هذه الدراسة تم تحديد وحدات طبقية قابلة ان تكون مكامن نفطية جيدة بواسطة بناء نمذجة صخور التریاسي السفلي في تكوين الخف. وكما تم استنتاج عدد من السيناريوهات للمسامية التي قد تنتج من العمليات اللاحقة المختلفة, والتي استفيد منها في فهم المكامن المماثلة في المناطق المختلفة. لعمل النموذج الجيولوجي لمنطقة الدراسة, تم استخدام العينات الحقلية للمكشف الصخري. حيث تم عمل ست مجموعات من اسطح او فواصل والتي بدورها تحدد خمسة نطاقات صخرية. كل نطاق يمثل بيئة ترسيبية معينة, حيث النطاق الاول والثاني يشتملان علي رسوبيات المقدمة والمياه الضحلة, والنطاق الثالث والرابع يحتويان علي رسوبيات المياه الضحلة و خلف الحاجز الرسوبي, والنطاق الخامس يحتوي علي رسوبيات المد والجزر. توزيع السحنات الرسوبية داخل النطاقات تم باستخدام خوارزمية جيواحصائية لكل نطاق. كما تم تقسيم النموزج الصخري الثلاثي الابعاد لثلاث وحدات رئيسية. الوحدة السفلي (النطاق الاول والثاني) والتي ترسبت على الحد الفاصل بين رسوبيات البيرمي والتریاسي وتميزت بترسيب وحدات اوليتية عندما كان سطح البحر في ازدياد سريع وغياب تام للكائنات الحية, الوسطى (النطاق الثالث والرابع) ترسبت عندما كان سطح البحر في تذبذب وظهور نسبي للكائنات الحية وتميزتا بمسامية قالبية وبين حبيبية, العليا (النطاق الخامس) وكان سطح البحر في تقهقر ونتيجة لذلك ترسبت صخور كربونات دولمتية زات مسامات بين بلورية و بين حبيبة.

تم تطوير السيناريوهات المتعددة للمسامية في نموذج ثلاثي الابعاد لكل نطاق على حدة. ومن خلالها يمكن فهم انواع المسامية الممكنة في المكامن الصخرية الشبيهة. وكما بواسطة هذه الدراسة يمكن فهم وتحسين استكشاف واستغلال الموارد النفطية المخزونة داخل تلك المكامن.

# CHAPTER 1

# INTRODUCTION

## 1.1 Introduction

The subsurface heterogeneity is an important issue to be understood and modeled for delineation of reservoir 3D architecture, reservoir management and performance predictions (Deutsch, 1999; Falivene et al., 2007). Reservoir models that are built by using subsurface data always suffer from the insufficiency of information or large scale-based data which has shortage to resolve the small variations within the reservoir properties (Eltom, et al., 2012, Felletti, 2004). The lithofacies is one of the main factors that affects the reservoir petrophysical properties. Sedimentological facies variability that could affect the reservoir quality prediction may occur either at seismically irresolvable scale or out of the typical inter-well spacing (Falivene et al., 2006). However, the strategies for subsurface modeling could be tackled through using geocellular outcrop-based modeling. The geostatistical methods meet the aim of the modelers and effectively enable them to overcome the limitations of the traditional techniques. Moreover, the integration of geostatistical analysis on outcrop data allows the construction of a quantitative lithofacies model which enhance the practicality of outcrop analogue to be a predictive tool to estimate the sedimentologic heterogeneity in subsurface reservoir geology (Felletti, 2004).

The Permian-Triassic Khuff reservoir is one of the largest gas field in the world, containing 38.4% of the world natural gas reserve (BP Statistical Review of World Energy, 2012). Khuff Formation units which crop out in central Saudi Arabia are documented in a different quadrangles falling in one belt (Vaslet et al., 2005). The Khuff Formation was intensively studied in the outcrop scale. Furthermore, Vaslet, et. al., (2005) and Eltom, et. al., (2016) have used the outcrop data to build the depositional model for the members within Khuff interval. Outcrops of the Upper Khuff Formation exposed in Buraydah City, in central Saudi Arabia, will provide an important analogue data that could effectively help in understanding the Khuff subsurface reservoir complexity through conducting detailed sedimentological and high-resolution stratigraphic studies this will allow capturing important information for subsurface reservoirs. The present study was conducted to fulfill the following objectives; to improve the understanding of spatial facies distribution by constructing 3D geostatistical models for lithofacies, and to predict the petrophysical properties through constructing 3D geostatistical models for the porosity and permeability of the Upper Khartam Member outcrop.

## 1.2 Problem Statement

The focus of this study is to address the difficulties of the understanding of Upper Khartam Member of Khuff Formation which are explained by the following points:

- Most of the previous studies focused on establishing 1D and 2D models of the facies and petrophysical properties ($\phi$, k) of the Upper Khartam Member. However, 3D model is the best to visualize such geologic properties.

- The understanding of subsurface reservoir heterogeneity is masked by the large inter-well spacing. Therefore, in this study the Upper Khuff Formation's outcrop analog is integrated with geostatistical approaches to capture the small scale variations within the reservoir properties.

## 1.3 Objectives

Outcrop of the Upper Khuff Formation exposed in Buraydah City, in central Saudi Arabia, will provide an important analogue data that could effectively help in understanding the complexity of Upper Khuff reservoir. Conducting a detailed sedimentological and high resolution stratigraphic study will allow capturing important information for subsurface reservoirs. The present study aims to fulfill the following objectives:

- To improve the understanding of spatial facies distribution by constructing 3D geostatistical models for lithofacies of the Upper Khartam member. n
- To predict the petrophysical properties through constructing 3D geostatistical models for the porosity and permeability of the Upper Khartam member outcrop.
- To characterize reservoir quality and architecture.

## 1.4 Study Area

Khuff Formation has been documented by the different researchers as an elongated belt of outcrops that extends N-S in the central Saudi Arabia. This study focuses on the upper part of Khartam Member of Khuff Formation which crops out in the north of Buraydah in the central part of Saudi Arabia (Figure 0.1). The studied interval is well exposed as road cuts trending west to east. The stepped and inclined outcrop walls

easily enabled logging and sampling of the whole interval of the upper Khartam Member.

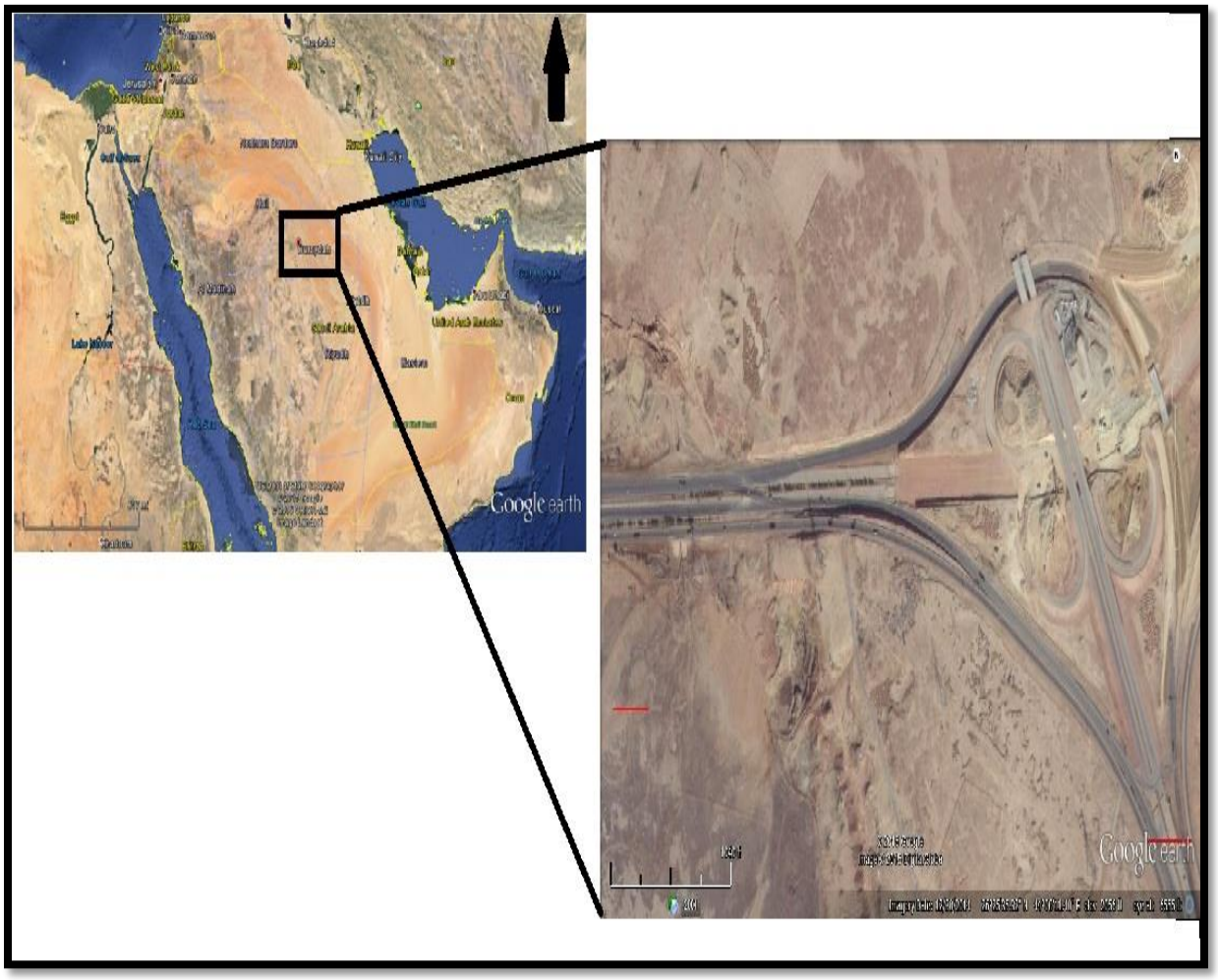


Figure 1.1: The study area in Buraydah city (Google Earth, 2015).

## 1.4 Geological Setting

Permian-Triassic Khuff Formation crops out as a North-South belt in the middle of Saudi Arabia with a length of 1200km (Figure 0.2). The extended Khuff outcrop dips in the east direction. Khuff Formation unconformably overlies the Precambrian basement in the quadrangles of Darma, Ad-Dawadimi,WadiArRayn, Wadi Al Mulayh, Sulayyimah, and WadiTathlith quadrangles. Khuff Formation was defined by Steinekeet al., (1958) close to ‘Ayn Khuff in Ad-Dawadimi quadrangle. Delfour et al., (1982) studied Khuff Formation in Ad-Dawadimi area and subdivided it into five members, started from the oldest with Unayzah, Huqayl, Duahysan, and Midhnab then topped by the Khartam Member. Vaslet et al. (2005) and Manivit et al. (1986), modified the reference section andchanged the UnayzahMember to Ash Shiqqah member, these authors also established four new members overlying the Ash Shiqqah Member (Figure 0.3).

Osman, 2014 conducted digital outcropmodeling using Light Detection And Ranging (LiDAR) technique for the upper Khartam Member of the Khuff Formation. Furthermore, the sedimentologic and stratigraphic analyses of the outcrop data have been integrated with the digital modeling to characterize the lateral and vertical facies heterogeneity. The stratigraphic horizons were defined in the digital model as well as the reservoir units (A, B, C). Additionally, the heterogeneities within the reservoir zones were studied and classified effectively in 2D framework.

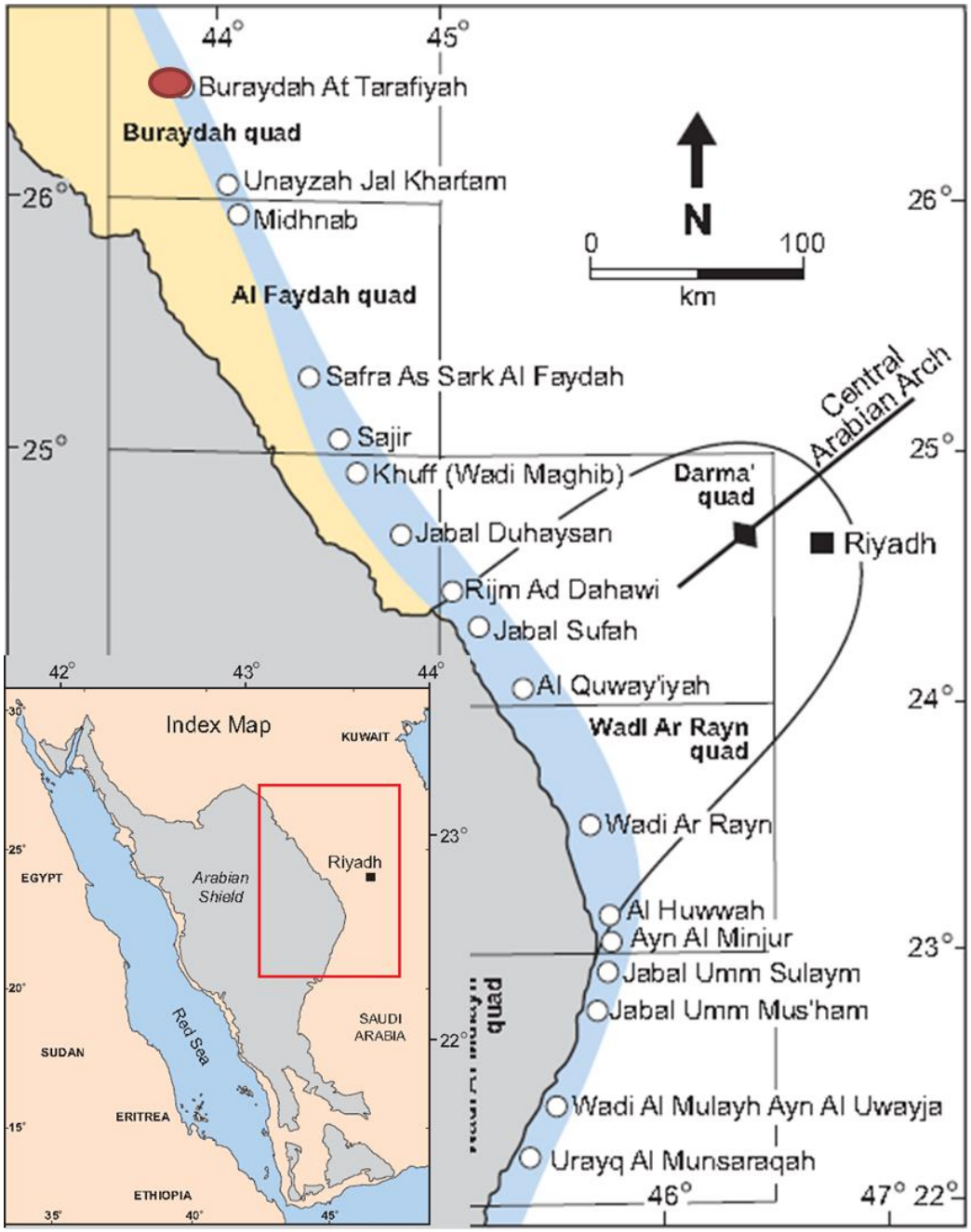


Figure 1.2: The belt of Khuff Formation outcrops in Central Saudi Arabia including the study area (red circle) (modified after Vaslet et al., 2005).

## 1.5 Sedimentary Environment and Depositional Evolution

Khuff Formation is composed of sequences of siliclastic and carbonate rocks. The siliclastic percentage showed an increase southward. The basal interval is siliclastic of Ash Shiqqah Member. While the overlying four members (Huqayl, Duahysan, Midhnab and Khartam) are characterized by sedimentation of repeated cycles. Each cycle is composed of transgressive part of subtidal grainstones at the bottom that are considered as reservoirs.The grainstonesare topped by the regressive part of intertidal and supratidal muddy and evaporitic deposits which represents the seals (Figure 0.4) (Ziegler, 2001).

In central Saudi Arabia, the Khuff formation is exposed as a curved belt of outcrops overlying the older Paleozoic sedimentary rocks and unconformably overlying the Proterozoic Arabian Shield basement complex rocks in the south (Powers, 1968). These lithological variations are due to several factors such as changes in paleolatitudinal, paleoclimatic position from higher latitude to lower latitude of the Arabian Plate as well as the subsidence that accompanied the Neo-Tethys opening and the deglaciation of continental ice at that time (Al-Aswad, 1997).

Eltom, et al., (2016) studied the upper Khartam Member in the outcrops at four different locations (Figure 0.5). Using the geochemical analysis and spectral gamma ray responses, they defined the Permo-Triassic boundary (PTrB) between lower and upper Khartam which separates the Permian sequences from the early Triassic units (Figure 0.6). Sedimentologic and stratigraphic description was also made by using 11 stratigraphic sections distributed along the road-cut at At Tarafiyah area (Abdulraziq, 2013). Moreover, the intensive analysis of the stratigraphic sections and the rock samples revealed the existence of 8

lithofacies, comprising the upper Khartam at that location. The depositional environments model was constructed for the lithofacies (Figure 0.7). Stratigraphically, five high frequency sequences (HFS) with shallowing upward trend were documented.

## 1.6 Permian-Triassic Khuff Reservoir

The Permian-Triassic petroleum system in the Gulf region contain a huge amount of non-associated gas recovery which holds about 15-20 % of the non-associated gas reserves inthe world. To the east direction, the Khuff Formation extends into subsurface where itforms an important reservoir of non-associated gas in the Saudi Arabia, Iran, United Arab Emirates, Qatar, Oman, and Bahrain as well (Alsharhan, 2006). Therefore, prediction ofthe reservoir quality at different scales starting from inter-well scale to micro-scale atstratigraphic hierarchy will be helpful to evaluate the reservoir quality and highlight theheterogeneity of the reservoir. In the subsurface Khuff Formation is composed of fivemembers (Khuff A to E) as shown in (Figure 1.8) (Dasgupta, et al., 2002). The UpperKhartam Member of the outcrop was found equivalent to Khuff-A and the upper parts ofthe Khuff-B reservoirs of subsurface in eastern Saudi Arabia (Al Dukhayyil, 2007; AlDukhayyil and Al Tawil, 2007). Regionally, Khuff Formation was correlated from theoutcrop and subsurface in Saudi Arabia to the equivalents in Iran, United Arab Emiratesand Oman. As shown in figure 1.9, the Permian-Triassic boundary was regionallydocumented and mapped within Khuff Formation and its equivalent within these regions (Vaslet et al., 2005; Insalaco et al., 2006; Hughes, 2009; Maurer et al., 2009; Koehrer et al., 2010; Eltom et al., 2016).

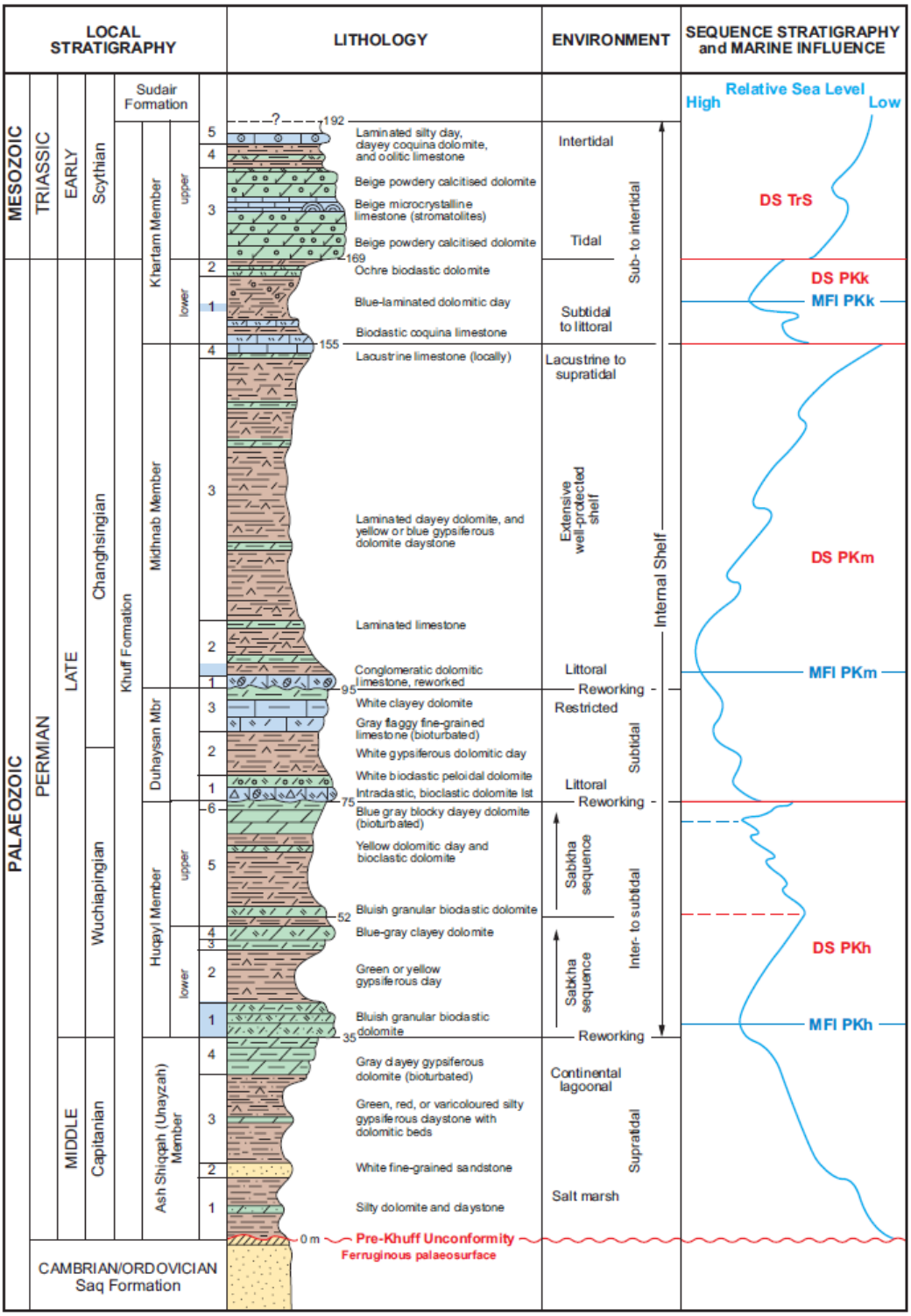


Figure 1.3: Stratigraphic type section showing the four members of Khuff Formation at Ad Dawadimi quadrangle (Vaslet, et al., 2005).


Figure 1.4: Depositional environment of the Khuff Formation (Ziegler, 2001).

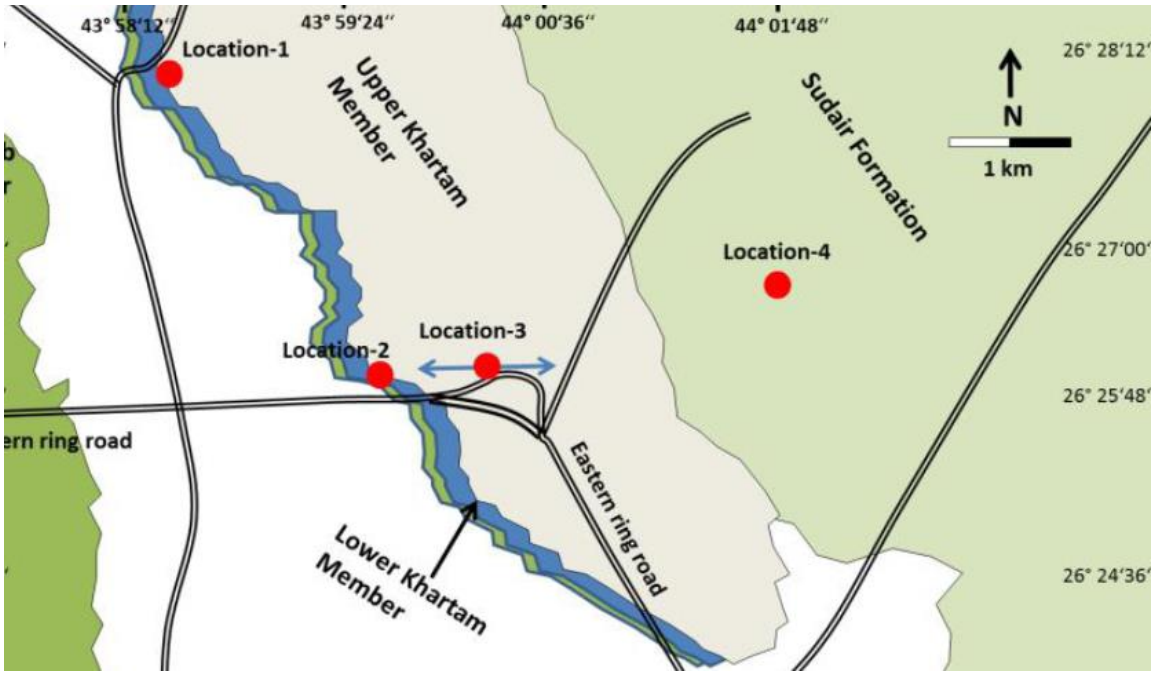


Figure 1.5: Illustrates the four locations where the upper Khartam member is well exposed (Eltom, et al., 2016).

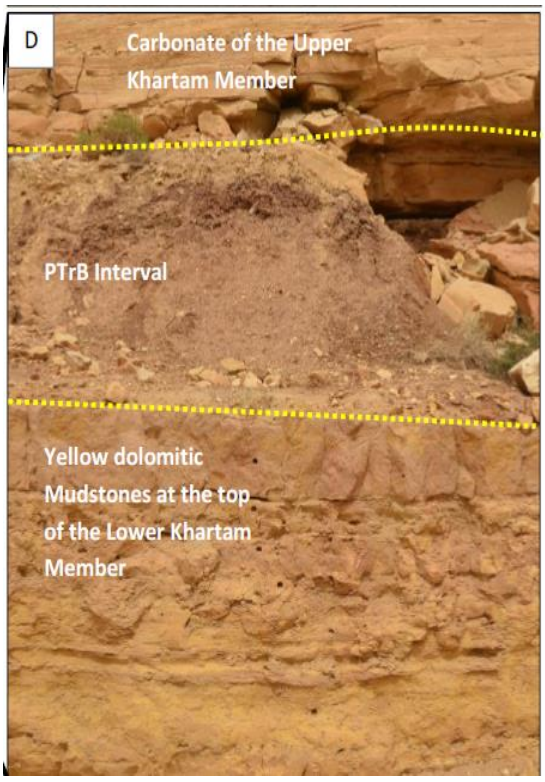


Figure 1.6: The Permian-Triassic Boundary (Eltom, et al., 2016).

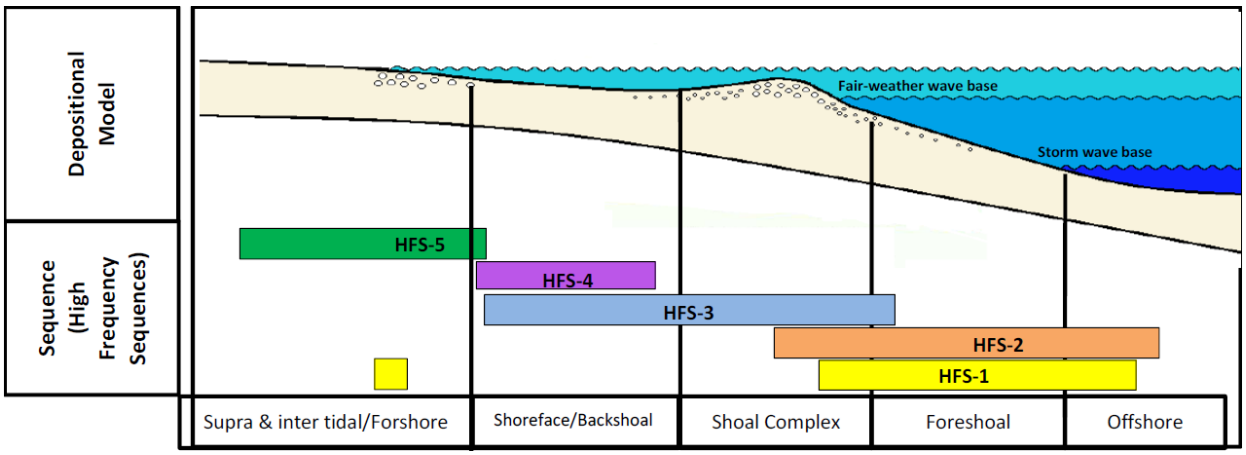


Figure 1.7: Shows the distribution of high frequency sequence with the depositional environments (Eltom, et al., in press).

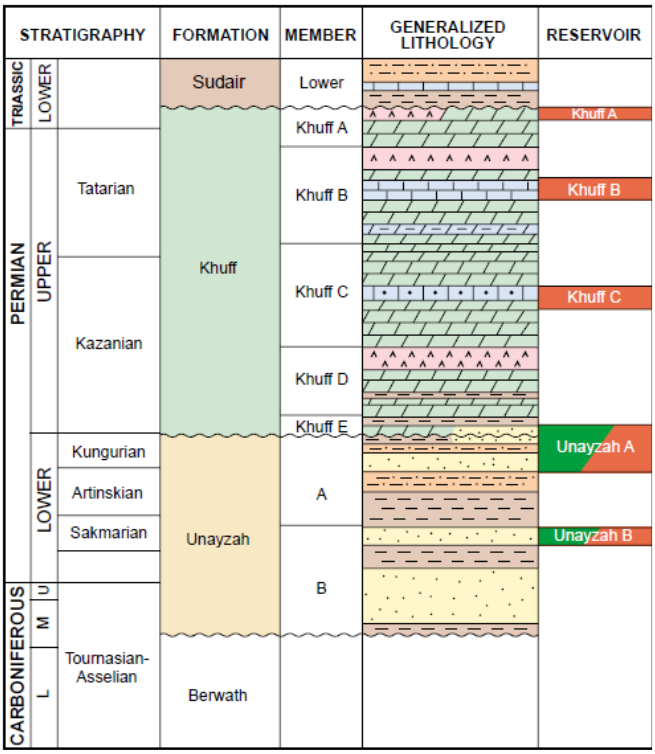


Figure 1.8: The stratigraphic column of Khuff Formation in the subsurface (Dasgupta, et al, 2002).

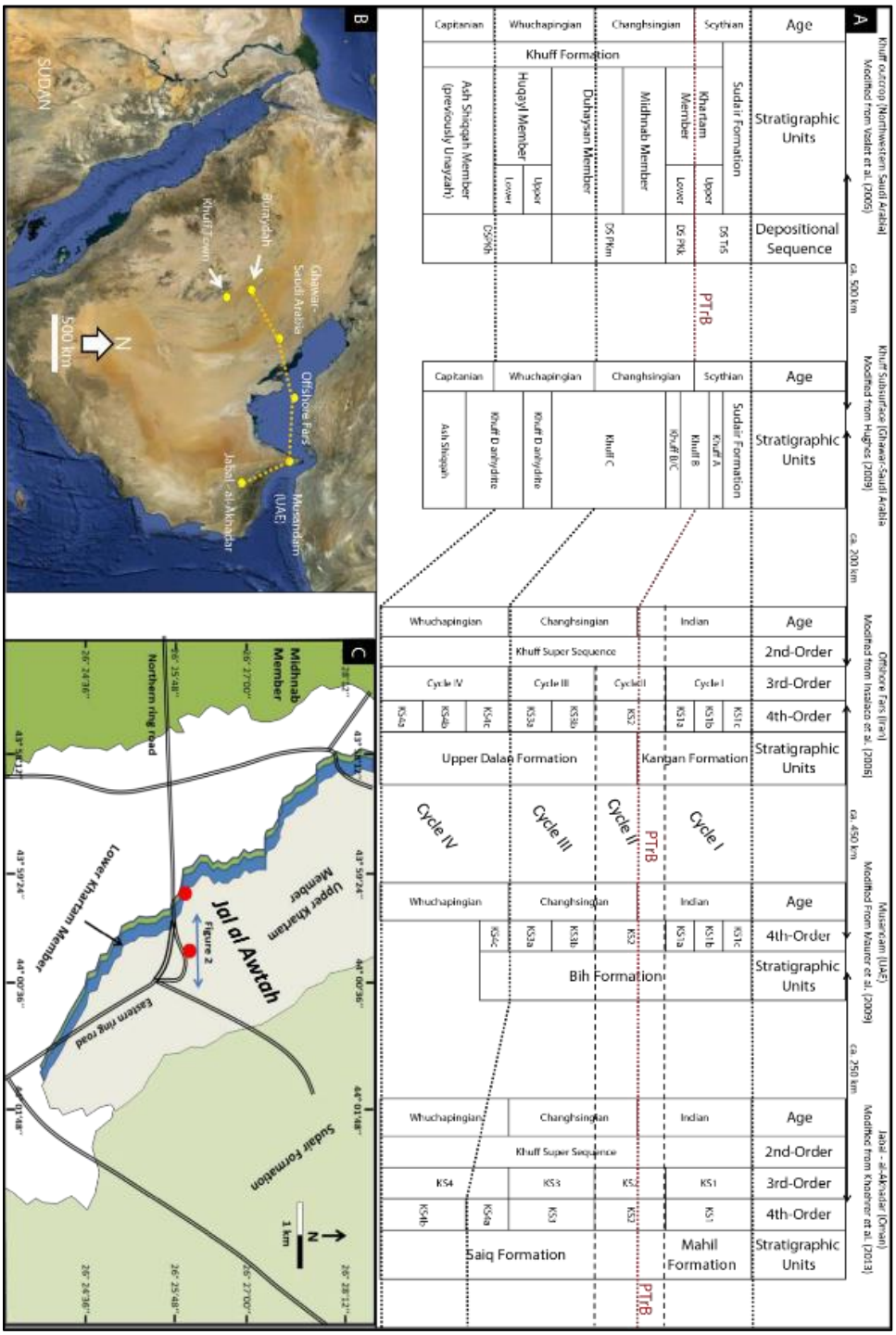


Figure 1.9: Khuff stratigraphic column from Middle East and Arabian Plate map; a) Regional correlation of the Khuff stratigraphy; b) Map of the Arabian Peninsula with the locations of the correlated stratigraphic sequences in Figure 1a; c) Geologic map of the study area in central Saudi Arabia, the red dotted line represent the Permian-Triassic Boundary (Eltom et al., 2016

# CHAPTER 2

# LITERATURE REVIEW

## 2.1 Introduction

The outcrop analog can be properly worked out the different scales of heterogeneity e.g. that included in carbonate deposits (larg-, medium- and small scale sequences) in different trends (spatialy). Thus, analogues approachsare used to emphasis the interwell scale of the subsurface data by generating the geometric of facies bodies as well as the petrophysical data. Moreover, the integration of geostatistical analysis on outcrop data allows the construction of a quantitative lithofacies model which enhance the practicality of outcrop analogue to be a predictive tool to estimate the sedimentologic heterogeneity in subsurface reservoir geology (Felletti, 2004).

## 2.2 Variogram

To have such a powerful outputs from geostatistical studies, it is necessarily to build reliable relationship between the geology and variogram analysis. On the other hand, the poor correlation may yield incorrect information in the later stages of estimation and simulation. The variogram behavior might be controlled by the stacking pattern of stratigraphy, various lithologic types and their structure as well (Sahin, et al., 1998).

## 2.3 Indicator Kriging (IK)

The Kriging algorithm estimates the properties on the unsampled location. Based on the type of the data, there are different types of Kriging such as; simple, block, ordinary

(continuous data) and indicator (categorical data) Kriging. The indicator Kriging estimates the value below and above specific threshold (Al-Khalifa, 2001).

## 2.4 Sequential Indicator Simulation (SIS)

Amour et al., (2012) and Benson et al., (2014) reached that the SIS is the best algorithm to reproduce the distribution of the mosaic-like lithofacies. Additionally, SIS is not controlled by the trend of the geologic features. Meanwhile, it allows assigning unique semivariogram for each lithofacies. Based on these criteria, SIS can adequately capture the small geologic variability in such depositional environment.

## 2.5 Truncated Gaussian Simulation (TGS)

The Truncated Gaussian Simulation (TGS) works better to model the ordered geologic features (such as facies). Moreover, Truncated Gaussian Simulation enforces the facies modeling to follow Walter's concept. However, TGS algorithm allows assigning single semivariogram for lithofacies types, rather than using many semivariogram as in SIS algorithm (Amour et al., 2012; White et al., 2003, Benson et al., 2014) (Figure 2.1).

Palermo, et al., 2010 conducted outcrop-based study on the Upper Muschelkalk carbonates were investigated in different scales. They collected and analysed data for the simple 1D model. The defined facies types were correlated in different locations (2D). Accordingly, 3D modelling techniques were used to figure out the architecture of the carbonate bodies as well as the dimensions in the different directions. After many iterations, proper geostatistical workflowwas selected and used for the modelling. Sequentail Gaussian simulation tool was effectively used to reproduce the input data. The resultant 3D model properly highlighted the cyclcity within the Upper Muschelkalk Member. The shoal bodies

were clearly delineated and traced for kilometeres in the 3D model. To include different scales of geologic data in single 3D model, different geostatistical techniques are crucial to be used instead of one algorithm to accommodate the various scales of heterogenieties. Most researchers work was based on one simulation concept, where as some of them applied more than one simulation methods for the modeling. A scale-dependent study was conducted by Amour, et al., (2012)to model the carbonate bodies at different scale of heterogeneities in area located in Atlas Mountains of Morocco. They three types of carbonate deposits scales were investigated and modelled; depositional sequences stacking pattern, facies associations, and the lower scale of lithofacies distribution. The suitable simulation workflow depends on the required scale of modeling. Lithofacies scale have shown more complexity of carbonate deposits than that shown in facies association scale. The variogram analysis was used to compute the spatial range of carbonate bodies dimensions as well as the morphological features. The larger scale of carbonate heterogeneity (depositional sequences) was deterministically modeled. Thus, general trend of the carbonate deposits was clearly shown at this scale of modeling. Then, facies associations were stochastically modeled as a medium scale of carbonate heterogeneity. Truncated Gaussian simulation algorithm was selected to reconstruct the ordered facies associations within the geocellular model. The simulated facies associations reflected transition changes along the carbonate ramp. To simulate the randomly distributed lithofacies types, Sequential Indicator simulation was chosen for its capability to honor the facies independently of trends. Also it enables to use unique variogram for each lithofacies individually. Where the domal-shape facies types such as molluskan-coral bioherms was simulated by using object-based algorithm. The stacking pattern of the carbonate deposits

reflects the role of tectonic (accommodation space changes) as controlling factor in the deposition. Where in the lithofacies scale heterogeneity is controlled by the local environmental conditions.

The resultant models were qualitatively validated by direct comparison to the field observations. Meanwhile, the quantitative validation were made through computing the degree of similarity between the input and output data.

Eltom et al.,(2012)established high resolution facies and porosity models for the upper Jurassic Arab-D reservoir using an outcrop analog approach. They aimed to capture the fine facies variability of the reservoir that may affect the spatial porosity and permeability distributions. To achieve the goal of study, a detailed sedimentologic analysis for the outcrop acquired data was done. The facies in 14 stratigraphic sections of the analog were correlated to the subsurface data of the Shudgum, Uthmanyah, and Ain Dar areas of the Ghawar. And the published porosity logs and core measurements were sorted for each individual lithofacies in the three fields. A 3D facies model was constructed using the outcrop analog data and the indicator simulation used to model the data. For the comparison with the lithofacies model, the Spectrum Gamma Ray (SGR) utilized to log the investigated outcrop and its measurements inserted into a 3D model. The porosity measurements were assigned into the 3D facies framework and modeled by using Sequential Gaussian Simulation (SGS). To capture the uncertainty within the porosity model, realizations were generated repeatedly. The high resolution 3D model of the facies provides an understanding for the reservoir architecture as well as the petrophysical properties, furthermore the small variations in the porosity ascribed to the facies changes.

Barbier et al., (2012) used a sophisticated approach to reconstruct both lithofacies and diagenetic imprints in a conceptual model. However, the study relied on an outcrop of Madison Formation in Wyoming in United States. The data was acquired by logging of five sedimentologic sections. Also, the lithofacies and diagenetic phase's description were made on the collected rock samples from the studied outcrop. The facies associations were built and attributed to their correspondent depositional environments. The bounding surfaces of the facies units were defined and utilized as the main input to constrain the lithofacies distribution and their relationships. The diagenetic analysis was focused on the early diagenetic phases. The simulation of both facies and their diagenesis showed the 3D distribution of the lithofacies in different stratigraphic units effectively as well as the subsequent diagenetic phases.

Benson, et al., (2014), constructed reservoir-analogue model using an outcrop from south east of Spain. They integrated lithofacies distribution and the diagentic parameters to understand the various reservoir properties such as porosity and permeability. The stratigraphic sections were used to build the lithofacies distribution model through using the geostatistical methods.

The characterization of facies architecture is a crucial for the reservoir/aquifer development.Falivene, et al., (2007), studied the hydrofacies heterogeneity in As Pontes Basins of Cenozoic in NW Spain. The stratigraphic subdivisions of the basin were used to control the modeling process.

The indicator Kriging algorithm has showed a robust model of hydrofacies distribution as the data coverage was sufficient. The characterization of aquifer sedimentologic bodies could be helpful in the creation of numerical models that concern with the groundwater

flow as well as the solute transport. The stratigraphic occurrence and depositional environment understanding of the reservoir rocks is important for the different scales, including the regional, exploration scale and the field development scale.

Koehrer, et al., (2010)studied the dolomite bearing reservoir in the south German basin, to clarify facies distribution in well-exposed outcrop.The modeling of the facies, porosity and permeability showed the same variability trend as the observations seen in the multi-scale stratigraphic sections. While, the porosity is following the direction of facies distribution, the permeability distribution trend was more or less unpredictable.

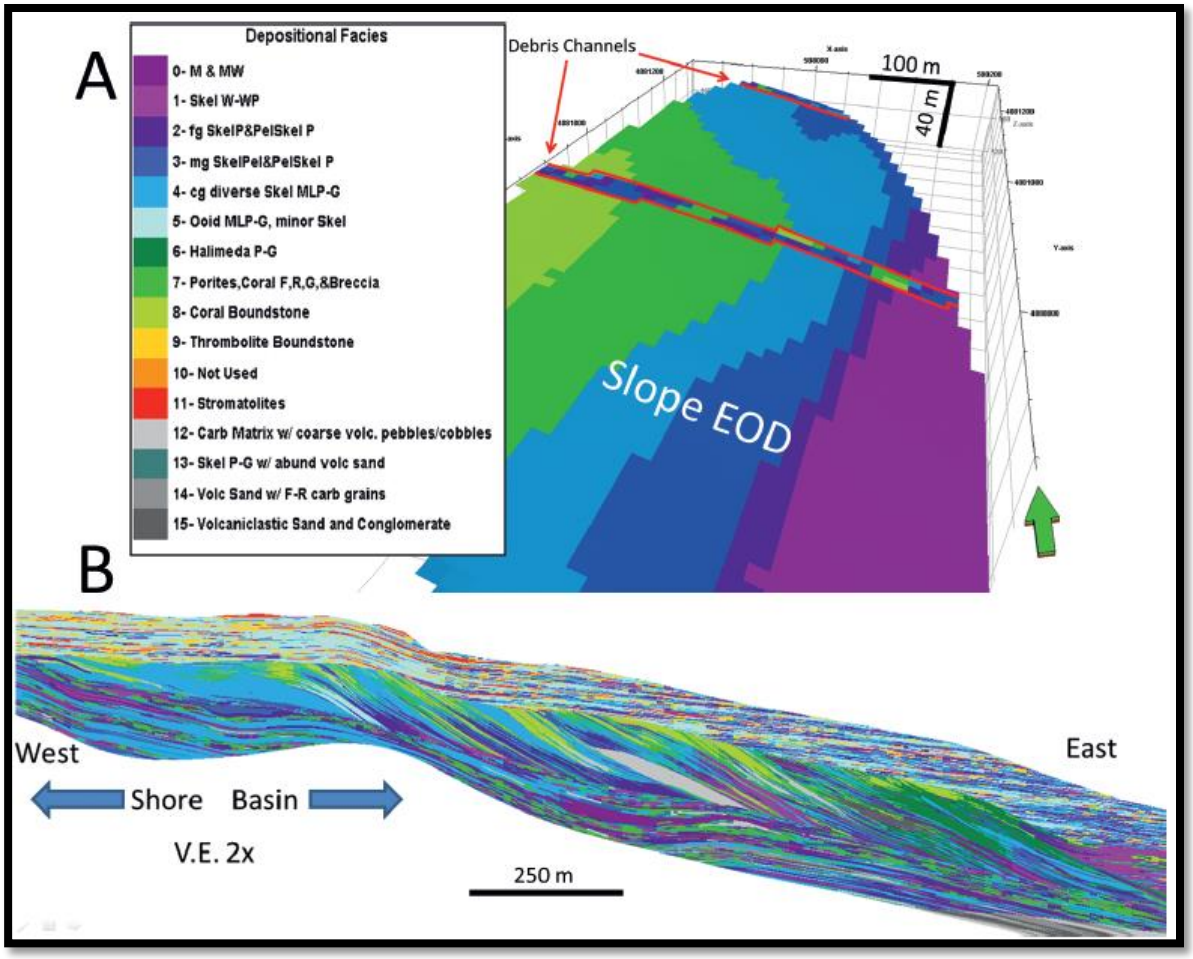


Figure 2.1: Shows the facies distribution models using; (A) Truncated Gaussian Simulation (TGS); and (B) Sequential Indicator Simulation (SIS) (Benson et al., 2014).

# CHAPTER 3

# METHODOLOGY

## 3.1 Introduction

To achieve the main objectives of this study, methodologies been used can be divided into three parts, and their integration will lead to the final results. Firstly, the field investigation at which the sedimentologic profiles were described and sampled. Secondly, the laboratory analyses to investigate the microscopic features and support the field observations. Finally, the three-dimensional modelling for the outcrop and petrophysical properties.Figure 3.1 shows the workflow been used in this study from the field stage and laboratory analyses to the 3D modeling of the facies, porosity and permeability properties.

## 3.2 Sedimentological and Stratigraphical Analysis

Eleven outcrop sections were sedimentological described, profiled and sampled. The description and sampling along the profiles were planned and made bed by bed.

Following Dunham (1962) classification for carbonate rocks, the texture was described. In addition, also description includes; lithology, color, bed thickness, sedimentary structures and lateral continuity and other distinctive remarks. For the laboratory analyses, representative samples were taken from each bed covering the whole interval. Also, high resolution images were obtained for the investigated part to depict the lateral bed continuity.

## 3.3 Laboratory and Petrophysical Analysis

For microscopic analysis, thin sections were prepared from the collected samples and studied under polarized microscope. To differentiate between the carbonate minerals, the samples stained by Alizarin Red. Also blue dye was added to the samples for investigating the visual pore systems. Core plugs were drilled and prepared from the collected samples. A 2.5 cm (1 in) core diameter and 5.1 cm (2 in) core length were used for the porosity and permeability the measurements in the laboratory.

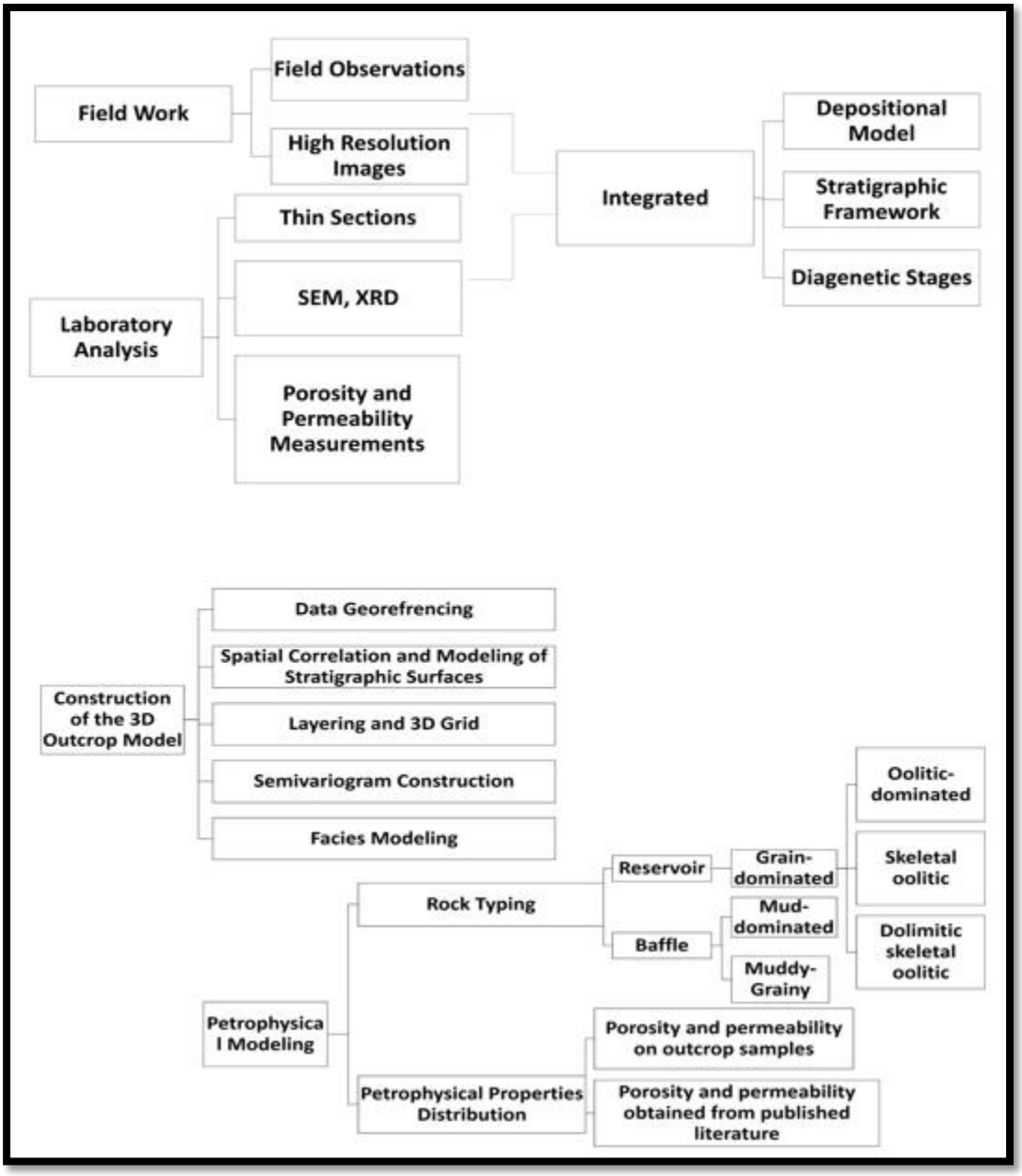


Figure 3.1: Illustrates the workflow been followed from field work to the constructed 3D models for outcrop facies, porosity, and permeability.

All core plugs were examined in the saturation apparatus assembly their porosity (Φ) and permeability (k) values respectively. The porosity was calculated using the saturation method, in the same manner, permeability was counted by injecting saturation fluid inside the sample and then measuring the amount of discharge water during different time intervals.Porosity and permeability measurements are important to characterize the geobodies or reservoir units which are relatively highly porous and permeable. In addition to the porosity and permeability measurements that have been carried out on the samples from the lateral stratigraphic sections, detailed analysis techniques were conducted on selected samples. These techniques include Scanning Electron Microscopy (SEM) and X-Ray Diffraction (XRD). The integration between the microfacies analysis from the thin sections and the petrophysical analysis for the samples collected laterally; resulted in an interpretation for the heterogeneity within the potential reservoir units.

### 3.3.1 X-ray diffraction analysis (XRD)

Powdered X-ray diffraction was carried out on selected samples to identify the mineralogical phases contained in the rock facies. The minerals were identified base on their reflected angles (2-Theta).

### 3.3.2 Scanning electro-microscope (SEM)

For detailed microscopic characterization, scanning electron microscope is conducted to image rock fabric. Also, the pore types and grain to grain contact were clearly emphasized on reservoir facies. Furthermore, EDS obtained to identify the minerals within the certain sample.

## 3.4 Statistical analysis of the Data

The facies and the petrophysical properties datawerestatistically analyzed and checked for the normality of the distribution by using the various statistical parameters (center, spread and shape parameters). Also this stage is useful to investigate the erratic values within the datasets. However, thecoefficient of variation was computed to study the homogeneity of the measurements. The facies grouped into three rock types based on the texture. Then, the porosity and permeability values were investigated within each group.

## 3.5 Data Analysis

The trends of data distribution were determined by conducting the variogram analysis which measures the spatial variability within the data set, and mathematically described by the following equation:

$$\gamma(h) = \frac{1}{2N(h)} \sum_{\alpha=1}^{N(h)} [Z(u_\alpha + h) - Z(u_\alpha)]^2$$

Where;

$\gamma(h)$variogram at the distance (h), $Z(u_\alpha)$ value at location $(u_\alpha)$ $Z(u_\alpha + h)$ value at location$(u_\alpha + h)$, $N(h)$number of pairs.

The experimental semivariograms were measured for the discrete data (facies) and continuous data (porosity, permeability) respectively. The graphic plot of the calculated variogram and the lag distance (h) are fitted to one of the following mathematical equations; a) Gaussian, b) Spherical or c) Exponential model (Figure 3.2). The modeled

variogram will help in the estimation of the unsampled location in the further geostatistical analysis stages (e.g. Kriging and Simulation).

To obtain the spatial continuity/ heterogeneiety of the facies associations within Upper Khartam Member, the indicator variograms were computed after defining parameters of lag distance, angle, trend, etc. Horizontal Lag distances were chosen based on the average distances between sample points in the horizontal directions for both minor major variogram. Where in the vertical direction, experimental variograms were computed for each facies log individualy.

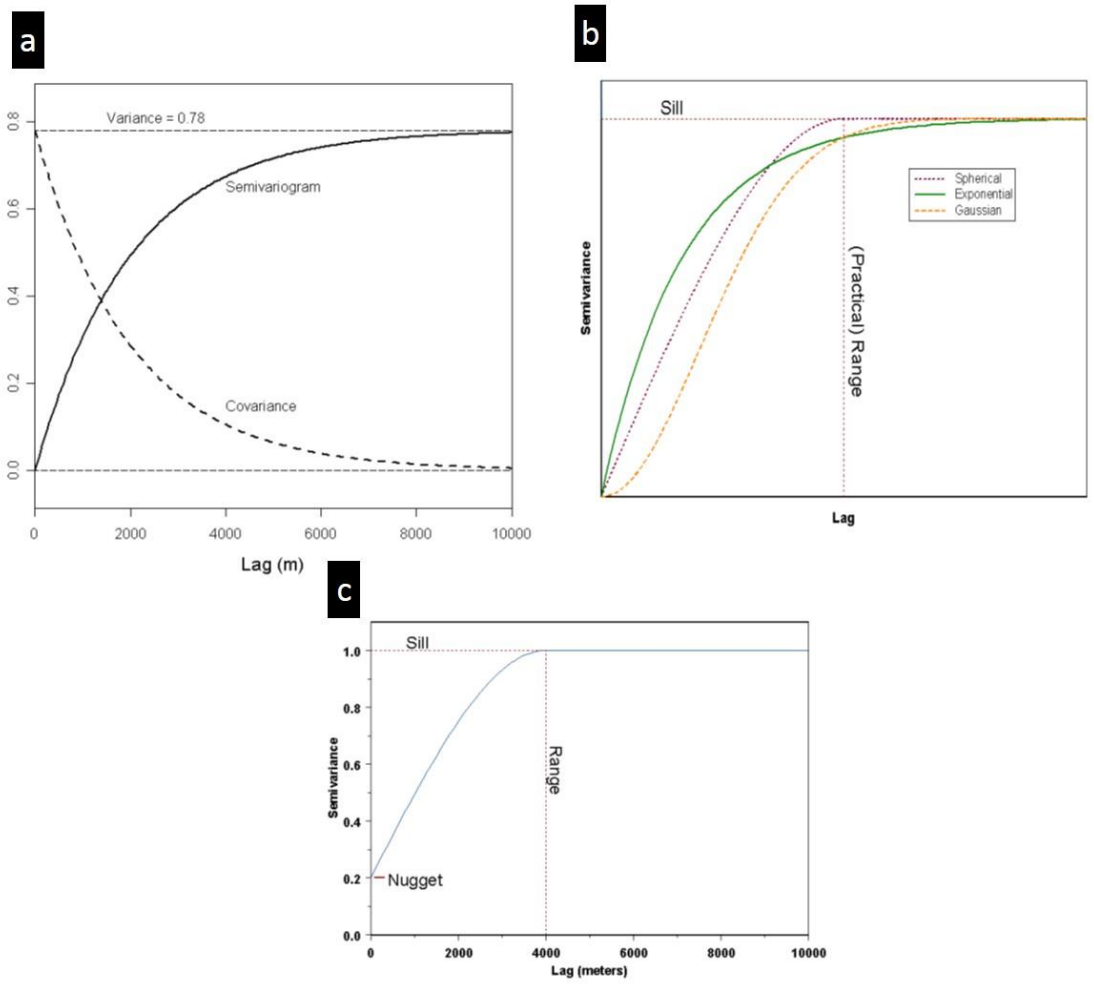


Figure 3.2: Variogram a) experimental variogram, b) types of variogram models and c) its parameters (Bohling, 2005).

## 3.6 Geostatistical Modelling

The majority of classical statistical techniques do not consider the spatial relationships within the geologic phenomena (Issak, et al., 1989).On the other hand, the geostatistical methods have the advantage to model the geologic features either in 2D or 3D space (Felletti, 2004). The PETREL software was used for the modelling however, the software does not consider the geology in the modeling, unless the modeler control the operation in a geological-perspective manner(Benson et al., 2014). The modelling workflow established by Aigner et al. (2007) was followed to achieve the aims of this study. Data geo-referencing performed using the global positioning system (GPS) for 23 stratigraphic sections of which 11 were logged a long road-cut in the study area and 12 sections were obtained using photomosaic and hand-drawn of 2D panels of the road-cut. Major sequence boundaries that separate major stratigraphic units in the studied outcrop were selected to construct the surfaces and zones of the model framework. The five cycle sets were digitized and corresponded to five zones of 3D model. The bed thicknesses, porosity and permeability measurements were statistically analyzed and their distributions were investigated as well. Then, the dimensions of the studied window; the long, wide and thickness are; 2km, 1.5km and 32m, respectively. To capture the small features, the horizontal cells sizes should be no longer than the dimension of the facies bodies (Fabuel-Pe´rez, 2008). Several indicator semivariograms were computed using pairs of facies codes obtained from the 23 stratigraphic sections. However, only one common semivariograms (major, minor and vertical) were used to guide facies modeling to avoid complexity that may occur by using many different semivariograms. The concept of stochastic simulation involves three main points should be considered. These points are; 1) the geological hypothesis, data density

and distribution; 2) the stochastic algorithm behavior and its effect on the facies simulation; and 3) the selection of the proper algorithm (Amour et al., 2012). Afterward, the reproducing of the lithofacies within the 3D grid has performed using three of modeling strategies; Indicator Kriging, Sequential Indicator Simulation and Truncated Gaussian Simulation. Because, Petrel software provides only these three algorithms for facies modeling. Meanwhile, the constructed models were validated with the conceptual depositional model of the lithofacies. The stochastic algorithms were guided by the semivariogram, thus the SIS algorithm allows using a single semivariogram per each lithofacies. On the other, TGS algorithm assigns one common semivariogram for whole lithofacies.The 3D petrophysical models were constructed by assigning porosity and permeability data to lithofacies in the 3D facies model. The porosity and permeability data were obtained by two means: 1) porosity and permeability measurements of outcrop samples 2) porosity and permeability data were obtained from equivalent oolite reservoir units in subsurface Khuff-equivalent reservoirs in Iran (Esrafili-Dizajiand Rahimpour-Bonab, 2014).

# CHAPTER 4

# RESULTS AND DISCUSSIONS

## 4.1 Introduction

Due to the opening of the Neotethys, epicontinental, platform was located in the north-east part of the Arabian plate. Based on the literature and previous works in the Khuff Formation and its equivlant Formations in the Gulf regions comprises of (Eltom et al., (2016), Koherer, et al. (2011)), an eipiric carbonate ramp used as depositional model in the area. Most of the Triassic carbonate ramp shows similar facies profile such as Upper Muschelkalk in central Europe (Ziegler, 1990). The cyclic pattern has been encountered in most of the eipiric carbonate ramp of depositional model. Thus, cyclicity documented in this study and process-base interpretation was established. The cycles comprises of repetitive transgressive and regressive depositional sequences. Three types of depositional cycle scale were identified during this study. Within the carbonate ramp, the facies associations always show a gradational facies change along the ramp. Whereas, the lithofacies of carbonate deposits often exists arbitrarily and without transition trend (Amour et. al, 2012). The different stratigraphic hierarchy displays different distribution pattern for the facies. The stratigraphic surfaces were delineated on the outcrop wall. Accordingly, the stratigraphic framework was built and genetic process-base depositional cycles were developed in the studied interval.

A comperhensive study was done on the upper part of Khuff Formation at Attrafiyia road-cut. Based on the field, macroscopic and microscopic observations, sedimentary facies were subdivided into 11 lithofacies and coded for the upper Khartam Member within the study area **(**Table1**)(**Eltom et. al, in press). The lateral facies successions were dveloped from the vertical facies stacking according to Walter's law.

## 4.2 Facies Analysis and Interpretation

Numerous lithostratigraphic schemes of the Khuff Formation have been published (Vaslet et al., 2005; Insalaco et al. 2006; Maurer et al. 2009; Koehrer et al. 2010; Walz et al. 2013; Eltom et al., *in press*).

In the studied interval, eleven vertical stratigraphic sections were sampled and described. Four of the vertical sections are covering the whole interval (32 m thick); KS-3, -7, -9 and -10. The following points are summary for these sections:

- **KS-3:** This section is about 6 m thick
- **KS-7:** This section is about 9.6 m thick
- **KS-9:** This section is about 5.6m thick
- **KS-10:**This section is about 13.6 m thick

The lithofacies were identified and described in the outcrop and thin sections as follows:

### 4.2.1 Graded peloidal wackestone and packstones (LF1)

Description: yellowish to whitish colors, comprises of; peloids and ooids particles. This lithofacies shows structures of, Horizontal lamination and hummocky cross stratification (Figure 4.1 (B)). The thickness of lithofacies ranges from 30 to 50 cm and shows fine ooids and peloids particles in the thin section. The depositional energy for this lithofacies is low

to moderate and more precisely below a fair-weather wave base and above a storm wave weather base. This was inferred from the sedimentary structures and the grain size. This lithofacies is interpreted to have been deposited as offshore to distal foreshoal tempestites in a transitional zone between deep and middle ramps (Eltom et al. (*in press*)).

### 4.2.2 Graded wackestone to grainstone (LF2)

Description: whitish to light beige, comprises of; very fine to fine ooid, detrital peloids and calcisiltites and Flat pebble at the base. This lithofacies shows massive wackestones and hummocky cross stratified, low angle trough cross-bedded grainstones. Also, the grainy part shows ooids particles with different sizes (Figures 4.1 (C, D, E and F)). The thickness of this lithofacies ranges from 20 to 70 cm. However, this lithofacies deposited in proximal foreshore sub-environment (Eltom et al. (*in press*)).

### 4.2.3 Massive oolitic grainstone (Emerge Shoal) (LF3)

Description: brownish, comprises of; ooids, and disperse peloids. This lithofacies shows Massive at the base and cross-bedded at the top (Figure 4.2 (C)). Its thickness ranges from 10 to 50 cm, and 100 cm for the stacked bed sets. In the thin section showed dominance of ooids and peloids. Above this unit there are a lot of microbiolites, which are present in the forms of thrombolites(Figure 4.2 (B)). This lithofacies deposited in stabilized shoal sub-environment and prograded into the foreshoal deposits, so interbeded with packstone and wackestone lithofacies (Eltom et al. (in press)).

### 4.2.4 Trough cross-bedded Peloidal oolitic grainstones (LF4)

Description: brownish, comprises of micritizedooids.This lithofacies shows horizontal lamination, cross bedding and cross bedding to massive bedding (Figure 4.2 (E)). In the

thin sections, grains are of ooids and peloids types. Lithofacies thickness ranges from 1 to 3 m and interpreted as sand bars deposits (Eltom et al. (*in press*)).

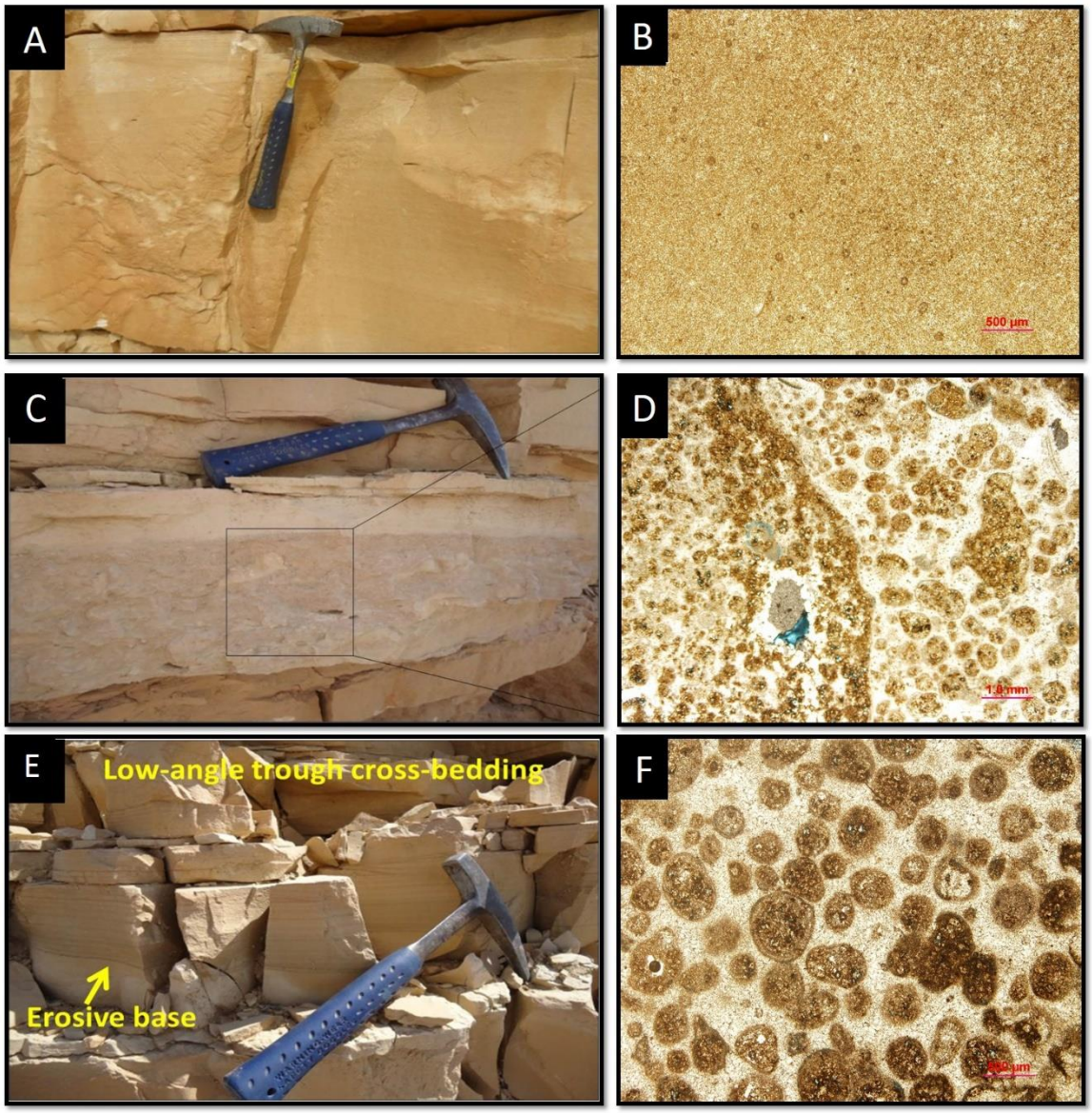


Figure 4.1: Outcrop observations and photomicrographs of foreshoal lithofacies; (A) and (B) show the graded peloidalwackestone and packstones, (C) and (D) show flat pebbles and (E) and (F) show trough cross beds within gradedwackestonetograinstone lithofacies (Eltom et al., in press).

### 4.2.5 Rippled oolitic Peloidal grainstones (LF5)

Description: whitish to brownish, comprises of; fine to medium well-sorted ooids and peloids. It shows mega ripples (Figure 4.2 (D)). Lithofacies thickness is 50 cm and in thin sections shows grains are dominated by fine ooids and peloids interpreted as rippled oolitic sands (Eltom et al. (*in press*)).

### 4.2.6 Poorly sorted peloidal oolitic grainstone (LF6)

Description: brownish, comprises of poorly sorted ooids and peloids (Figures 4.2 E). This lithofacies shows cross-beds structure. In the context of the depositional environment, this lithofacies was interpreted to having been deposited in a tidal channels (Eltom et al. (*in press*)). Also, this unit prograded into the intercalated layers of wackeston and packestone.

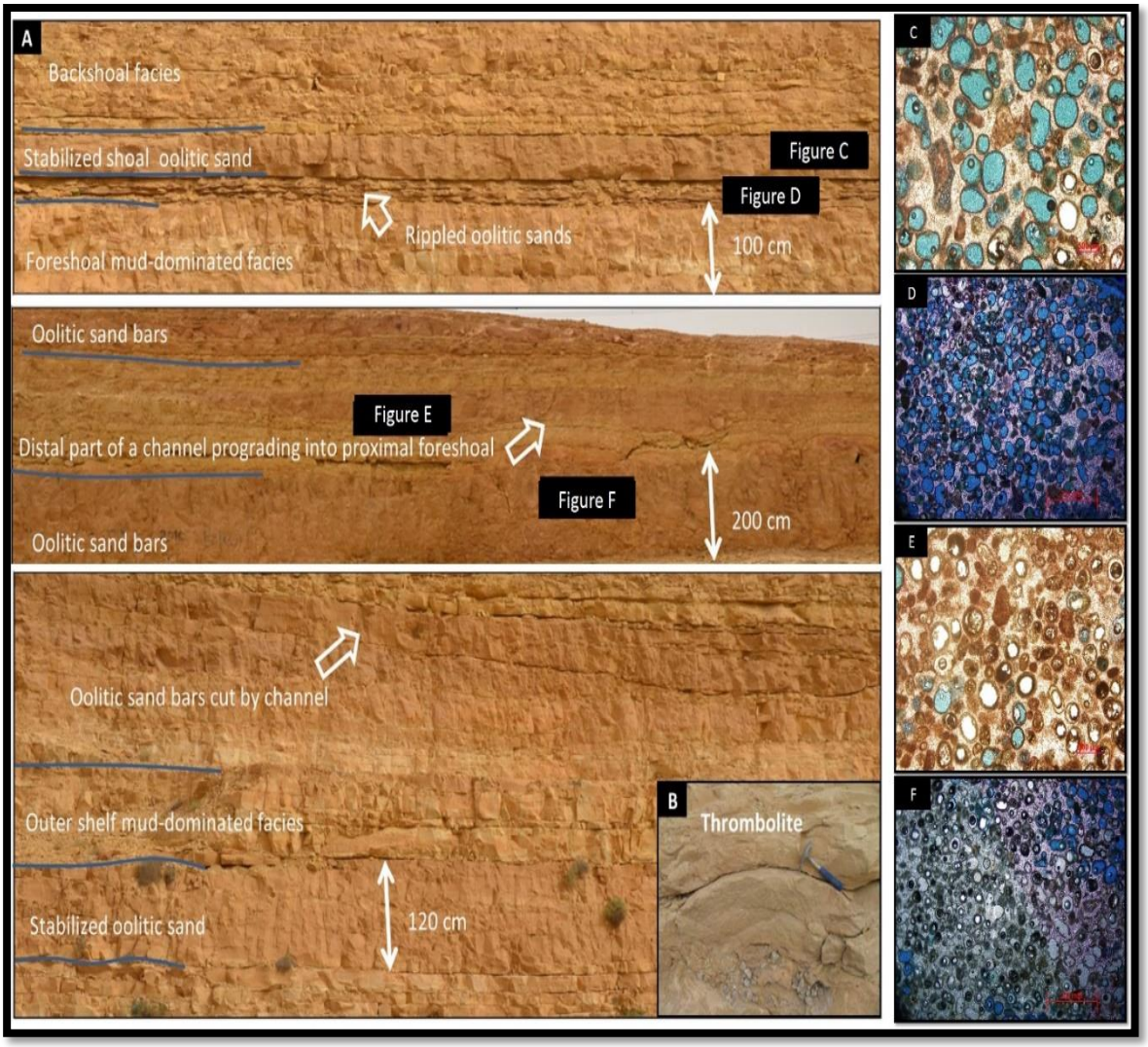


Figure 4.2: Outcrop observations and photomicrographs of shoal complex lithofacies; (A) shows lateral and vertical stacking of shoal complex, (B) shows thrombolite structure within shoal complex, (C) shows massive oolitic grainstone, (D) shows trough cross-bedded peloidal oolitic grainstones, (E) shows rippled oolitic Peloidal grainstones and (E) shows oolitic sand bars (Eltom et al., in press).

### 4.2.7 Poorly sorted skeletal intraclastic oolitic grainstones and packstones (LF7)

Description: gray, light brown to tan, comprises of; inetrclasts, peloids and ooids particles. It shows structures of, massive associated with cut and fill structures (Figure 4.3 (B, C)). This lithofacies has thickness ranges from 50 to 70 cm and interpreted to as intercalated layers of distal backshoal and shoal deposits (Eltom et al. (*in press*)).

### 4.2.8 Poorly sorted skeletal peloidal oolitic grainstones and packstones (LF8)

Description: dark brown to reddish, comprises of; brachiopods, gastropods, and bivalves shells. It shows structures of massive beds (Figure 4.3 (D)). Lithofacies thickness ranges from 30 to 50 cm (Eltom et al. (in press)).

### 4.2.9 Dolomitic skeletal oolitic grainstones (LF9)

Description: red to beige, comprises of dolomitized ooids, brachiopods, bivalves, and gastropods skeletals. It shows structures of, wavy ripples, convolute beds, soft sediment deformation and lenticular beds (Figure 04.4 (B)). This lithofacies has thickness ranges from 10 to 20 cm. This lithofacies interpreted as Subtidal deposits (Eltom et al. (in press)).

### 4.2.10 Hetrolithic (LF10)

Description: red to beige, comprises of dolomitized ooids. It shows structures of, wavy ripples, convolute beds, soft sediment deformation and lenticular beds. This lithofacies has thickness ranges from 10 to 20 cm.

The heterolithic facies is deposited in the subtidal zone (Eltom et al. (in press)) and is mainly dominated by dolmitic skeletal oolite as shown in thin sections (Figure 4.4 (C)).

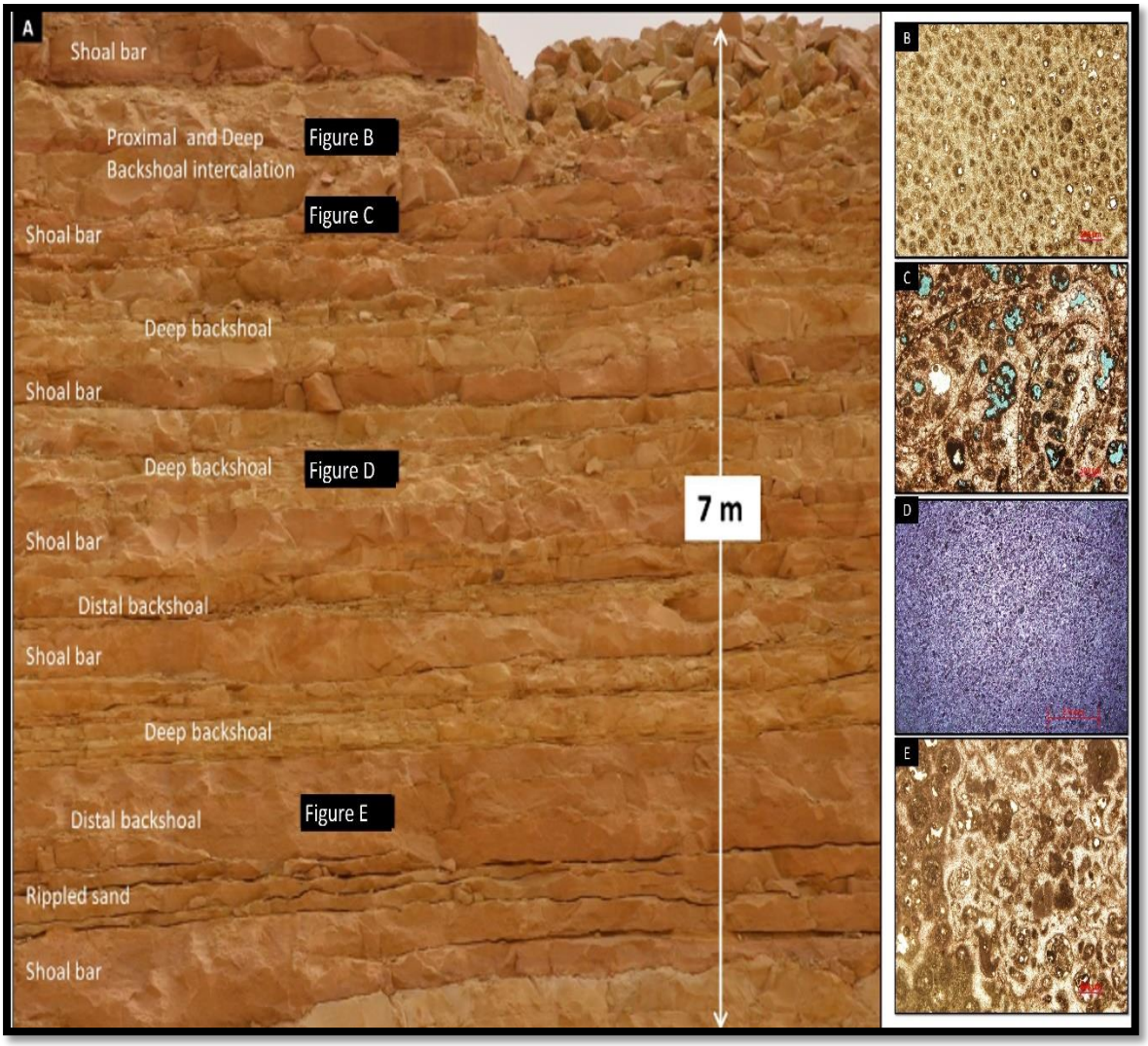


Figure 4.3: Outcrop observations and photomicrographs of backshoal lithofacies types; (A) lateral and vertical stacking of backshoal lithofacies, (B) and (C) show skeletal intraclastic Peloidal ooilitic grainstone, (D) shows skeletal intraclastic peloidal oolitic grainstone, (E) shows poorly sorted skeletal intraclastic oolitic grainstones and packstones (Eltom et al., in press).

### 4.2.11 Microbial laminates (LF11)

Description: tan, light gray to whitish, comprises of; debris of algal mats, poorly sorted peloids and medium to fine-grained quartz. Microbial laminates shows structures of massive (Figure 4.4 (D)) and its thickness ranges from 30to50cm. This lithofacies interpreted as Intertidal deposits (Eltom et al. (in press)).


Figure 4.4: Outcrop observations and photomicrographs of tidal flat lithofacies types; (A) the lateral and vertical stacking of the lithofacies, (B) Poorly sorted skeletal peloidal oolitic grainstones and packstones, (C) Hetrolithic and (D) microbial laminates lithofacies (Eltom et al., in press).

In this study, the Upper Khartam Member lithofacies and depositional environments are described and interpreted in the context of these published lithofacies schemes for the Khuff Formation. Observations of lithology, facies texture, sedimentary and structures are listed in Table 1. The depositional model for the upper part of the Khuff Formation was constructed by Eltom et al., 2016 as shown in figure 4.5. Six lithofacies associations (LFA) in the studied outcrop are interpreted to represent environments of sutidal to shoal complex depositional environments (DE) of a ramp platform setting. Table -1 summarize field observations and interpretation of these lithofacies associations.

Table 1: Shows lithofacies and their correspondent depositional environment and sub-environment in the study area (Eltom et. al, in press).

| Lithofacies Association (LFA) | Lithofacies | Thickness | Sedimentary Structures |
|---|---|---|---|
| LFA 6 | Microbial laminates | 30 to 50 cm | massive |
| LFA 5 | Heterolithic | 10 to 20 cm | wavy rippled filled by mud drapes, soft sediment deformation, convolute beds, lenticular beds, keystone vugs, and soft sediments deformation |
| LFA 4 | Poorly sorted skeletal peloidal oolitic grainstones and packstones | 30 to 50 cm | massive |
| LFA 3 | Poorly sorted intraclastic oolitic grainstones and packstones | 50 to 70 cm | massive with some cut and fill structures |
| | Thin bed fine limestones alternating with grainstones | 30 to 50 cm | Fessile, wavy-laminated beds, gutter casts, pot casts, hummocky cross stratification |
| LFA 2 | Cross-bedded micritized oolitic Peloidal grainstones | 1 to 3 m | horizontally laminated, cross-bedded, crossbedded to massive beds |
| | Massive oolitic grainstones | 100 cm | Massive at the base and crossbedded at the top |
| | Rippled oolitic peloidal grainstones | 50 cm | mega ripples |
| LFA 1 | Graded wackestone to Grainstone | 20 to 70 cm | wackestones and packstone are massive while the grainstones are characterized by climbing lamination, hummocky cross stratification, low angle trough cross-bedding and horizontal lamination. |

## 4.3 Stratigraphic architecture

Five meter-scale stratigraphic cycle sets were identified within the studied interval of Khartam Member (Figures 4.6 and 4.7). The lithofacies were used for cycle sets interpretation, thus each cycle comprises of hemi-cycle sets of transgressive and regressive sequences. The thickness of the cycle sets ranges from 4m to 8.5m with an average thickness of about 6.2m. Each one comprises of group of lithofacies as shown in table 1:

**Cycle sets-1** consists of transgressive part of poorly sorted intraclasts rudstones topped by open marine distal foreshoal mudstone to wackestone, then followed by the regressive part comprised of open marine distal foreshoal mudstone to wackestone. This cycle is bounded by the clay boundary of Permian-Triassic transition in the bottom and cycle 2 in the top.

**Cycle sets-2** as in the above cycle sets, it consists of foreshoal mudstones and graded beds mudstones to packstones as transgressive part and overlain by tempestites of the foreshoal deposits and thick shoal deposits of oolitic sand bars, channels and rippled oolitic sand as the regressive part of the cycle sets.

**Cycle sets-3** the transgressive part consists of thinnly-bedded deposits of shoal complex, thin beds of distal, deep or proximal backshoal deposits. The regressive part comprises of beds of poorly sorted skeletal-peloidal-oolitic grainstones, packstone of proximal backshoal and tidal flat deposits.

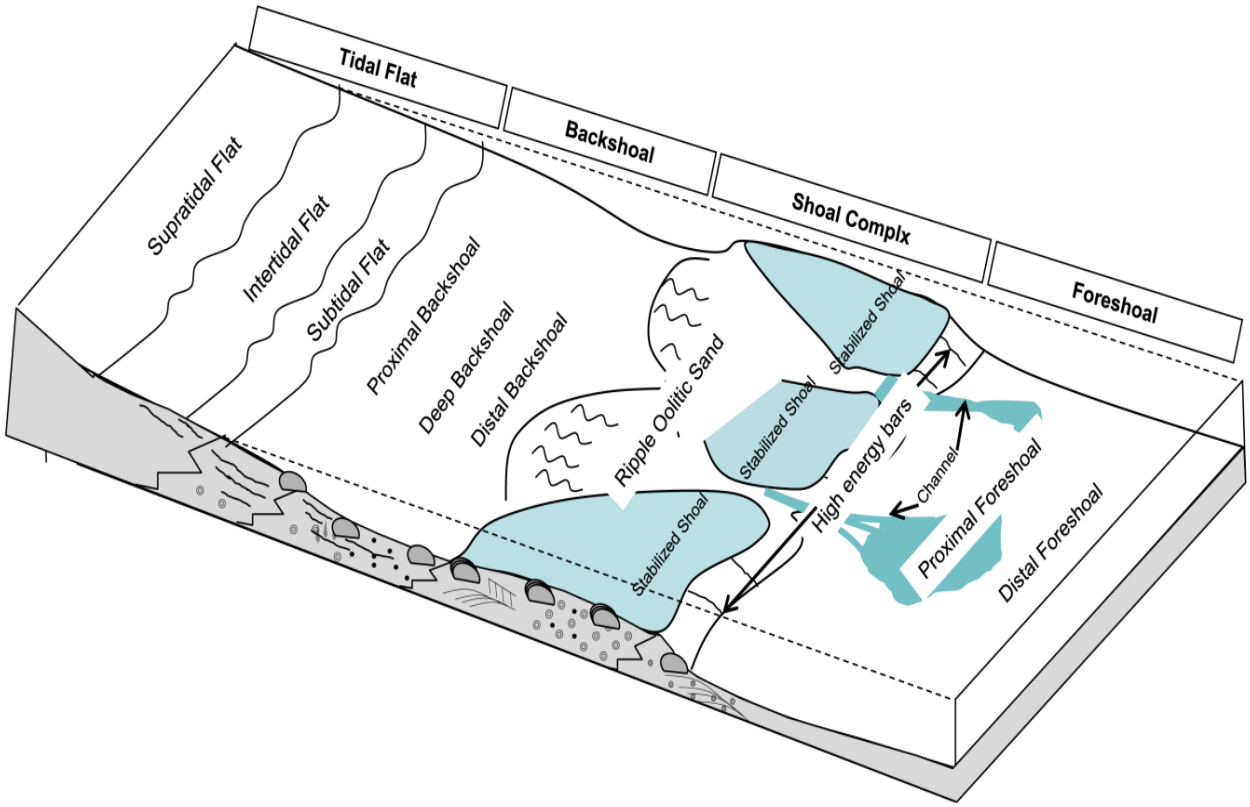


Figure 4.5: depositional model for the Upper Khartam Member at AtTrafiha outcrop (Eltom et al., in press).

**Cycle sets-4** has similar facies types as in cycle sets-3**.** The transgressive and regressive sequences were also encountered within this cycle set.

**Cycle sets-5** represents the uppermost part of Khuff Formation. it is overlain by the thick beds of collapsed breccia ( base of Sudair Formation). Subtidal to intertidal flat deposits of heterolithic facies represent the transgressive part, while supratidal flat deposits of microbial laminates repesent the regressive part of the cycle sets.

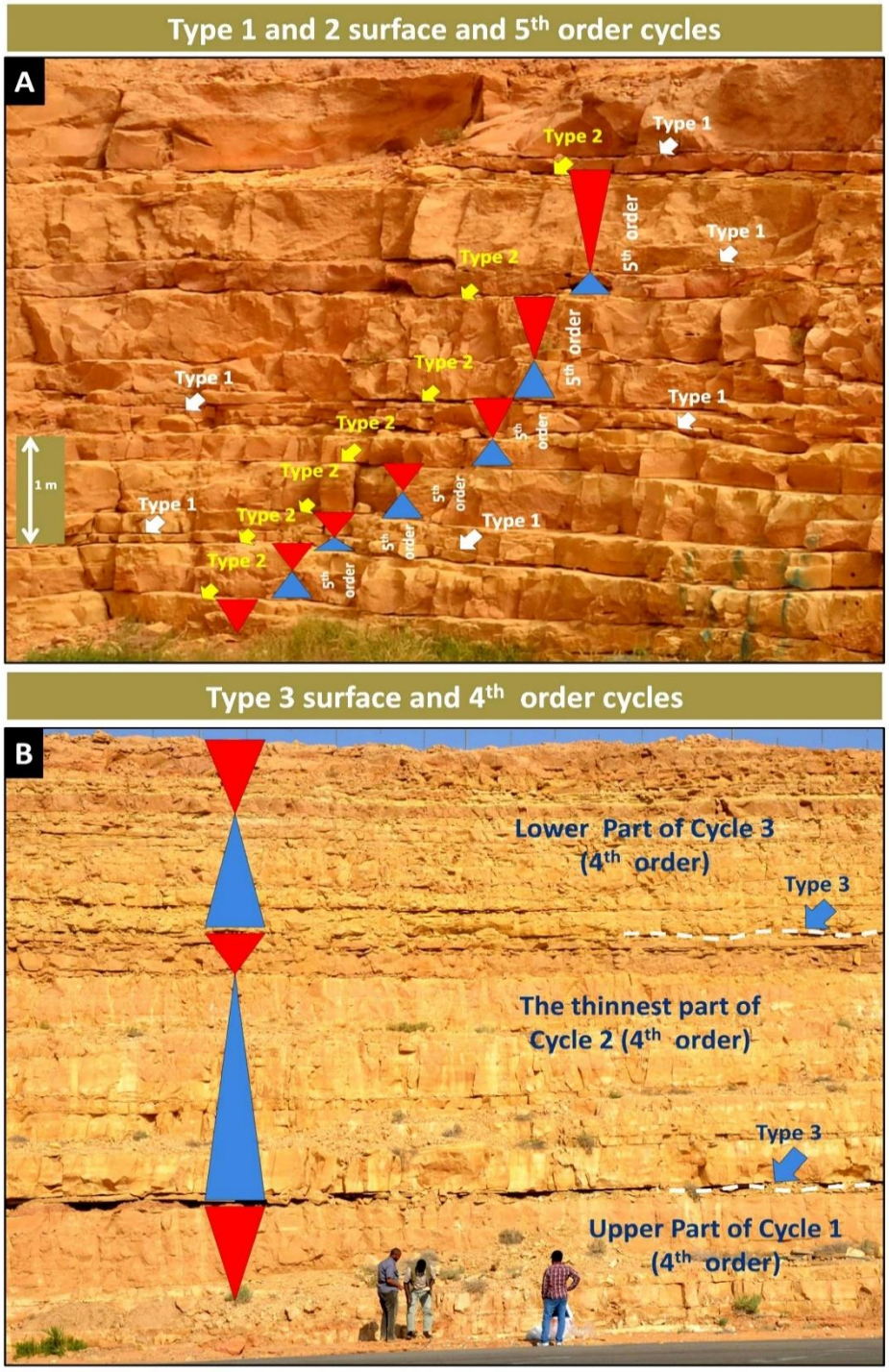


Figure 4.6: Outcrop view of the cycles and cycle sets with different surfaces indicated by arrows. White arrows show Type 1 surfaces; yellow arrows show Type 2 surfaces; blue arrows show Type 3 surfaces. The blue tringles indicted the transgressive part of cycles, inverted red tringle indicate regressive part of cycles.

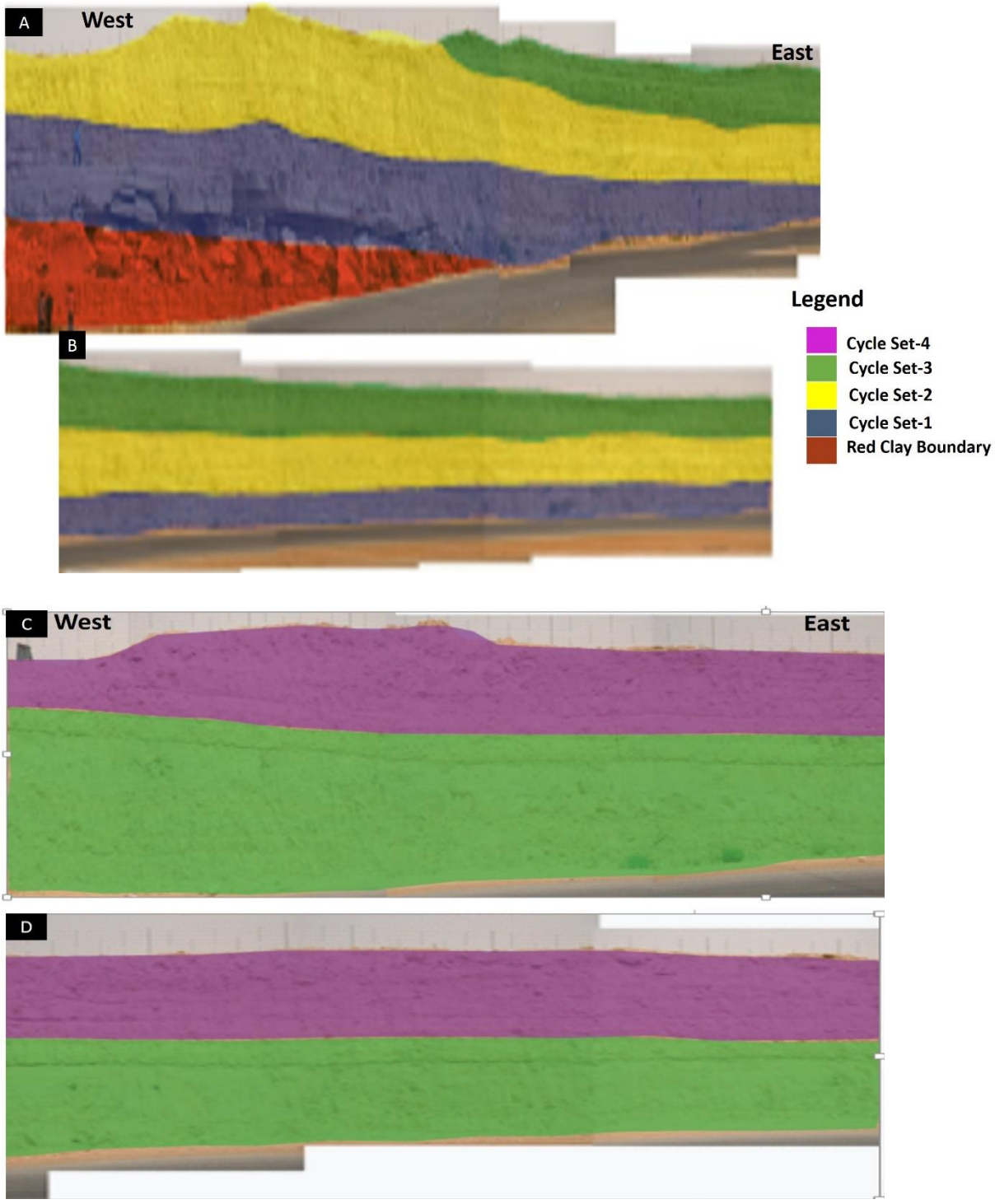


Figure 4.7: colored 2D outcrop panel showing the stacking of cycle sets (fourth order sequences) (A), (B), (C) and (D) from east to west.

## 4.4 Impact on Reservoir-Quality Evolution

Limestones have undergone to diagentic processes such as; 1- micritization around the grains; 2- partial dissolution of the grains (ooids, peloids, skeletal .etc.); 3- precepitaation of calcite cement in the interparticle pores; 4- total dissolution of the particles and precipitation calcite; 5- dolomite cement and displacement; and 6- quartz cementation.

### 4.4.1 Lithofacies and pore types

- **Massive oolitic peloidal grainstones**

  The lithofacies was deposited in a stabilized shoal sub-environment. Lithofacies prograded into the foreshoal deposits, and hence it is interbeded with packstone and wackestone lithofacies. Thin section showed dominance of ooids and peloids.

  However, grains of aragonitic mineralogy dissolved and precipitated in the interparticle pores as a calcite cement. Due to the meteoric effect, the most abundant pore type are moldic and intraparticle (Figure 4.8 (a), (b)).

- **Trough cross-bedded peloidal oolitic grainstones**

  The facies interpreted to have been deposited in high energy bars and channels. The facies has the similar features as the massive oolitic peloidal grainstones, however, the sedimentation energy is slightly higher. Due to the peturbation in the environmental conditions, the bimineralicooids were the main mineralogic type in the interval. Therefore, the pore types of intraparticle and interparticle were observed but with high degree of calcite cementaion (Figure 4.8 (c), (d) and (e)).

- **Rippled oolitic peloidal grainstones**

  The ripple mated oolitic-peloidal grainstone was deposited. The ripples structure indicate the weak energy of deposition. Due to the bimineralic mineralogy of the ooids, the facies shows the same pore types as in the lithofacies of the high energy bars and channels subenvironments. However, the trough cross-bedded peloidal oolitic grainstone is more cemented than the rippled oolitic peloidal grainstone (Figure 0.9 (a), (b)).

- **poorly sorted peloidal oolitic grainstone**

  this facies was deposited in tidal channels which pass seaward to the foreshoal deposits. As in the other shoal subenvironments units, it is dominted by bimineralic ooids and the main pore types are moldic and intraparticle.

- **Skeletal peloidal oolitic grainstones**

  Due to the energy activity in the proximal backshoal, skeletal peloidal oolitic grainstones deposited along with interbeds of , wackestones and packstones in deep and distal backshoal environments. The skeletal particles have firstly appeared in this facies. The ooids mineralogy still bimineralic, so the intraparticle, intraskeletal and modlic pore types were dominated in the interval (Figure 0.9 (c), (d)).

- **Dolomitic skeletal oolitic grainstones**

  This lithofacies was deposited in the subtidal zone and is mainly dominated by dolmitic skeletal oolite. The ooid mineralogy is aragonitic and main pore types are intercrystalline, moldic and intraskeletal (Figure 0.9 (e), (f)).

### 4.4.2 Diagenesis and stratigraphic framework

The diagentic effect has been studied and characterized within the stratigraphic framework of the studied interval. The sea level and original ooid mineralology are the main factors that control the prevailing diagentic stages within the stratigraphic sequences. By studying thin sections, X-ray diffraction and scanning electron microscopic analyses, the main diagenetic features were revealed within the five cycle sets. Meteoric diagenesis extensively affected the boundaries between the cycle sets as indicated by the dissolution of the particles.

Cycle sets 1 and 2 are mainly comprised of ooid-dominated lithofacies whichmineralogiclly composed of aragonitie. Marine fauna is completely absent in the facies of these cycles. The sea-level rose at the end of Permean-Triassic boundary. The meteoric diagenetic alteration dissolved the aragonitic particles to fill the initial interparticle porosity. The porosity was retained in this interval, because of rapid sea level rise which stop the advance of the tidal flat. However, moldic and intraparticle were expected to be the abundant pore types. In cycle sets 3 and 4, the marine fauna has partially recovered and rock types are mainly of skeletal oolite lithofacies. The facies analysis indicates that sea level at the time of deposition extremely fluctuated. The change of original mineralogy from aragonitic to bimineralic affected the expected pore types. Thus, the interparticle, intraskeletal and less moldic pore types were observed in this interval. In cycle set 5, the marine fauna fully recovered and dolomitic skeletal oolite lithofacies dominated within the interval. The ooid mineralology changed again to aragonite and thus, the pore types are moldic and interskeletal. Because of the extensive evaporation in tidal

flat subenvironment, dolomitization was extensively developed and intercrystalline pore type enhanced the porosity values within this interval (Figure 4.10).

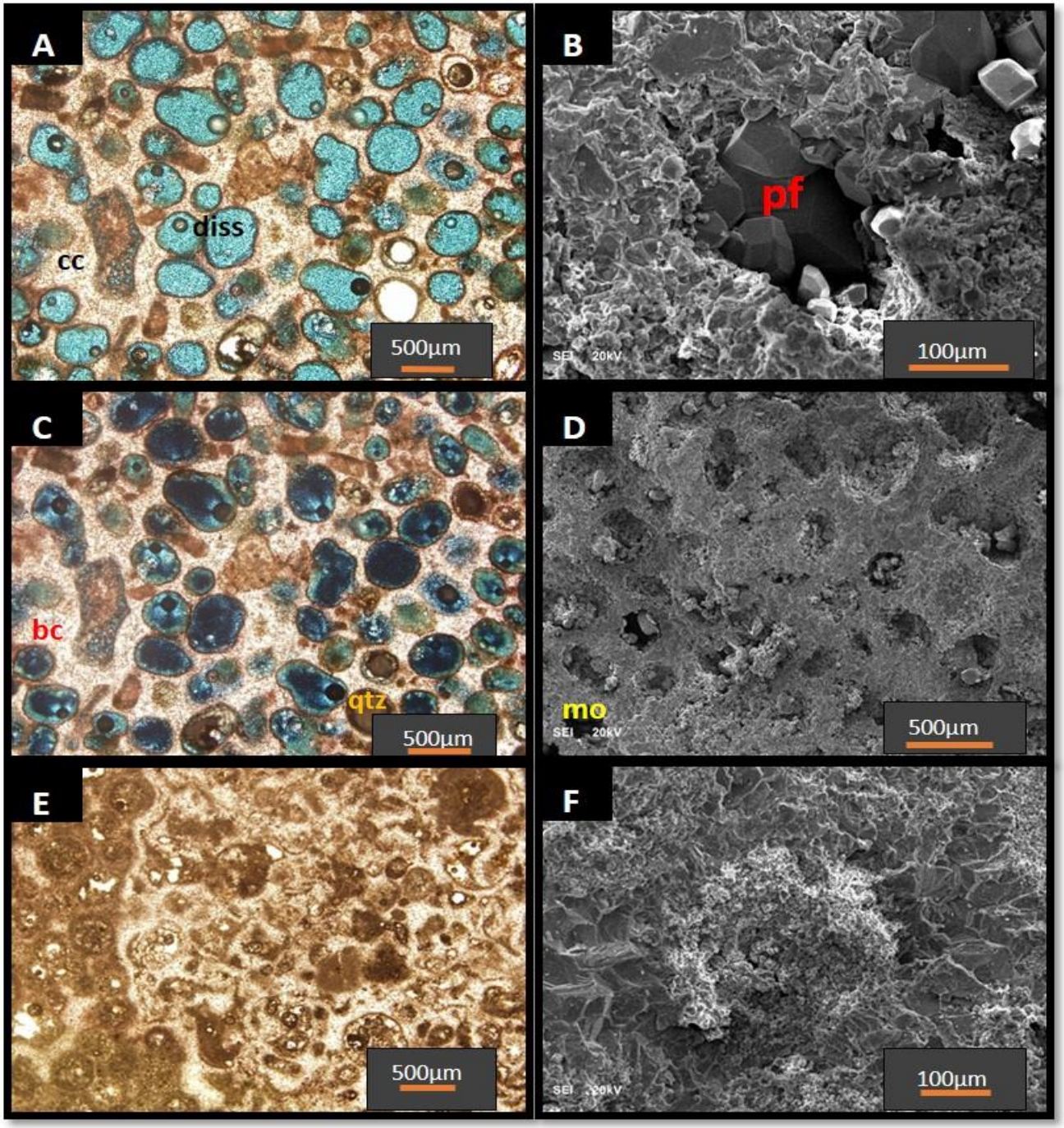


Figure 4.8: (A) oomoldicgrainstone (diss= dissolved ooids; cc= cemented interparticle pores); (B) SEM image shows the partially filled moldic pores (pf); (C) thin section image under cross polarized microscope shows quartz (qtz) and blocky calcite (bc) cement types; (D) SEM image shows moldic (mo) and cemented pores as well; (E) image of highly cemented grainstones and (F) shows the cement material of fine calcite.

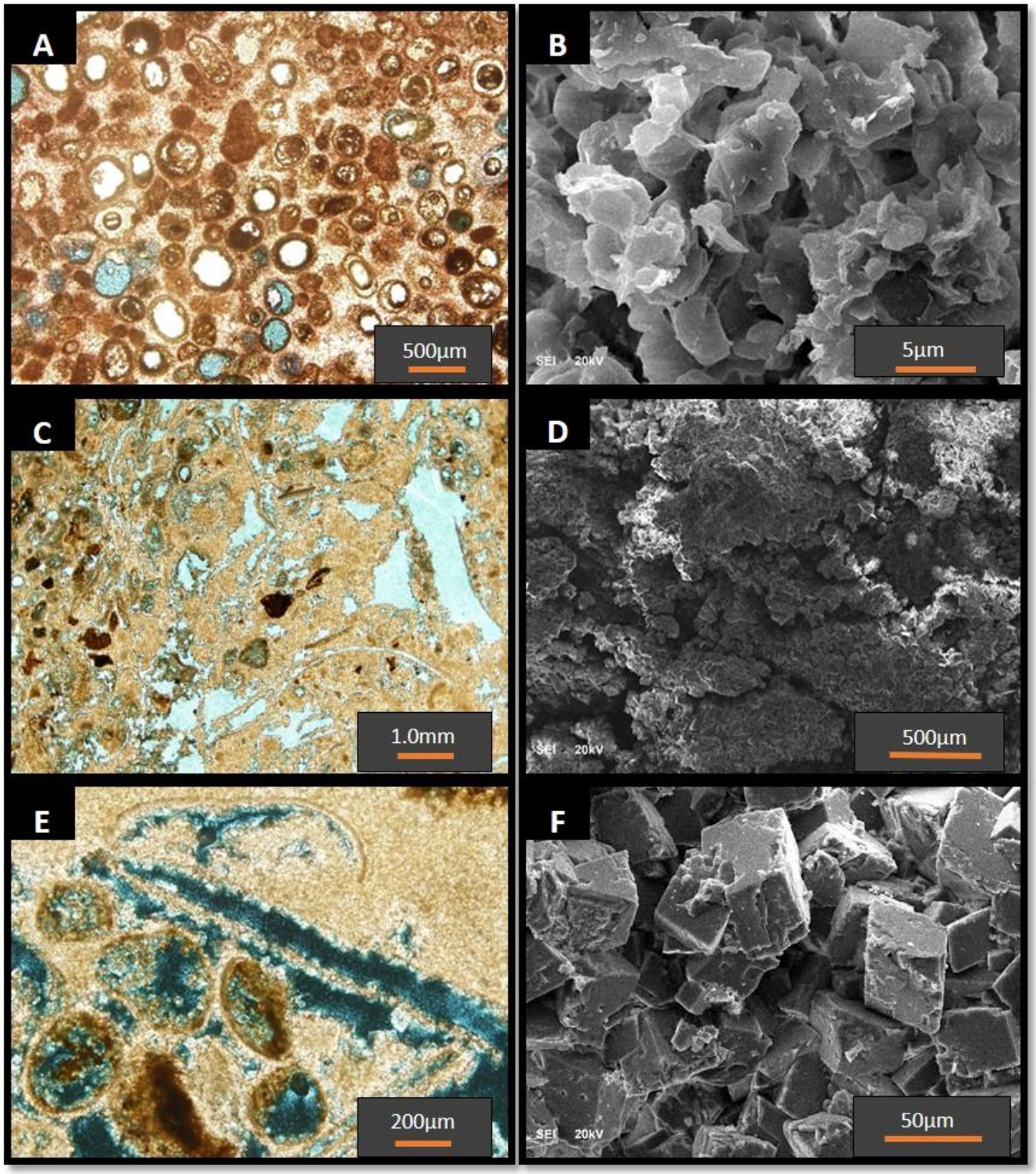


Figure 4.9: (A) Rippled oolitic peloidal grainstones; (B) SEM image shows calcite cement; (C) intercrystalline pore types (icp) and rhombic structure of dolomite (dol); (D) dolomitic skeletal oolitic grainstone composed of skeletal moldic pores (skm); (E) and in SEM image (F).

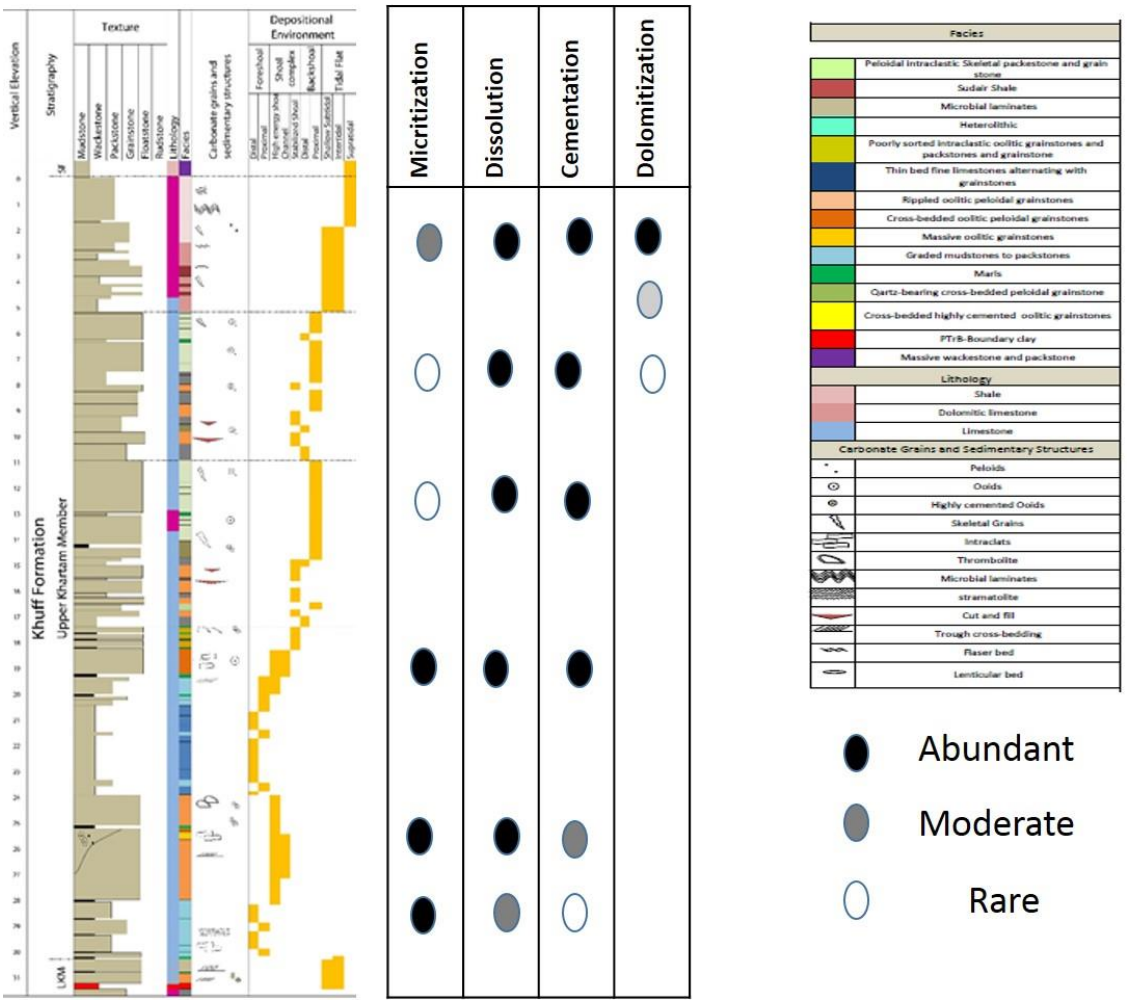


Figure 4.10: The effect of the diagenesis on the stratigraphic sequences, porosity and permeability. The plus indicates the degree of the diagenetic impact; abundant (black circle), fair (grey circle) or less (white circle).

## 4.5 Statistical Analysis

The petrophysical properties such as porosity and permeability measurements and their relationship are the heart of reservoir characterization operation. The distribution of these properties are commonly controlled by the depositional lithofacies (Saner and Sahin, 1999, Saner and Sahin, 2001). However, the outcrop analogue has a crucial role in providing data with high vertical and lateral continuity which resolves the spatial distribution of the facies. The statistical analysis of the petrophysical properties and their correlations effectively contribute to the characterization ofa reservoir zones. In case of carbonate reservoirs, the porosity-permeability plot shows scattered behavior of data points which reflects the complexity of the carbonate lithofacies. Furthermore, porosity and permeability distributions reveal the different zonations within the reservoir rocks (Srinivasan and Sen, 2009).

This study presents the porosity and permeability parameters which have been evaluated from cores plug obtained from outcrops samples of the Upper Khartam Member at AtTraffiyah area. The data sets of porosity and permeability were analyzed in statistical point of view based on the lithofacies type. The univariate statistics tested for the input data involves the center, spread and the shape parameters of the porosity and permeability distributions. In order to determine the distribution type, the histogram was constructed for each variable. The main objective of this study was to define the zonation of the reservoir rocks of the Upper Khartam Member using the integration of the lithofacies and the petrophysical properties ($\phi$ & k).

### 4.5.1 Input data

The sample data were georefrenced and coordinated as shown in table 2. The constructed map shows the distribution of the sample points which generated by Petrel software (Figure 4.11). The outcrop sections were taken as pseudo wells. The encountered lithofacies of the Upper Khartam Member outcrop were analysed statistically. Figure 4.12 shows the percentage for each facies sampled from the outcrop. Rippled oolitic peloidal grainstones (5) lithofacies is the most dominant among the lithofacies types. On the contrast, graded mudstones to packstones (8) lithofacies is the least one.

Table 2: Shows outcrop sections location, and measuredlengths.

| Name | Easting | Northing | Length (m) |
|---|---|---|---|
| Section-1 | 400022 | 2923389 | 6.2 |
| Section -2 | 400214.3 | 2923411 | 10.2 |
| Section -3 | 400506.8 | 2923419 | 6 |
| Section -4 | 400748.1 | 2923528 | 5.2 |
| Section -5 | 400880.9 | 2923594 | 7.6 |
| Section -6 | 401129.8 | 2923592 | 6.2 |
| Section -7 | 400093 | 2923268 | 9.6 |
| Section -8 | 400385.6 | 2923284 | 5 |
| Section -9 | 400670.4 | 2923249 | 5.6 |
| Section -10 | 400679.4 | 2923418 | 13.6 |
| Section -11 | 400844.3 | 2923525 | 8.2 |

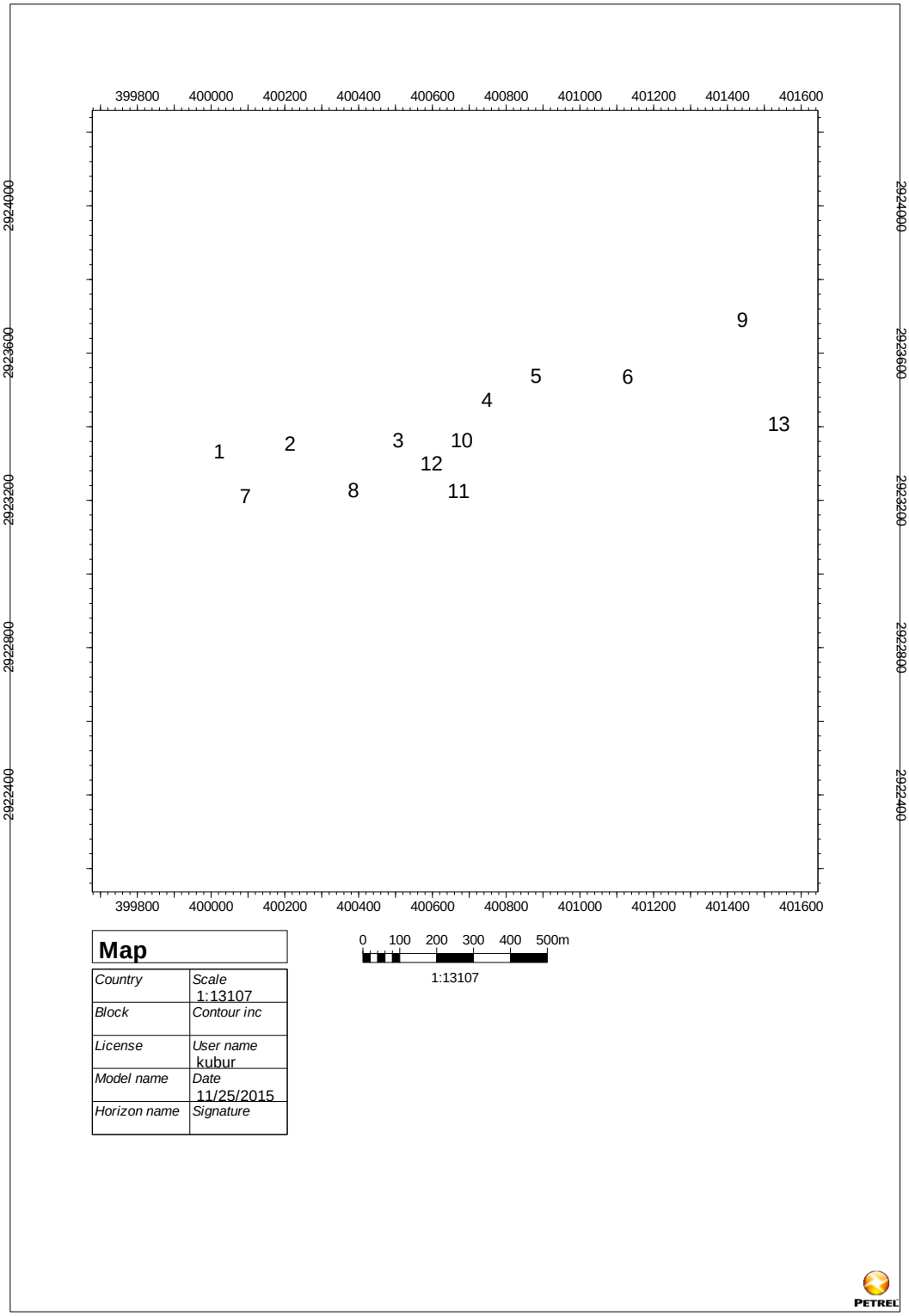


Figure 4.11: Map shows the distributions of the outcrop sections in the study area.

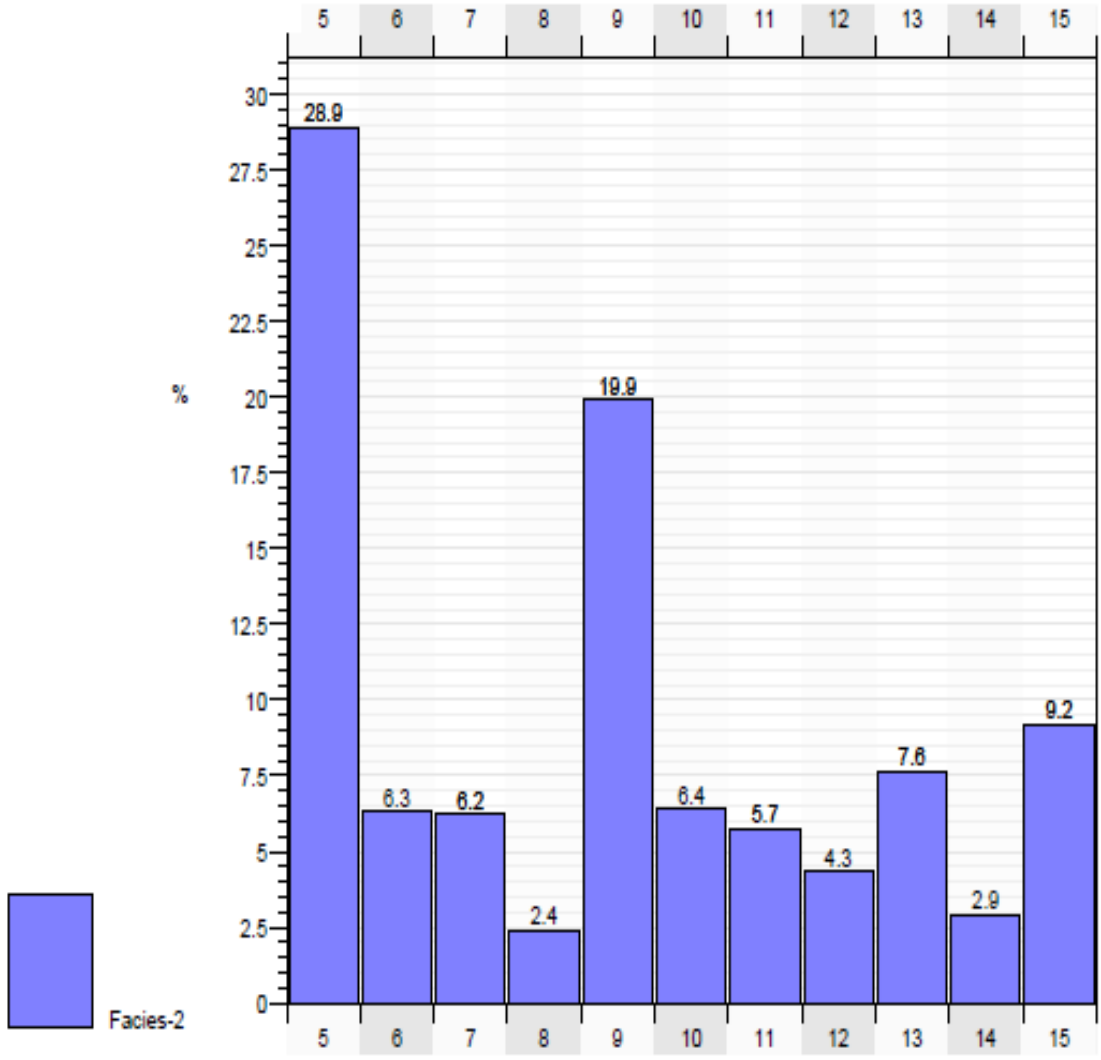


Figure 4.12: Histogram shows distribution of Facies percentages for the input data.

### 4.5.2 Univariate Statistics

The outcrops of Upper Khartam Member have been logged in 11 stratigraphic sections. The thickness of the sections ranges from 5 to 6m. Lithologically, the logged outcrop sections comprises of carbonate lithofacies range from; mudstone, wackstone, packstone, grainstone, through crystalline and dolomitized Limestone rocks. However, the occurrence of these lithofacies within the outcrops has been evaluated and statistically analyzed. The statistical parameters of center, spread and shape of the petrophysical properties have been calculated for each section individually.

### 4.5.3 Porosity and Permeability

The petrophysical data of the outcrop samples of the Upper Khartam Member have been statistically analyzed. The total number of samples are 244; includes 244 and 233 measurements of porosity and vertical permeability, respectively. Table 3 shows the summary statistics for porosity and permeability after data cleaned up. The data distributions showed sub-populations within the main populations of the porosity and permeability measurements (Figure 4.13). Then, accordingly four outliers (23.46, 54.23, 145.5, 202.3 md) have been removed from the permeability data. The previous investigation of these permeability outliers by Abdulraziq (2014), attributed them to an artificial fractures made during samples preparation. Porosity-permeability relationships have been investigated using the cross plot (Figure 4.14). Based on the statistical analysis, both porosity and permeability measurements showed presence of many patterns within the main populations. These patterns are due to the depositional facies heterogeneity and diagentic effect.

Table 3: Statistical summary of the porosity and permeability datasets obtained from Upper Khartam Member outcrop.

| Parameter | Porosity | Permeability |
|---|---|---|
| Mean | 10.88 | 1.18 |
| Median | 8.18 | 0.56 |
| Standard Deviation | 7.93 | 2.41 |
| Sample Variance | 62.97 | 5.79 |
| Kurtosis | 1.20 | 44.45 |
| Skewness | 1.33 | 5.87 |
| Range | 36.09 | 23.62 |
| Minimum | 1.52 | 0.02 |
| Maximum | 37.60 | 23.64 |
| Coefficient of Variation | 0.73 | 2.04 |

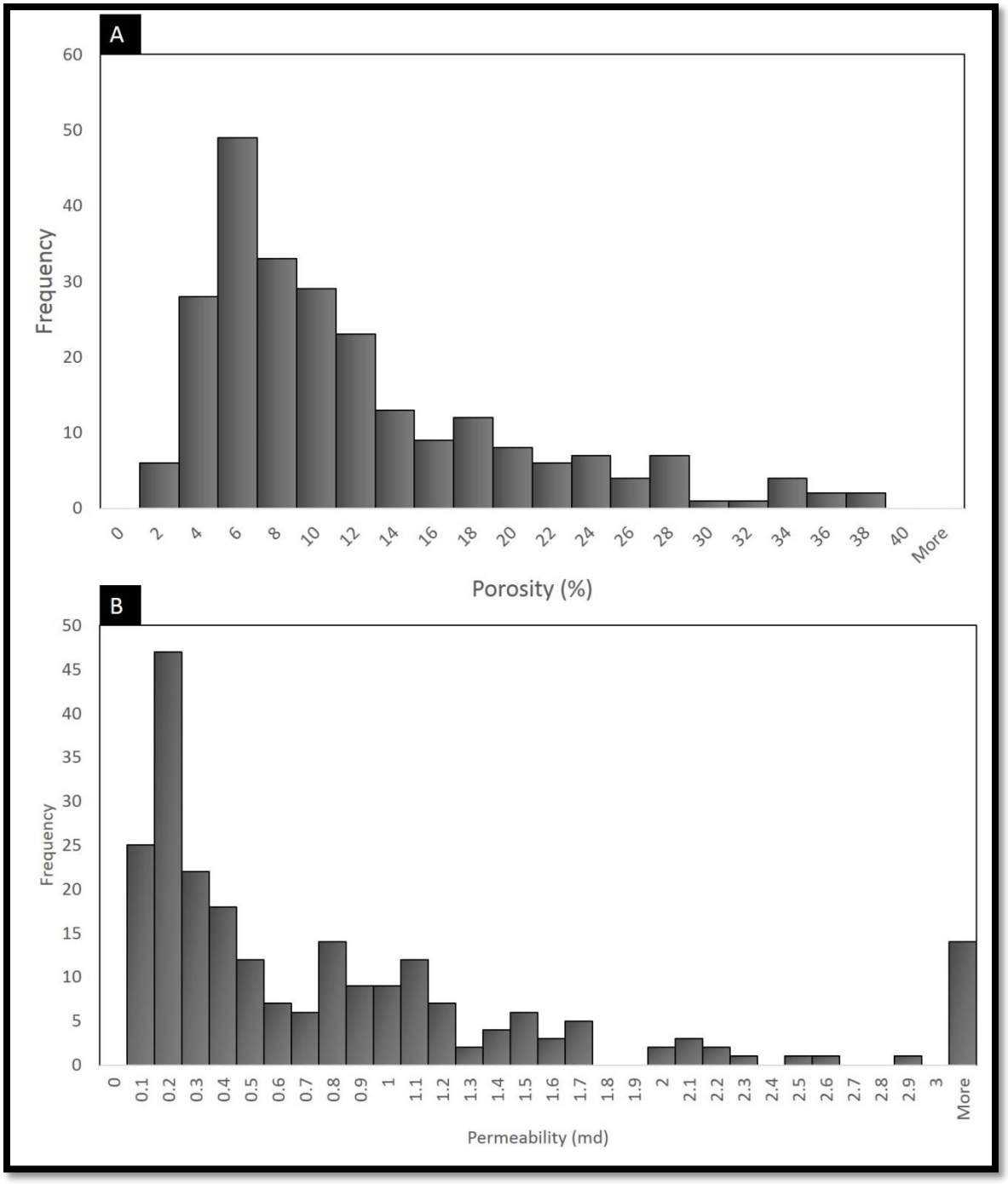


Figure 4.13: Histograms of porosity (a) and permeability (b) measured from the outcrop data.

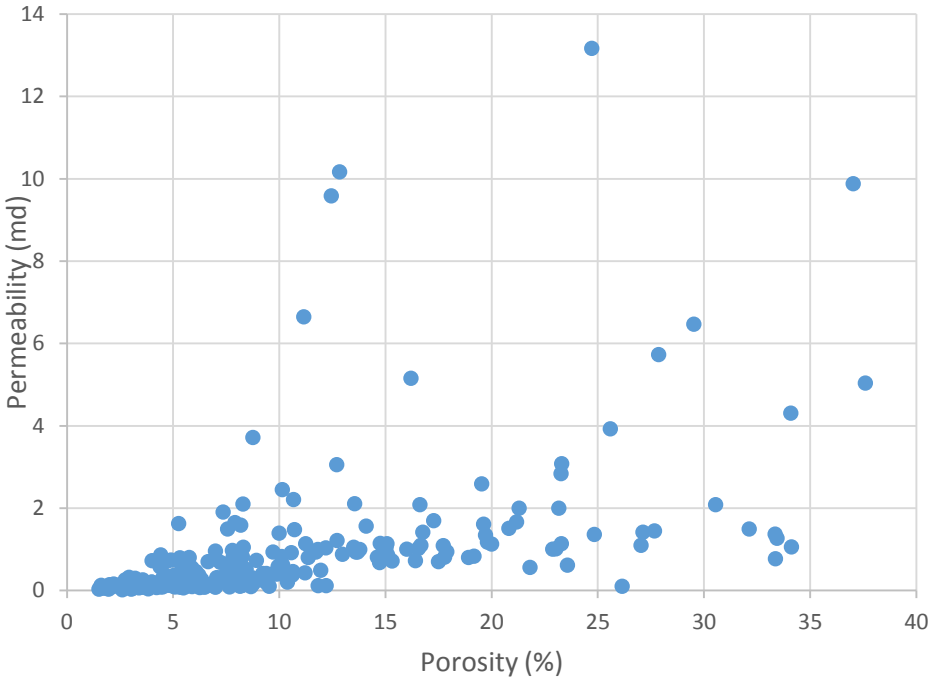


Figure 4.14: Shows cross plot of Porosity-Permeability measurements of Upper Khartam Member.

### 4.5.4 Porosity and Permeability of Texture-based Rock types

In this stage, the porosity and permeability distributions were analyzed based on the dominant texture. The sample data sets were grouped into three types of textures; grain-, muddy grainy- and muddy-dominated lithofacies. Each group of rock types has similar characteristics, so it reflects to some extent the pattern of the petrophysical properties.

The grainy rock types include different lithofacies of grainstones; massive oolitic Peloidal grainstones, trough cross-bedded peloidal oolitic grainstones, rippled oolitic Peloidal grainstones, poorly sorted peloidal oolitic grainstone, skeletal peloidal oolitic grainstones and dolomitic skeletal oolitc grainstones. The muddier rock type comprises of lime mudstone, microbial laminates and dolo-mudstone lithofacies. The muddy-grainy rock types represent transitional between the grainy and muddy ones. Thus, this type of fabric is comprised of graded peloidalwackestones to packstones, peloidal oolitic wackestone and packstones, skeletal intraclasticpeloidal oolitic packestones and graded Peloidal packstones to grainstones (Figure 4.15).

### 4.5.5 Porosity Distribution

The univariate statistics were used to study measured porosity distributions for the three lithofacies textural types. For the grainy rock types, porosity values range from 2 to 37.6% and mean of 13.49% (Figure4.16). The porosity values showed positively skewed distribution (mean is greater than median). The muddier facies have shown porosity values ranging from 1.5 to 30.6% around mean value of 9.2%. As in the grainy rock types, their porosity distribution shape is positively skewed (Figure4.17). The last texture lithofacies type (muddy-grainy) has porosity values with a mean of 8.92% and ranges from 1.6 to 34.1% (Figure 4.18). The coefficient of variation explains the heterogeneity within each rock types group. Muddy-grainy rock type has the greatest

coefficient of variation value (CV=0.724) among the other two types, indicating facies complexity of grainy-muddy rock types. Thus, the porosity values are highly varied because of the existence of different rock types with different textures. A coefficient of variation of 0.66 reflect the heterogeneity of porosity values within the grainy-dominated rock types. Most of these types are located in the shoal complex sub-environment. There is a variability in the energy strength in the shoal area, and thus may have affected petrophysical properties of the different lithotypes.

### 4.5.6 Permeability Distribution

Permeability values showed to some extent the same distribution as the measuredporosity. Permeability measurements showed bimodal distribution with values of 0.2md and 0.8md. Based on the statistical parameters, permeability values for the three textures are log normally distributed. Therefore, the log-normal distribution of the logarithmicpermeability values was observed for the three rock types (Figures 4.19, 4.20, 4.21).

The correlation of porosity versus permeability was enhanced by using texture of the rock types as criteria for datasets analysis. The correlation factors for grainy-, muddy grainyandmuddy-dominated rock types equal; 0.612, 0.311 and 0.735, respectively (Figure 4.22).

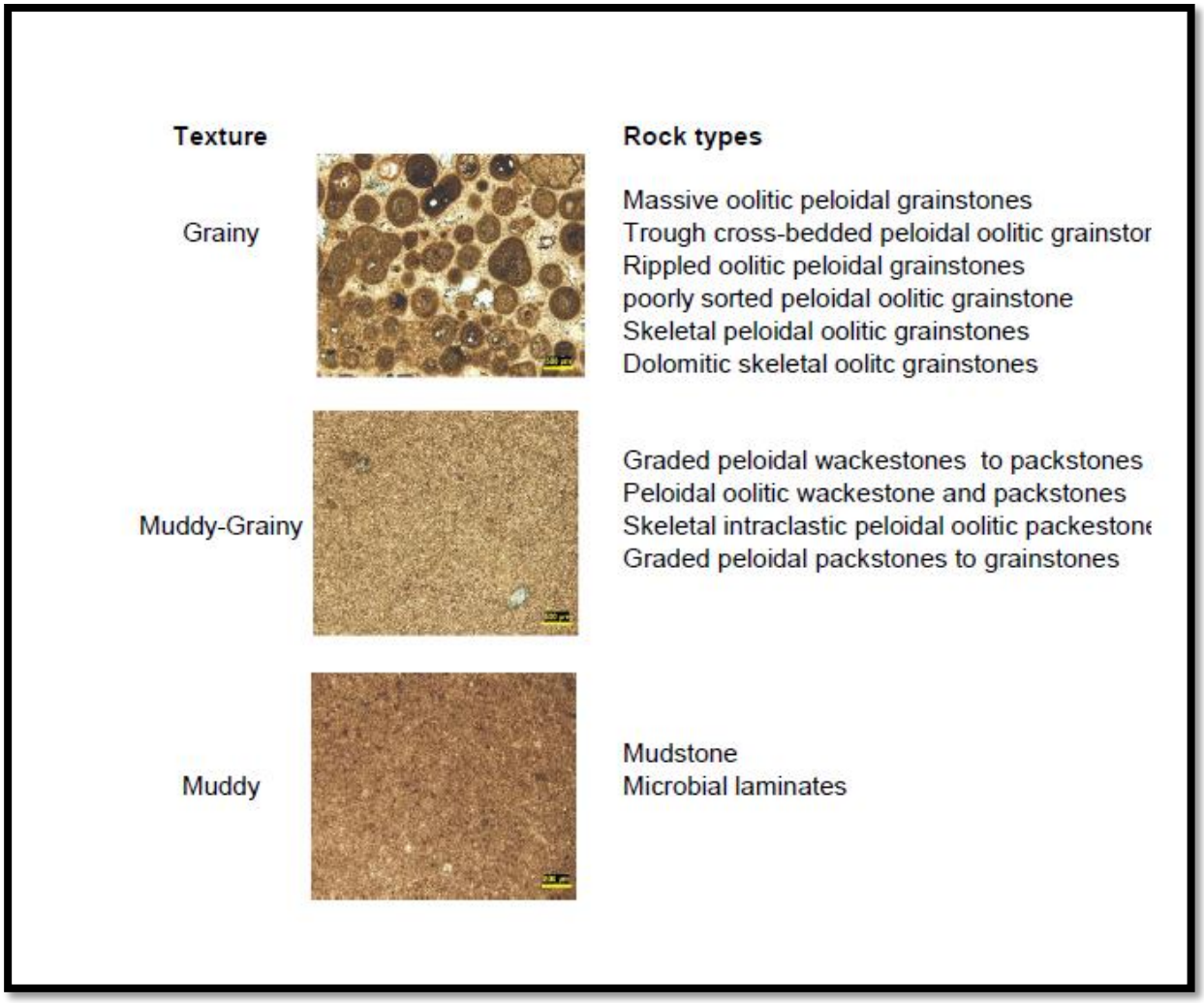


Figure 4.15: Shows rock typing based on the dominant texture and the list of the lithofacies within each rock type.

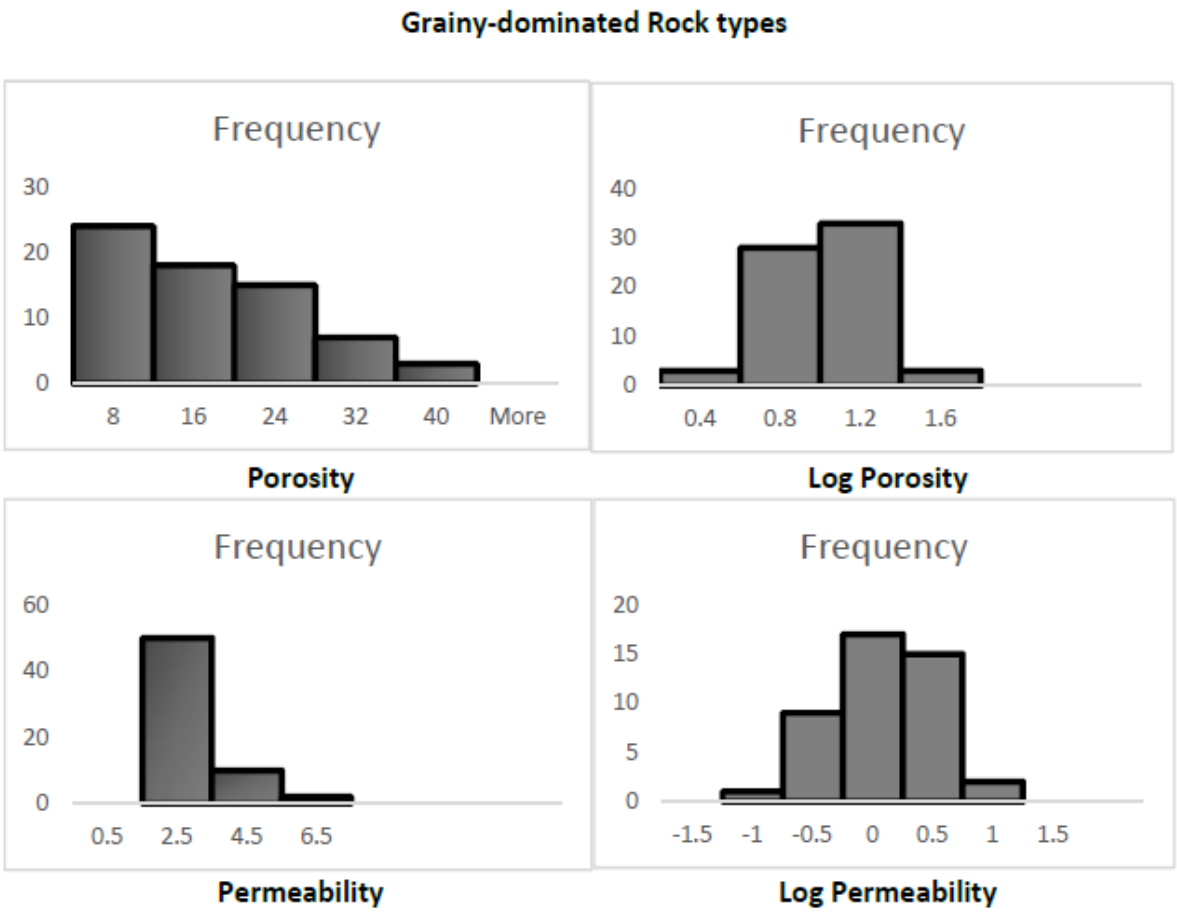


Figure 4.16: Histogram showing porosity permeability distributions for grainy-dominated rock types.

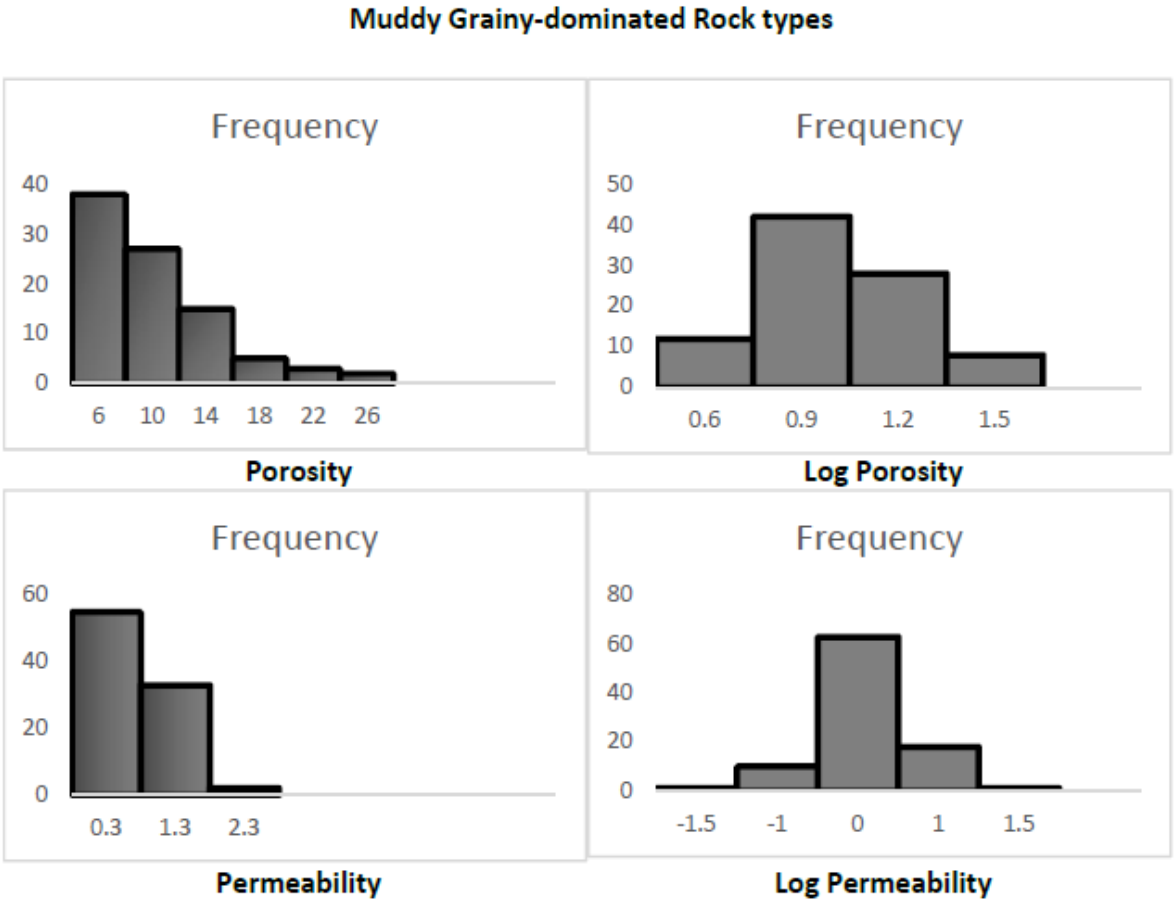


Figure 4.17: Histogram showing porosity permeability distributions for muddy-grainy-dominated rock types.

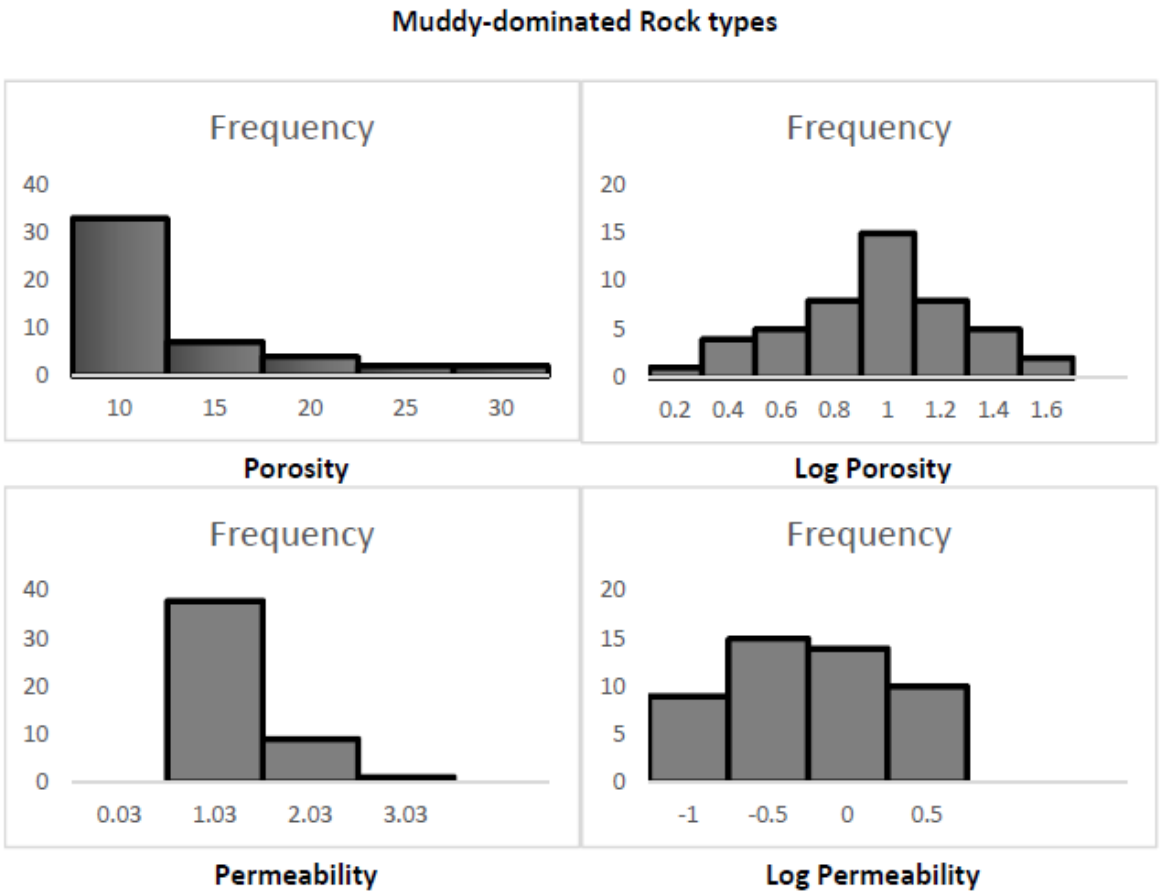


Figure 4.18: Histogram showing porosity permeability distributions for muddy-dominated rock types.

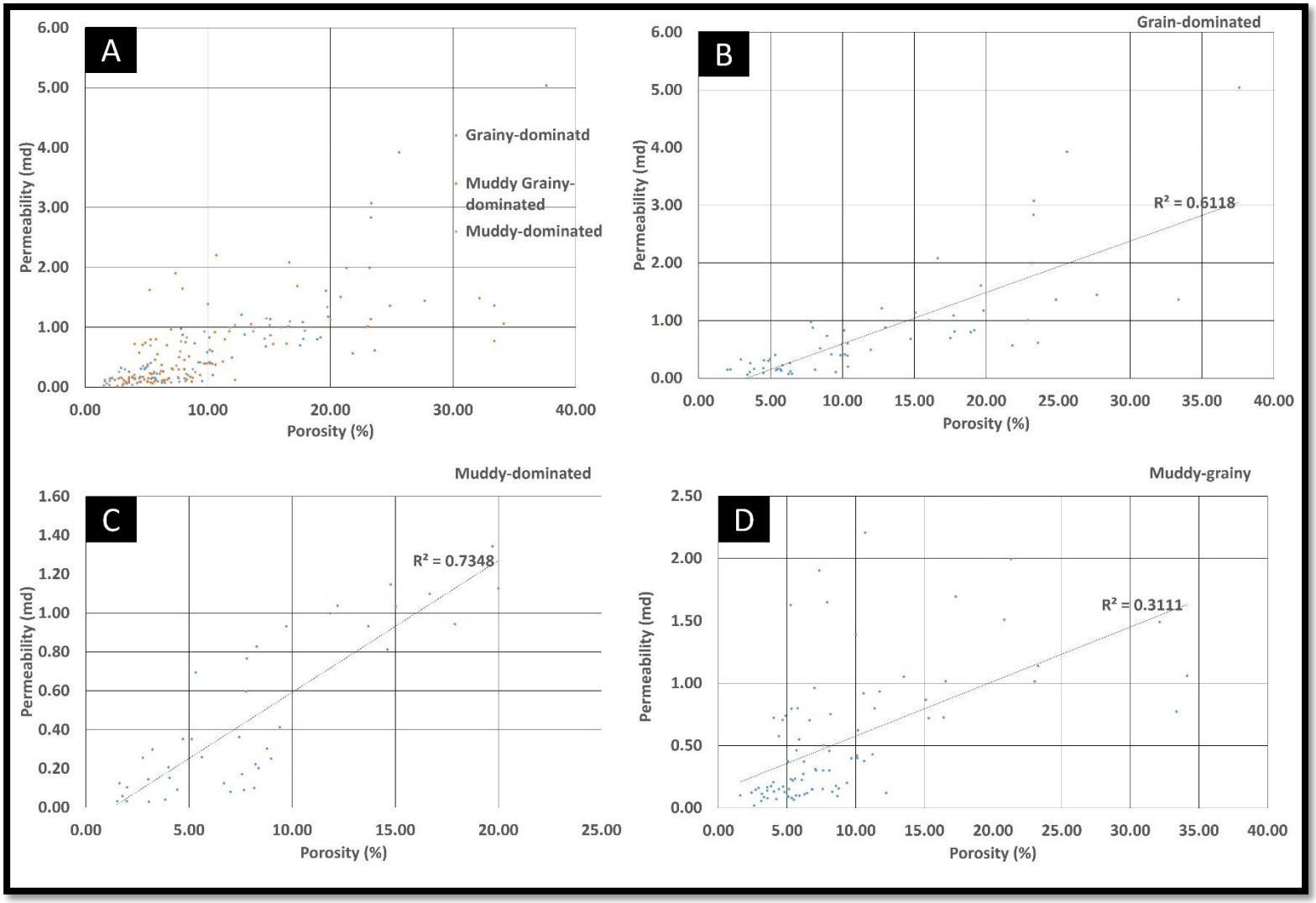


Figure 4.19:(A) Porosity-permeability correlation for the three rock types, (B) porosity-permeability correlation for grainy-dominated rock types, (C) porosity-permeability correlation for muddy-grainy-dominated rock types, (D) porosity-permeability correlation for muddy-dominated rock types.

## 4.6 Data Analysis

The variogram algorithm measures the geological variables (e.g. facies, porosity, permeability, .. etc.) behavior in specific trend. However, these variables often behave in different manners for the various directions. Thus, the facies distributions always show larger spatial correlation in the horizontal direction rather than its distribution in the vertical direction. Therefore, carbonate bodies dimensions and morphologies can be captured by using variogram analysis (Amour et al., 2012). Despite the importance of investigating directional continuity of geologic variables, the weak relationship between variogram and geology may cause problem in the understanding of the variable under study. Hence, the misunderstanding of this relationship leads to inappropriate modelling and consequently wrong estimation in the later analyses (Sahin et al., 1998).

### 4.6.1 Variogram construction and modelling

To obtain the spatial continuity/heterogeniety of the facies associations within the Upper Khartam Member, the indicator variograms were computed after defining parameters of lag distanc, angle, trend, etc. Horizontal Lag distances were chosen based on the average distances between sample points in the horizontal direction for both minor major variograms. On the other hand, in the vertical direction, experimental variograms were computed for each facies log individualy. To compute the experimental variograms, the lag distances were properly defined for each direction.A 100m was chosen for the horizontal directions as the smallest distance between sections. On the other hand, a lag distances ranging from 0.3 to 0.8m were chosen for the vertical sections to ensure capturing minimal beds thickness vertically.The experimental variograms were fitted to mathematical equations for further modelling processes and the spherical model was the best to represent the data points. Variogram modelling was made to recognize the nugget effect exsistence on the facies, the sill and the range of data set continuity.

### 4.6.2 Variograms analysis

Semivariograms provide information about spatial correlation and is used to guide the stochastic modeling. Several semivariograms were calculated using the upscaled lithofacies from the measured stratigraphic sections (the pseudo-wells). Horizontally, the semivariogram parameters (nugget, sill, and range) were calculated in the major and the minor directions. Due to the small horizontal area of the model, it is difficult to have accurate spatial correlation relationship and therefore uncertainty in the constructed semivariogram. Semivariogram uncertainty may introduce uncertainty in 3D facies model and consequently in petrophysical model (Kupfersberger and Deutsch, 1999). Previous studies on the Khuff indicate "layercake" layers which extend for tens to hundreds of kilometer and correspond to epeiric ramp settings interpretation of lithofacies belts. In such settings, semivariograms parameters are expected to have wide ranges; however, the calculated semivariograms parameters in the study area show narrow ranges. The most of beds thickness range from 10 to 30 cm which resulted in narrow variogram ranges. Most of these beds are interpreted as storm-dominated sediments and their lateral and vertical extend are very limited. This could have an effect on the calculated semivariogram and most likely the reason of having short ranges. Figures from 4.20 to 4.30 show the major, minor and vertical variograms for the grainy-dominated lithofacies and facies associations. Table 4 shows the parameters of the constructed variogram models for the facies sub environments of the Upper Khartam Member. The major range for the lithofacies was found to be oriented approximately north–south, and varies between 500 and 1000 m for all of the identified lithofacies. The minor range of the semivariogram varies between 300 and 700 m and is oriented approximately east to west. The vertical semivariograms were

computed using lithofacies of the same stratigraphic section. The spherical model was fitted to the computed experimental semivariograms. The software algorithm has the ability to assign an individual semivariograms for each facies; however, one common variogram was used for all of the facies to avoid complexity of using different variogram types. This common variogram has a 700-m major range (N–S), a
500-m minor range (E–W), and a 1-m vertical range.

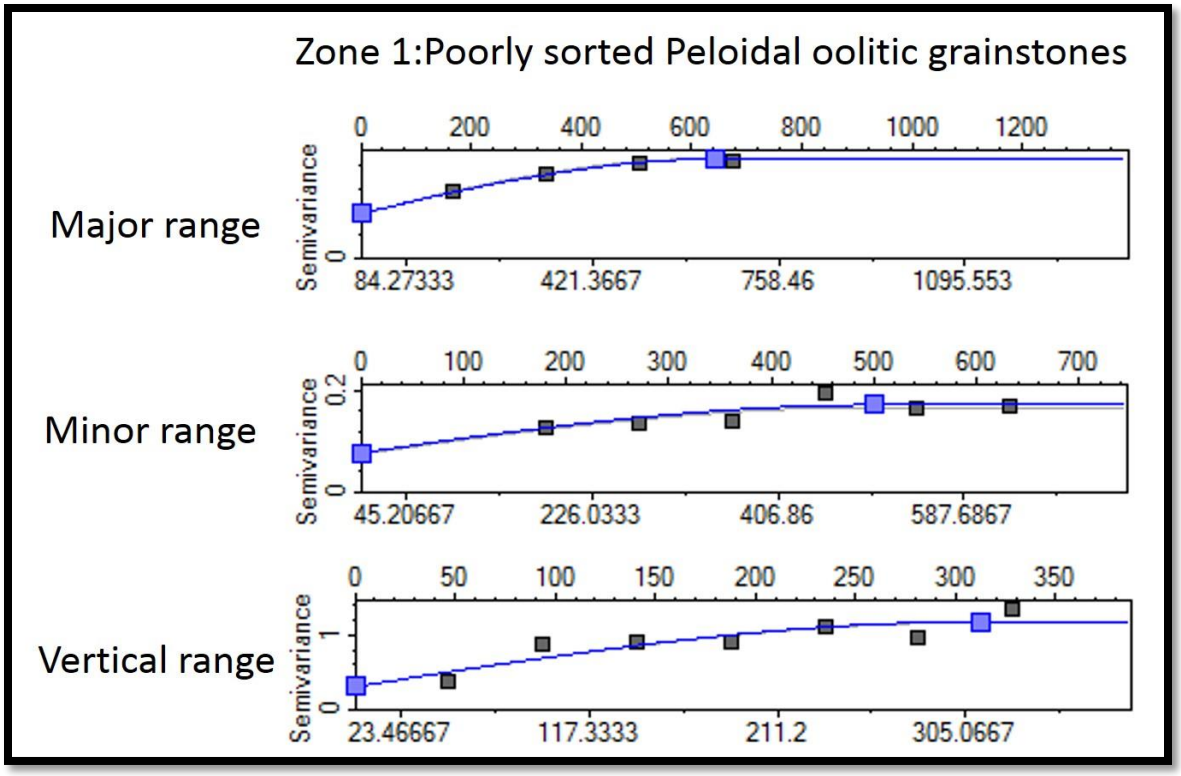


Figure 4.20: Variogram models for zone 1 lithofacies.

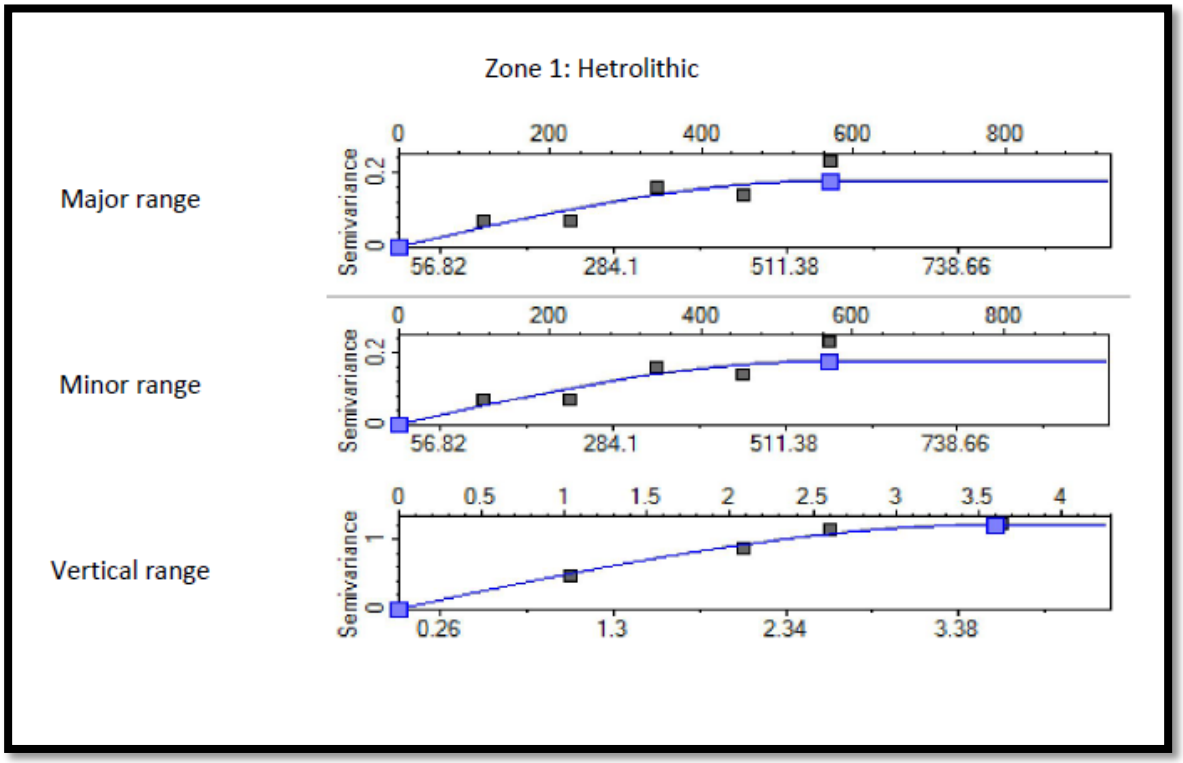


Figure 4.21: Variogram models for zone 1 lithofacies (hetrolithic).

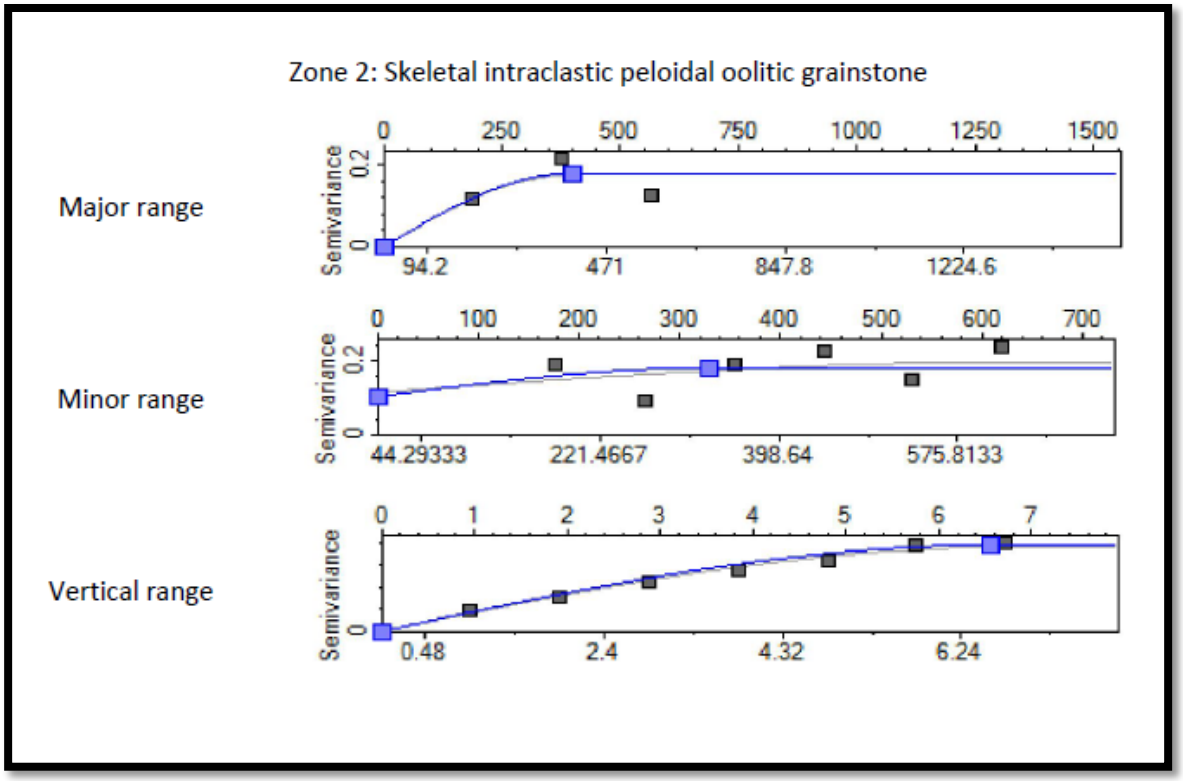


Figure 4.22: Variogram models for zone 1 lithofacies.

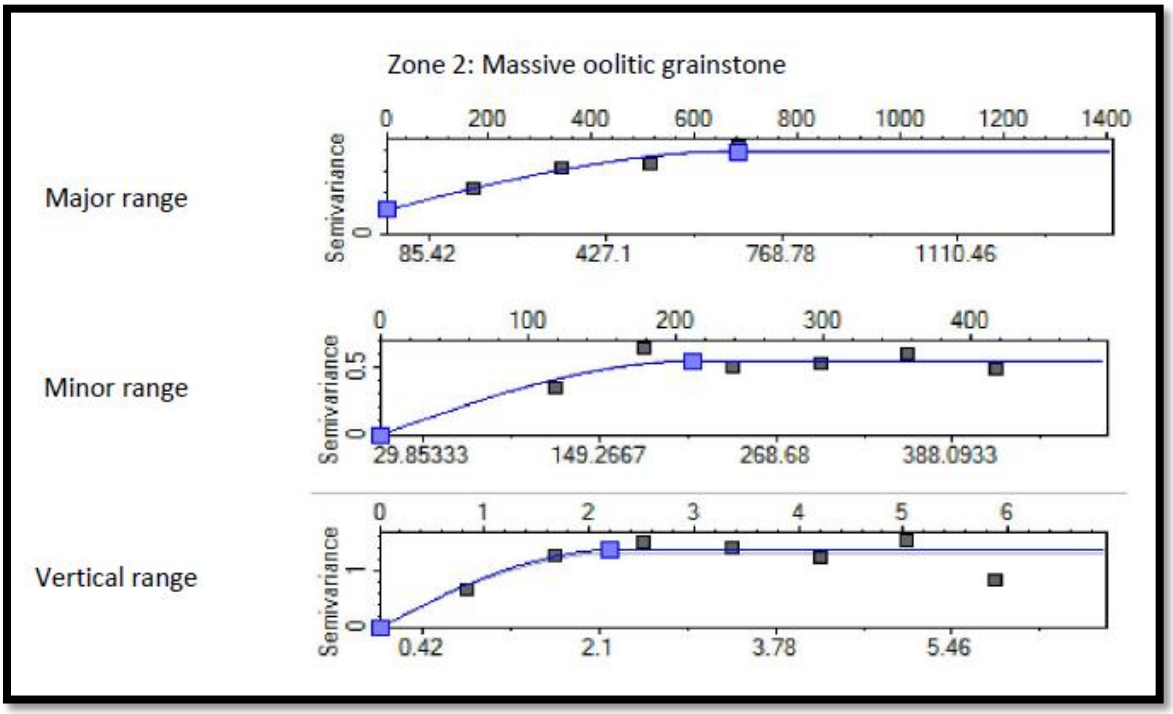


Figure 4.23: Variogram models for zone 1 lithofacies.

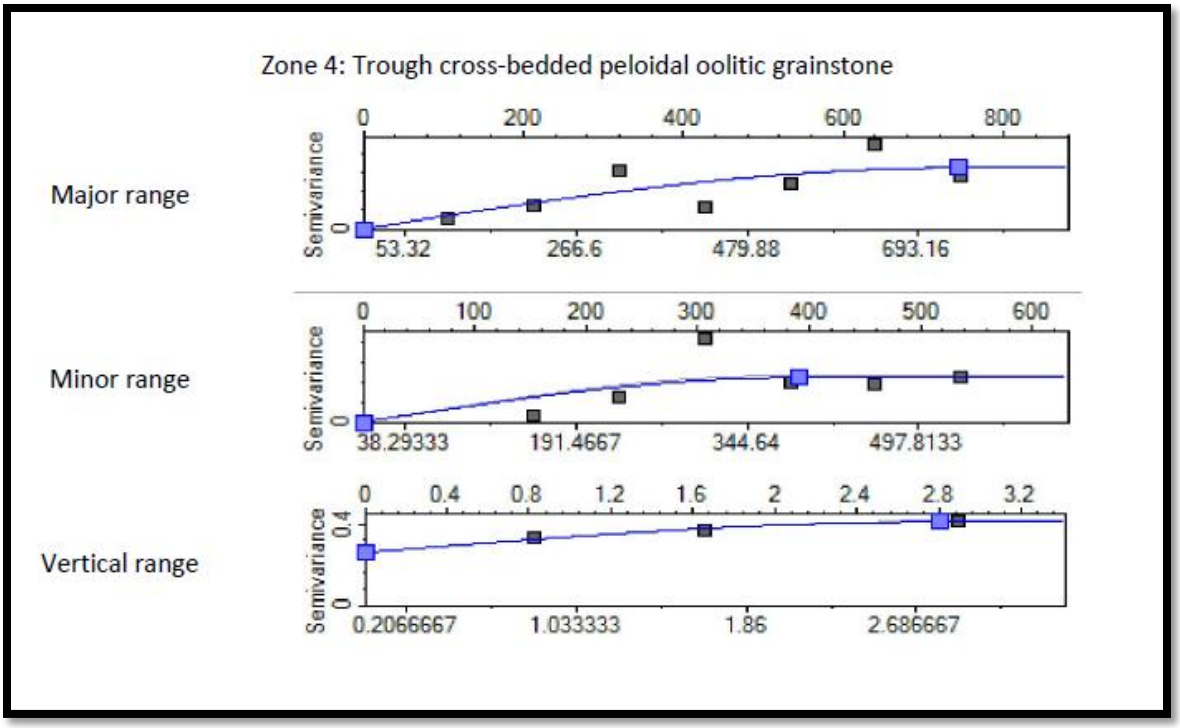


Figure 4.24: Variogram models for zone 1 lithofacies.

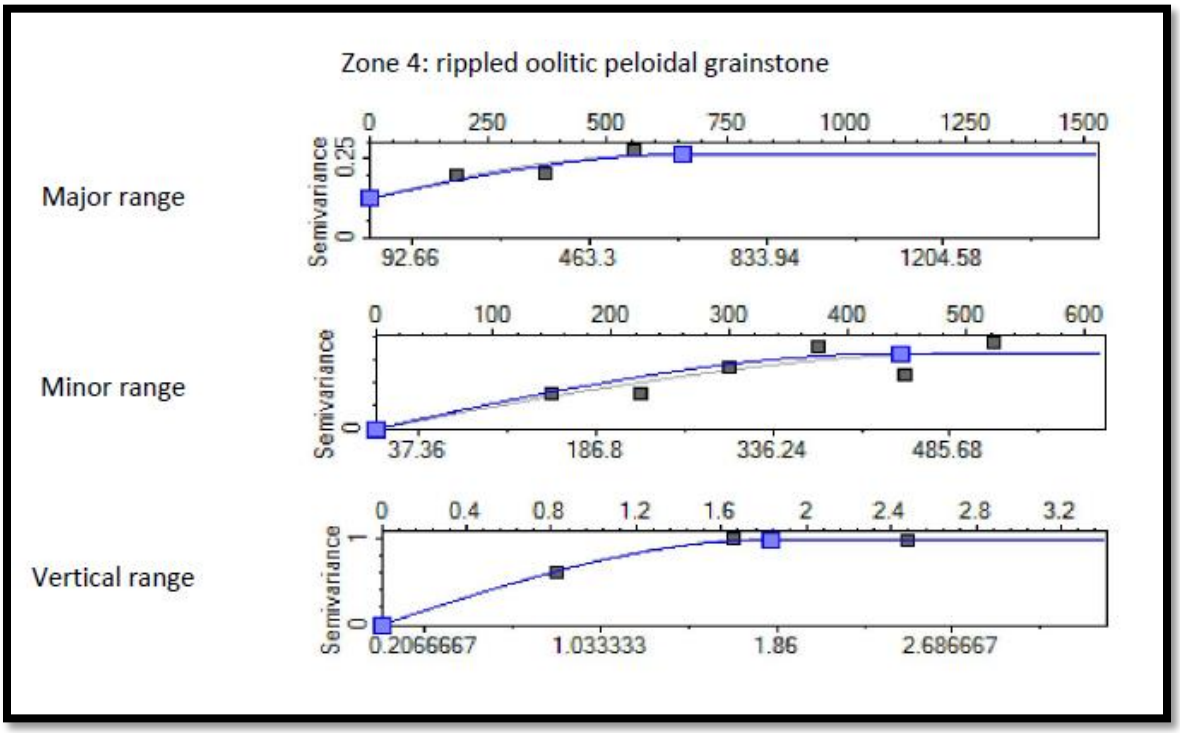


Figure 4.25: Variogram models for zone 1 lithofacies.

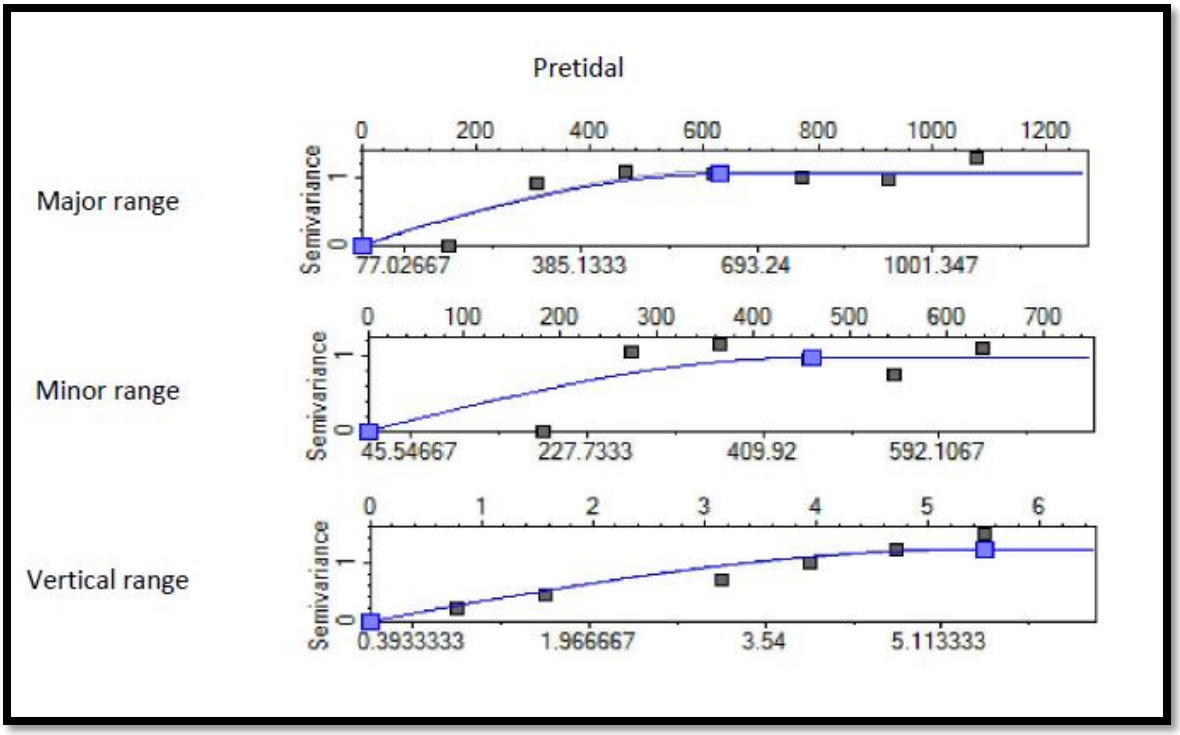


Figure 4.26: Variogram models for Pretidal lithofacies.

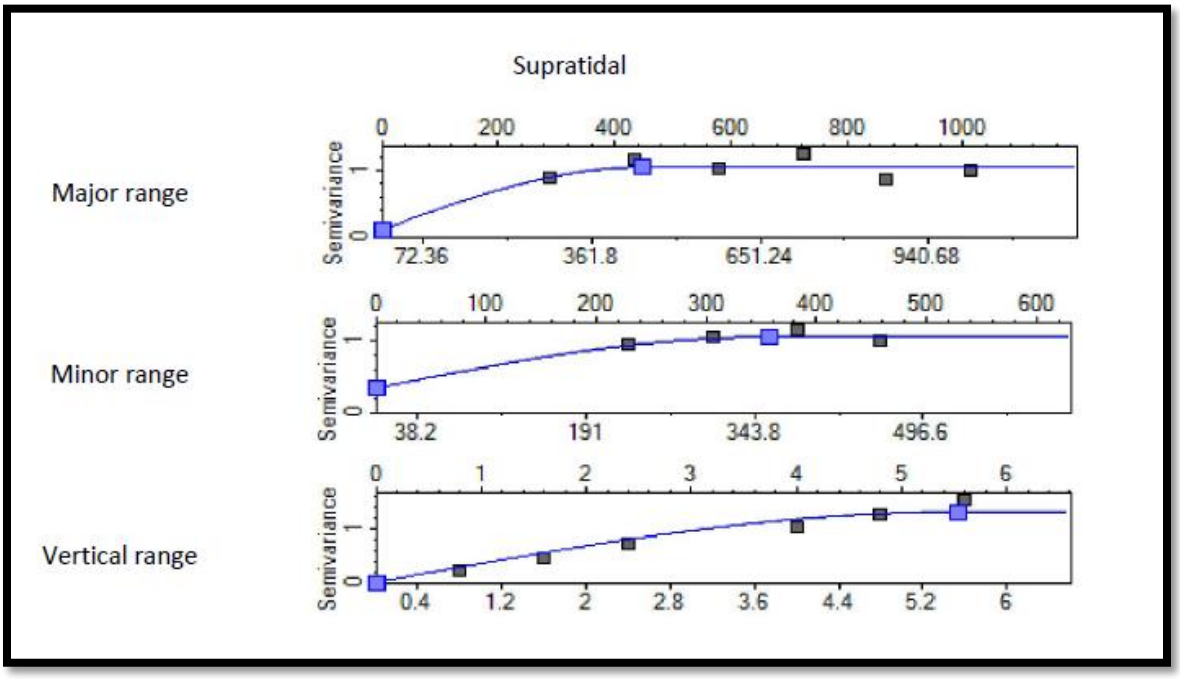


Figure 4.27: Variogram models for Supratidal lithofacies.

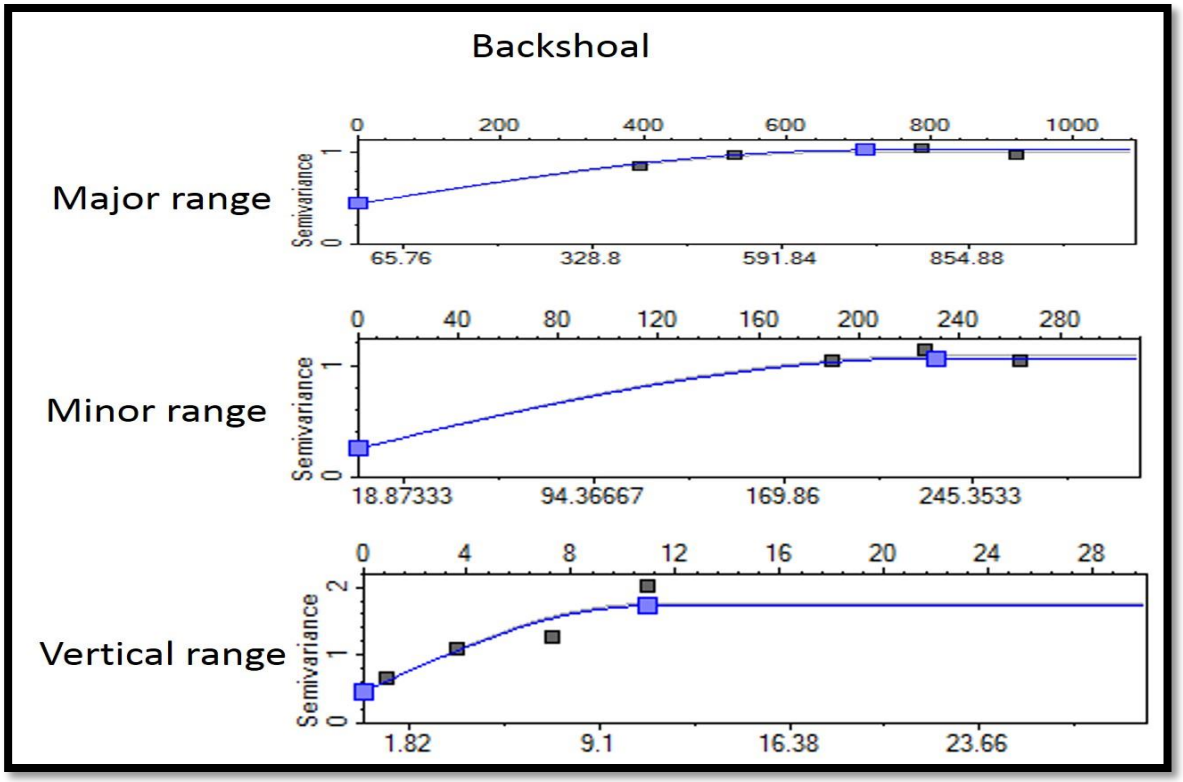


Figure 4.28: Variogram models for Backshoal lithofacies.

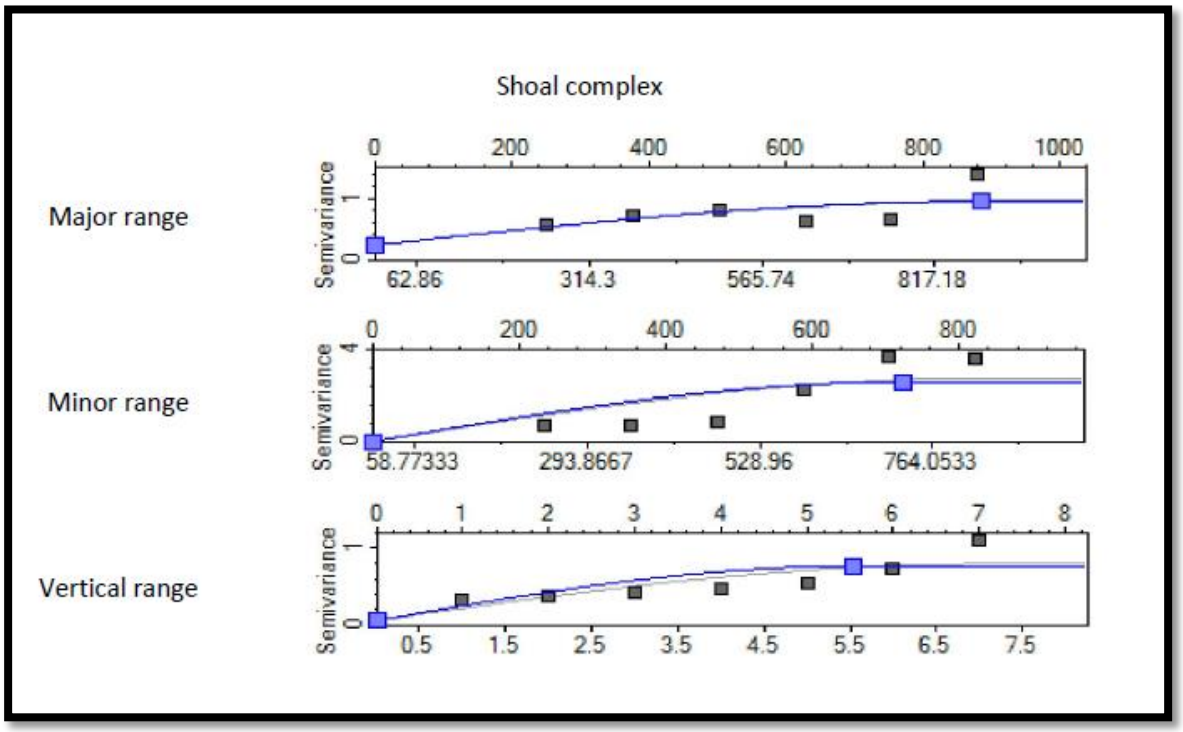


Figure 4.29: Variogram models for Shoal complex lithofacies.

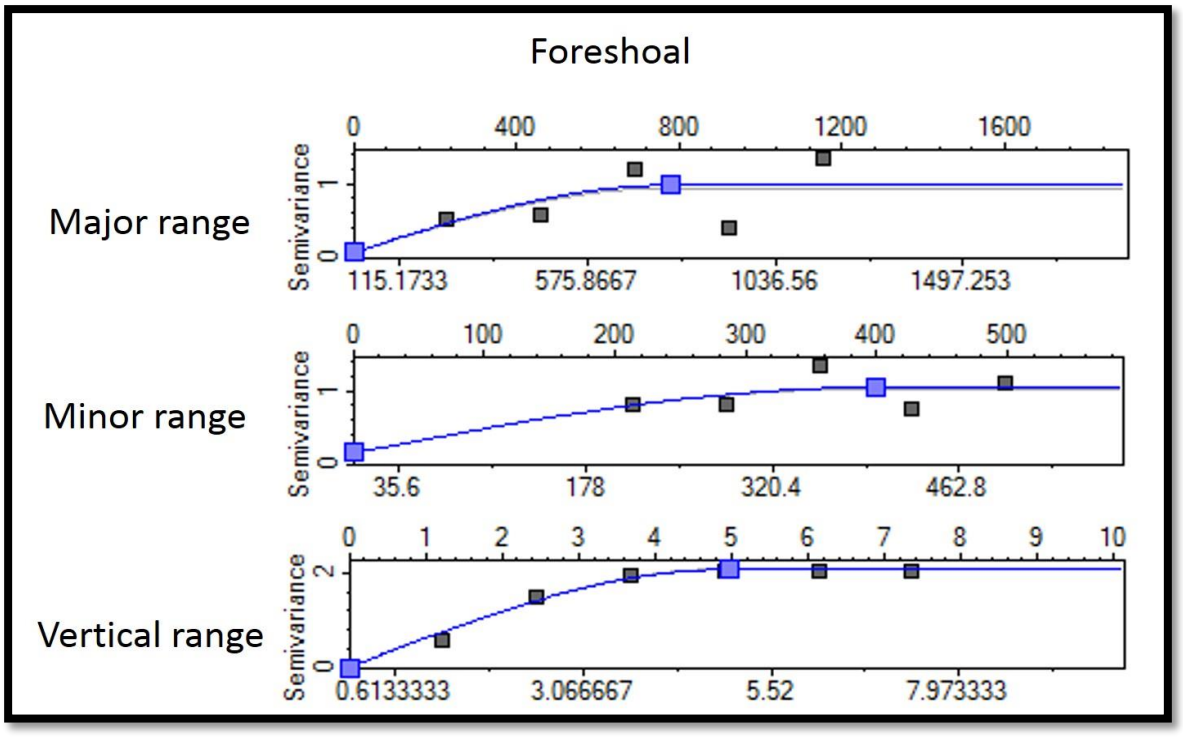


Figure 4.30: Variogram models for foreshoal lithofacies.

Table 4: Shows variogram models parameters for the encountered facies types of the studied interval.

| Facies | Major Range | Minor Range | Vertical Range | Sill | Nugget | Model type |
|---|---|---|---|---|---|---|
| Foreshoal | 613 | 155 | 4.7 | 1.0, 0.5, 2.1 | 0.062 | Spherical |
| Shoal | 886.1 | 700 | 5.5 | 1.2, 3.3, 1.00 | 0.228 | Spherical |
| Backshoal | 560 | 500 | 2.4 | 1.2, 1.1, 1.4 | 0 | Spherical |
| Supra tidal | 500 | 356.5 | 5.6 | 1.2, 1.2, 1.043 | 0.341 | Spherical |
| Pretidal | 626.5 | 467.1 | 5.5 | 1.2, 0.9, 1.0 | 0 | Spherical |
| Tidal Flat | 500 | 300 | 3.6 | 1.192 | 0 | Spherical |

## 4.7 Geostatistical Modelling

### 4.7.1 3D Model Construction

A total of 23 measured sections were used to construct the 3D facies model (yellow pins in Figure 4.31). We measured 11 stratigraphic sections along the road-cut in the study area. These 11 measured sections have facies interpretation performed by physically logging, outcrop and petrographic description. The 11 measured sections were correlated in a 2D stratigraphic panels using photomosaic of road cut controlled by field correlation and walking out lithofacies units. Total of 12 sections were obtained using the road-cut photomosaic and hand-drawn sections (red circles in Figure 4.32). We determined the geographical position of the measured sections using Global Positioning System (GPS), then the 23 measured sections were converted to pseudo-wells to guide the stochastic algorism for outcrop facies model. This step is essential for spatial correlation of all of the geological data from one section to a particular geographical location. The measured stratigraphic sections were converted to pseudo wells with facies logs to provide the primary input data for the 3D facies model. As these sections were measured in a road-cut, trigonometric correction to the well paths was not required.

### 4.7.2 2D Correlation

The facies associations were correlated along 23 outcrop sections using the stratigraphic framework of the studied interval. Physical tracing of the surfaces in the outcrop, hand drawing on the outcrop photomosaic and geochemical log signatures of lithofacies and sequence boundaries, were used for spatial correlation of the stratigraphic surfaces (Eltom et al., 2016). Major sequence boundaries separate the five fourth-order cycle sets. These sequence boundaries are distinctive bedding planes filled with very fine calcareous mud

and clay, and is a prominent morphological feature and can be correlated for several kilometers along the outcrop and photomosaic. Six major surfaces were constructed using the fourth-order sequence boundaries: these surfaces define five zones in the geomodel (Figure 4.33). These zones were identified as corresponding to depositional environments as follows: Zones 1 and 2 are foreshoal and shoal deposits; Zones 3 and 4 consist of shoal and backshoal deposits; and Zone 5 contains subtidal, intertidal and supratidal flat facies.

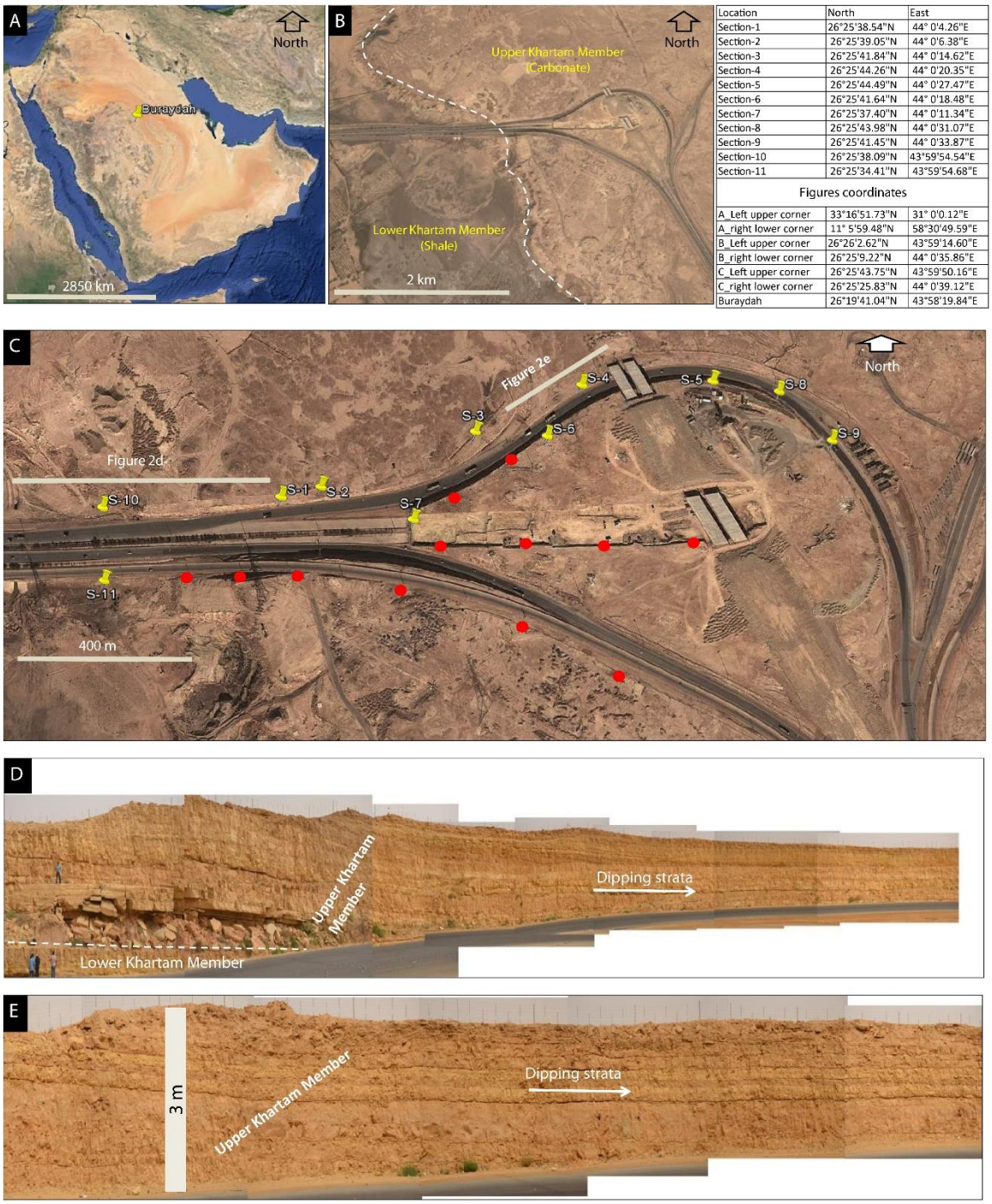


| Location | North | East |
|---|---|---|
| Section-1 | 26°25'38.54"N | 44° 0'4.26"E |
| Section-2 | 26°25'39.05"N | 44° 0'6.38"E |
| Section-3 | 26°25'41.84"N | 44° 0'14.62"E |
| Section-4 | 26°25'44.26"N | 44° 0'20.35"E |
| Section-5 | 26°25'44.49"N | 44° 0'27.47"E |
| Section-6 | 26°25'41.64"N | 44° 0'18.48"E |
| Section-7 | 26°25'37.40"N | 44° 0'11.34"E |
| Section-8 | 26°25'43.98"N | 44° 0'31.07"E |
| Section-9 | 26°25'41.45"N | 44° 0'33.87"E |
| Section-10 | 26°25'38.09"N | 43°59'54.54"E |
| Section-11 | 26°25'34.41"N | 43°59'54.68"E |
| Figures coordinates | | |
| A_Left upper corner | 33°16'51.73"N | 31° 0'0.12"E |
| A_right lower corner | 11° 5'59.48"N | 58°30'49.59"E |
| B_Left upper corner | 26°26'2.62"N | 43°59'14.60"E |
| B_right lower corner | 26°25'9.22"N | 44° 0'35.86"E |
| C_Left upper corner | 26°25'43.75"N | 43°59'50.16"E |
| C_right lower corner | 26°25'25.83"N | 44° 0'39.12"E |
| Buraydah | 26°19'41.04"N | 43°58'19.84"E |

Figure 4.31: The area under study. a) Satellite image showing Buraydah city in central Saudi Arabia; b) map of the study area, showing the contact between the Upper and Lower Khartam Member; c) aerial photograph of the study area, showing the locations of 11 measured sections; and d) and e) photomosaic of the road cut outcrops of the Upper Khartam Member.

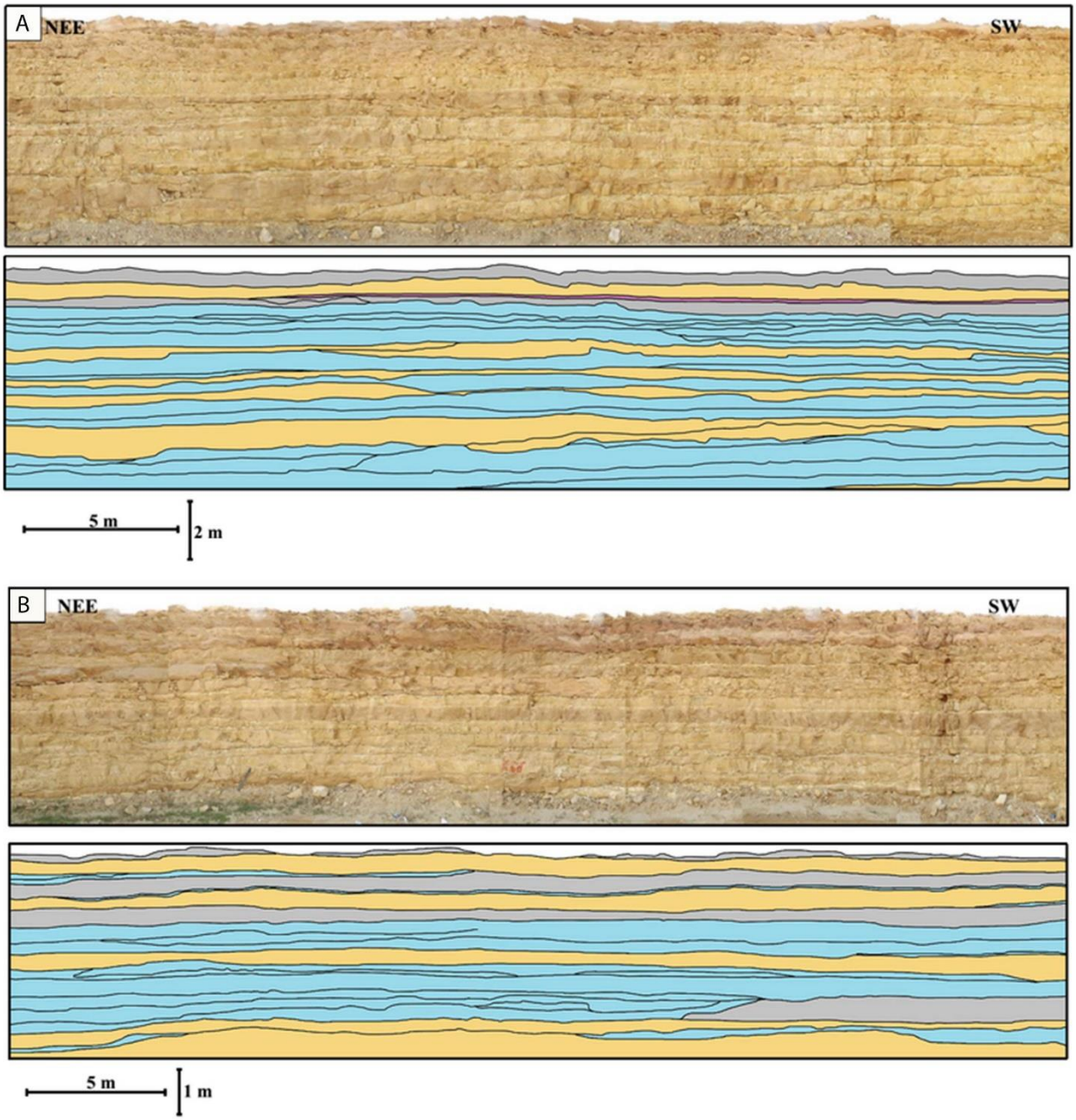


Figure 4.32: Photomosaic show road cut sections; at the bottom of each photomosaic a 2D panels illustrate beds within the road cut.

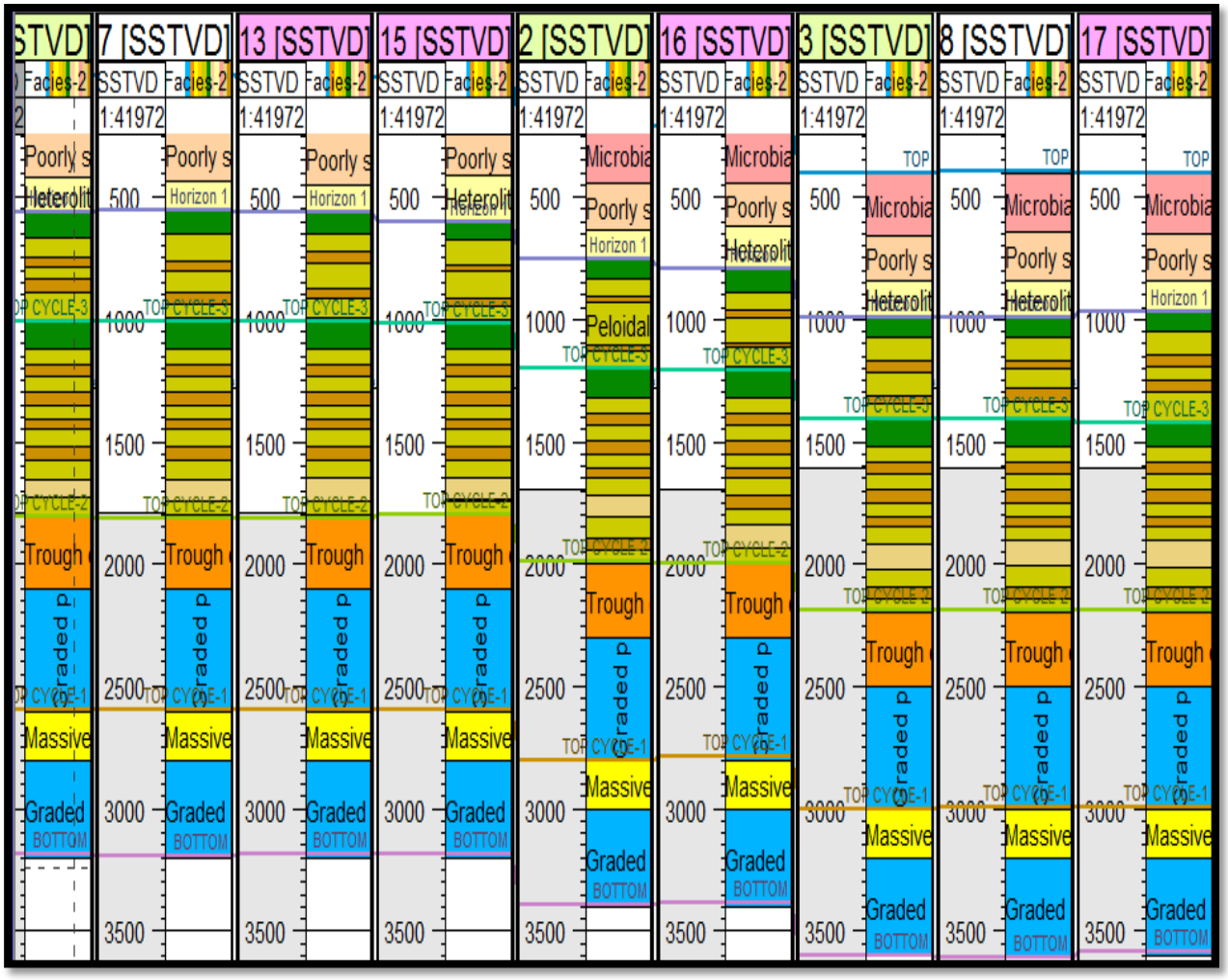


Figure 4.33: Shows the 2D correlation panel for the lithofacies of the Upper Khartam Member.

### 4.7.3 Grid construction and layering

A grid cell dimensions of 5*5m were selected to construct the geocellular outcrop model of the upper Khartam member with 5 zones. However, each zone represents cycles of transgressive and regressive sequences. The horizontal boundaries of the cells were directed to follow the base surface of each stratigraphic zone. The vertical dimensions of the grid cells were constructed and the vertically facies changes were considered. Thus layering was properly chosen to honor the small variations within the facies logs, therefore 20 conformable layers were made for each zone (total 100 layers). The resulting 3D grid was made for the 3D exposure of the outcrop (see Figure 4.31) which composed of 1,555,500 cells (Figure 4.34).

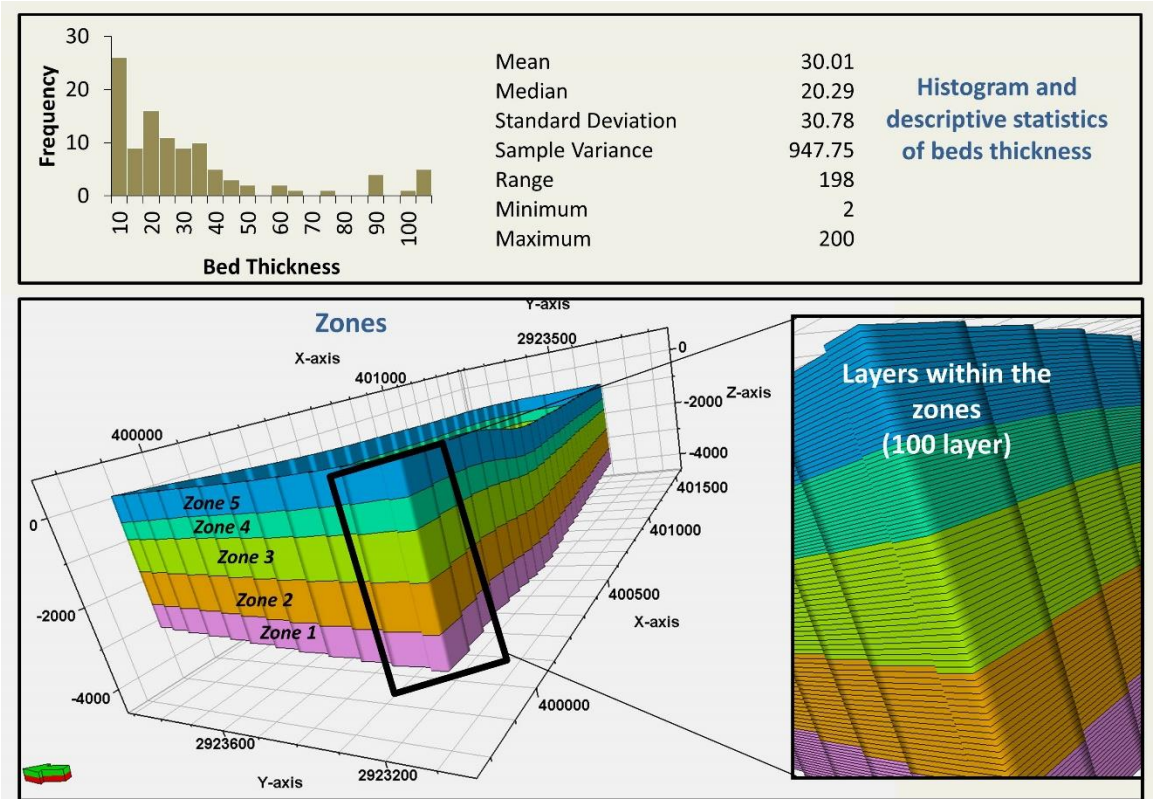


Figure 4.34: Visualizes the constructed zones and the layering

### 4.7.4 Facies Modelling

To develop a realistic distribution of facies in the outcrop geostatistical model, the 3D grid was populated with the lithofacies logs from the measured sections. The population of the lithofacies was performed separately within each zone using three different geostatistical algorithms (indicator Kriging, IK; sequential indicator simulation, SIS; and truncated indicator simulation, TGS) and was guided by the common semivariogram parameters that were computed in the previous step. This allows comparison of the resulting outcrop model from each algorithm with the outcrop facies percentage and the stacking patterns. The degrees of similarity between the resulting realizations of the models were visually evaluated to select which of the algorithms had best reproduced a realistic facies percentage and stacking patterns. Figure 4.35 shows the three models constructed using different algorithms, and figure 4.36 shows the lithofacies percentages of the output 3D models compared with the lithofacies percentages from the stratigraphic sections.

None of the three (IK, TGS, and SIS) models perfectly reproduced the outcrop stratigraphic architecture. All of the models introduced unreasonable geological features that are not in true stratigraphic order in the conceptual model. However, the three models collectively yielded reasonable representations of the outcrop facies, stacking pattern, and stratigraphic architectures. Based on the visual comparison and the facies percentage between the input and output data, the IK model possessed the best representation of a vertical stacking pattern, but lacks vertical continuity. Although the SIS model captured the small-scale variability, it had difficulty in representing the lateral continuities and facies transitions of the beds. The TGS model exhibited reasonable lateral facies continuity, but vertically introduced facies that are not in the true stratigraphic order.

Accordingly, the final facies model was constructed using all the three algorithms together to take advantage of the best geological representation of certain facies by particular algorithms and fix the problems encountered when using others. There are always uncertainties and some degree of error associated with each of these algorithms when building facies in place; therefore, the best algorithm to be selected for the facies model is the one that produces the least erroneous result (Benson et al., 2014). Because of the lateral facies transition, the Truncated Gaussian Simulation (TGS) introduced the best result within zones one and two. Thus, the ordered lithofacies in zones one and two enabled the TGS to work better than the others (IK and SIS). Because of the good coverage of zone three, IK showed the best representation of stacking patterns in this zone. However, IK model has perfectly captured the rapid facies change between shoal and backshoal facies within zone three. Due to the small geologic variability within zones four (backshoal) and five (tidal flat), the Sequential Indicator Simulation introduced the best output rather than TGS and IK algorithms. These realizations are equally probable, and their average may represent a realistic modelfor the outcrop (Figure 4.37). In general, the resulting average model of the realizationsadequately reproduced the continuity of the beds and fairly represented the stackingpattern of the stratigraphic architecture of the outcrop. SIS proposed as one of theapproaches that can adequately reproduce the facies within 3D outcrop model.

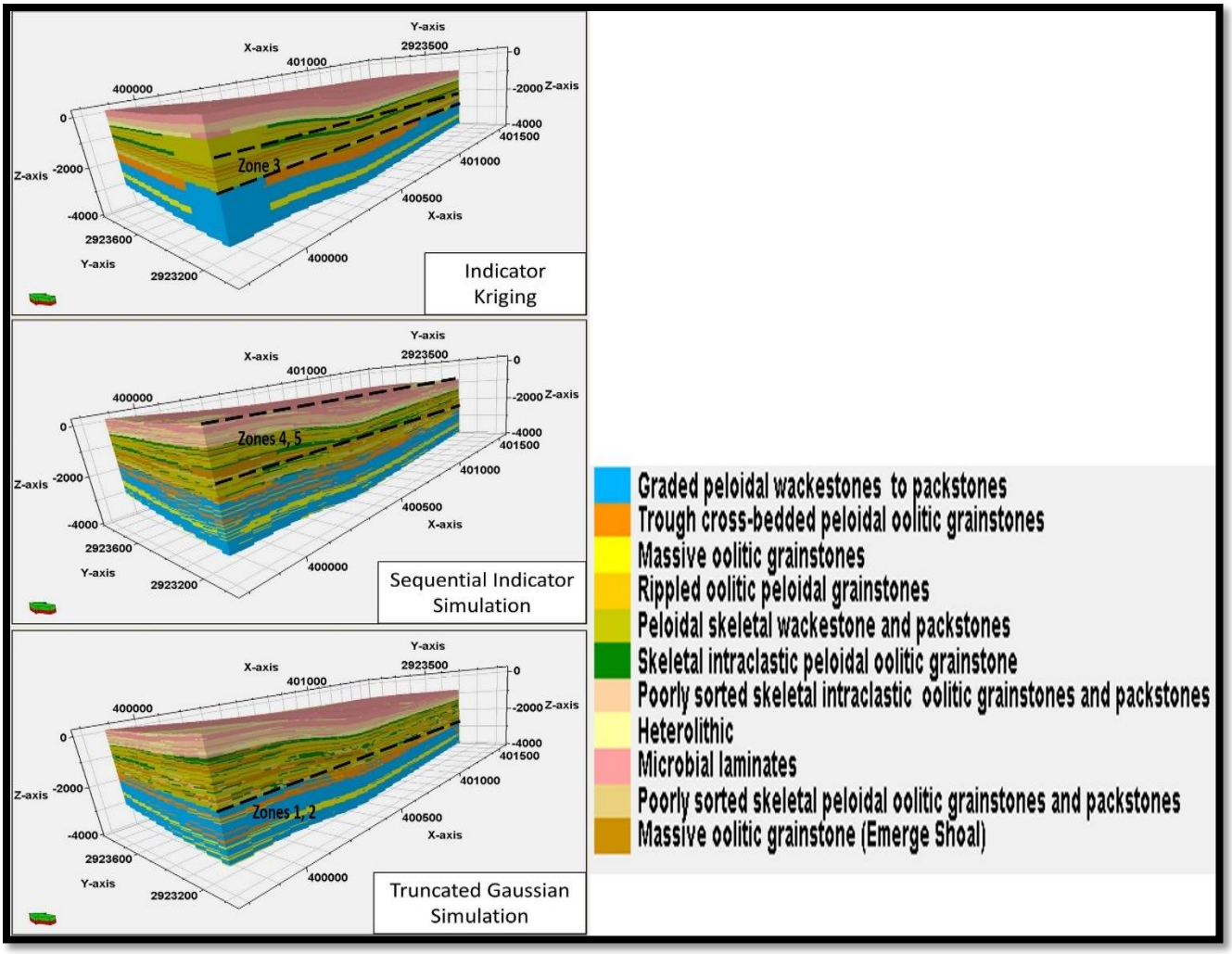


Figure 4.35: 3D outcrop models constructed by three different algorisms.

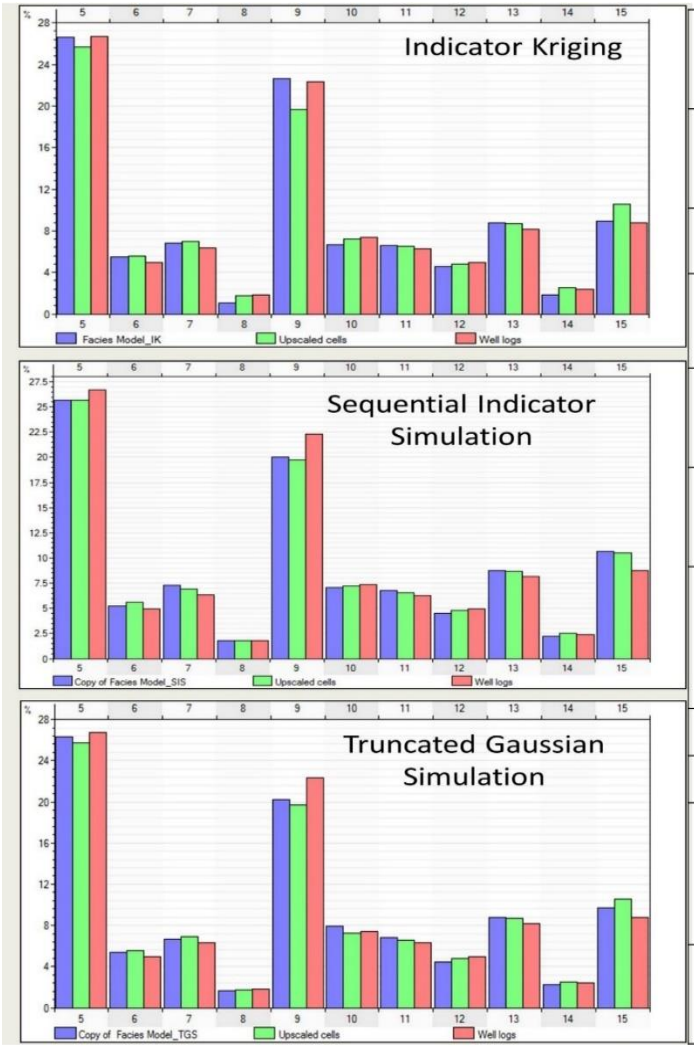


| | |
|---|---|
| 5 | Graded peloidal wackestones to packstones |
| 6 | Trough cross-bedded peloidal oolitic grainstones |
| 7 | Massive oolitic grainstones |
| 8 | Rippled oolitic peloidal grainstones |
| 9 | Peloidal skeletal wackestone and packstones |
| 10 | Skeletal intraclastic peloidal oolitic grainstone |
| 11 | Poorly sorted skeletal intraclastic oolitic grainstones and packstones |
| 12 | Heterolithic |
| 13 | Microbial laminates |
| 14 | Poorly sorted skeletal peloidal oolitic grainstones and packstones |
| 15 | Massive oolitic grainstone (Emerge Shoal) |

Figure 4.36: Facies proportions computed from the geo-model of the three different algorisms compared to the input data.

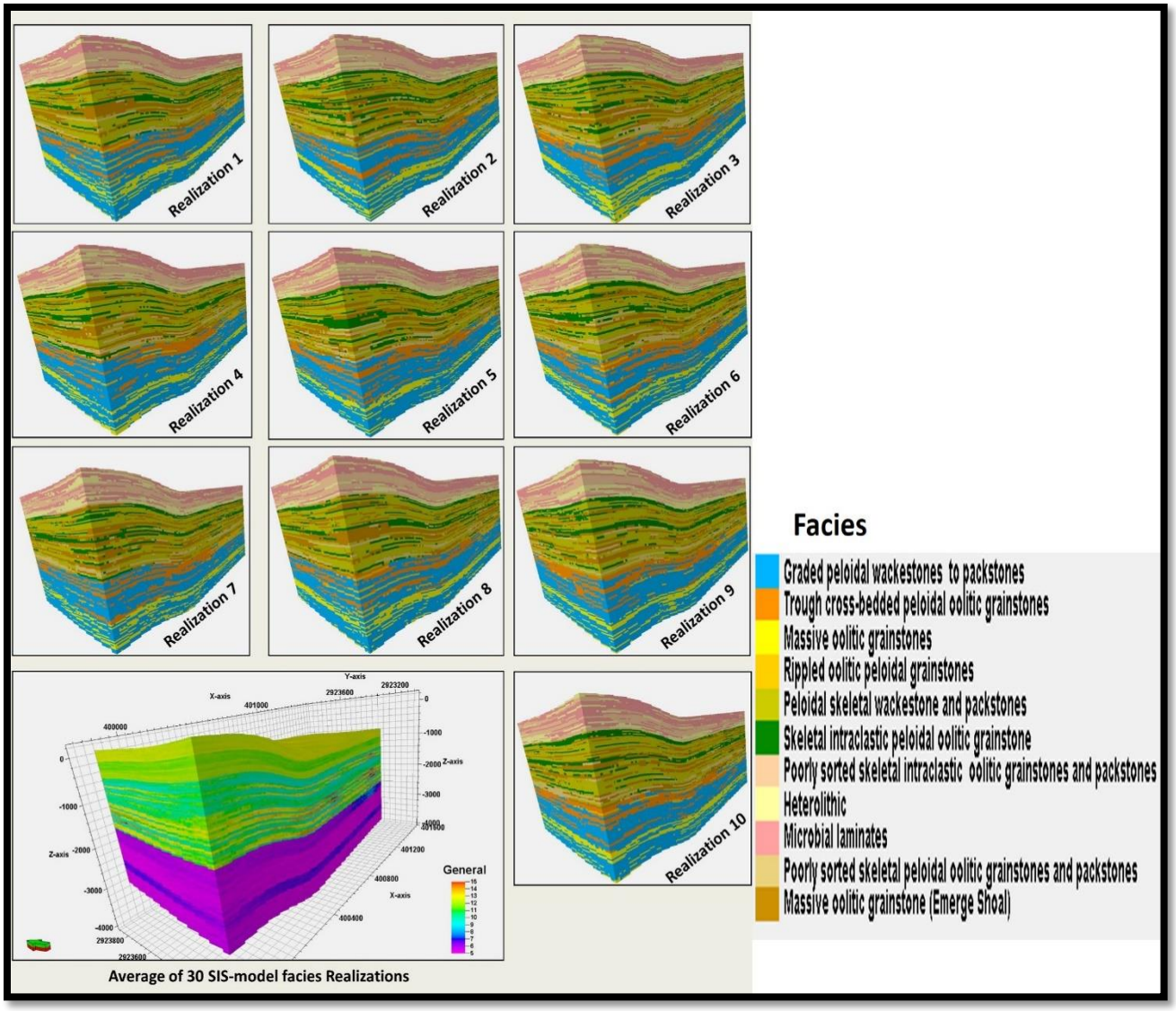


Figure 4.37: Equiprobable realizations of the geo-model constructed by SIS algorism.

### 4.7.5 Petrophysical Modeling

Oolitic grainstones reservoirs host most of the world's hydrocarbon accumulation. Therefore, the present study aims to enhance the characterization of oolite reservoirs of Khuff Formation and its equivalent ones of nearby gulf regions (Esrafili-Dizaji-Rahimpour-Bonab, 2014).

- **Outcrop and Subsurface Data**

Khuff Formation is one of the most known oomouldic grainstones reservoirs in the Middle East (Ehrenberg et al. 2007). Dalan and Kangan carbonates are the equivalent of the Khuff Formation of the Saudi Arabia (Sharland et al. (2001), Alsharhan (2006)). Meanwhile, Dalan-Kangan Formations are the major gas prone reservoirs. The subsurface equivalent of Khuff Formations was studied in South Par Field of Iran (Esrafili-Dizaji-Rahimpour-Bonab, 2014). The ooid shoal lithofacies shows different petrophysical properties (porosity and permeability values range from 0-35% and 0.01-1000 md, respectively). The lithofacies were grouped into two groups; the porous types (porous grainstones) and tight ones (tight grainstones) (Figure 0.38).

Porosity and permeability values were modelled following the same variogram parameters as in the previous facies model. Therefore, the spatial distribution of the petrophysical properties is controlled by the lithofacies. Values of each facies have been assigned in the facies model. The muddy-dominated facies showed the lowest values for both porosity and permeability. So it has been given values of 5% and 0.0001 md for both porosity and permeability respectively. These values were set as background for the other porosity and permeability values of the grainy-dominated interval (Figure 0.39).

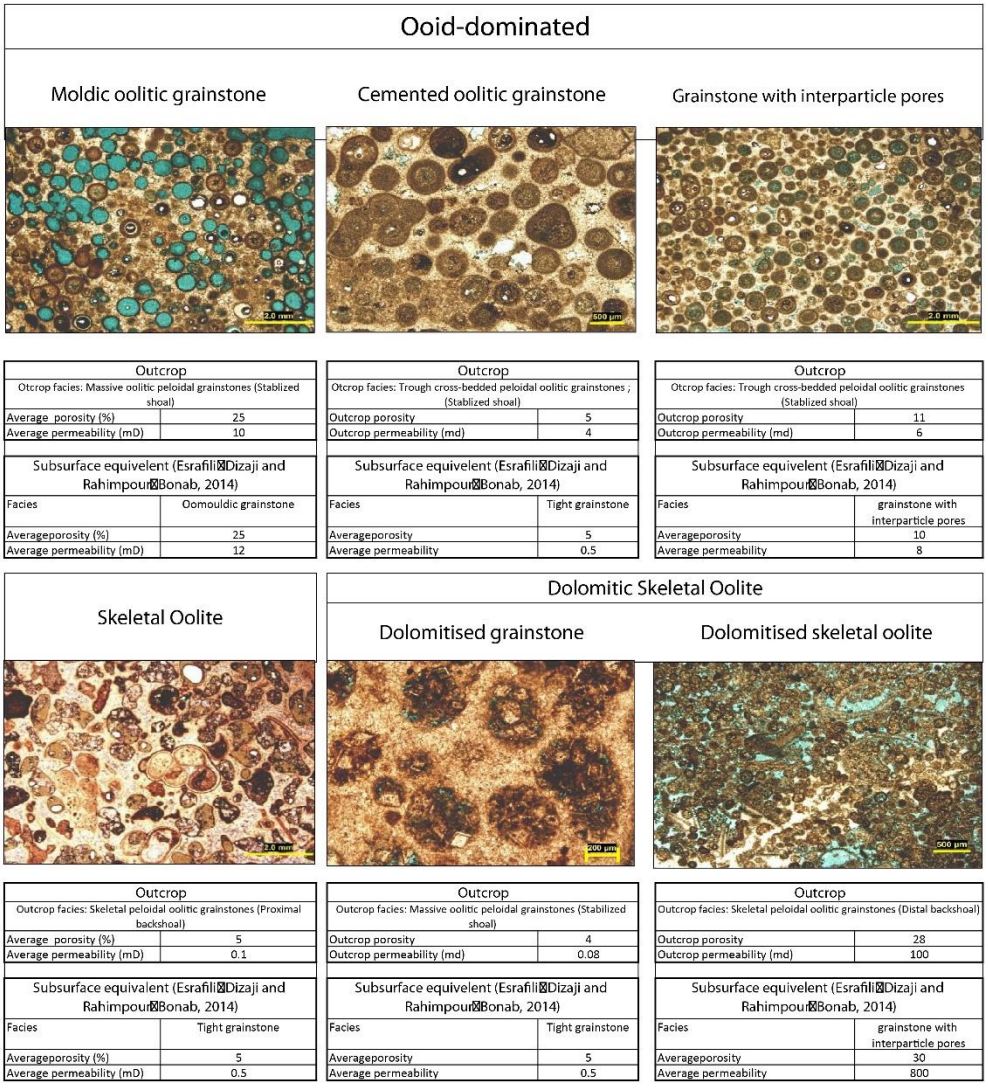


Figure 4.38: The groups of the grain-dominated lithofacies: ooitic-dominated, skeletal oolitic and dolomitic skeletal oolitic facies. Each facies in these groups has given porosity value from analogous reservoirs and average measured porosity value from samples collected from outcrop.

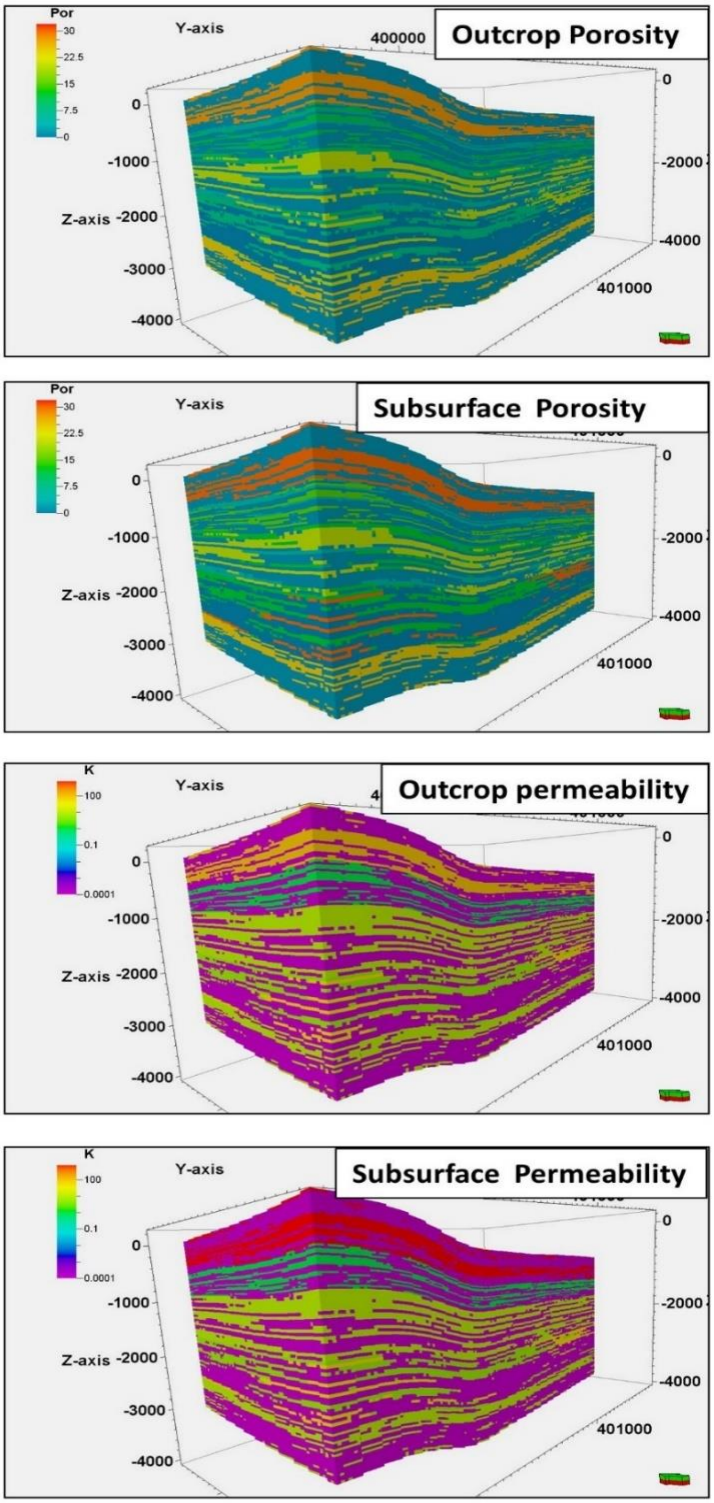


Figure 4.39:3D porosity and permeability models constructed using subsurface (South Par Field of Iran) data and outcrop measured porosity and permeability data from collected samples from the outcrop.

### 4.7.6 Multiple Scenarios of Porosity Evolution

The 3D volume of the reservoir units can be subdivided into three broad stratigraphic intervals containing different reservoir units (Figure 0.58):

- The lower interval (Zones 1 and 2), which mainly consists of ooid-dominated units, was deposited within a rapid sea-level rise at the Permian–Triassic boundary.
- The middle interval (Zones 3 and 4), which was deposited within a rapid sea-level fluctuation, was characterized by marine faunal recovery and is dominated by skeletal oolitic reservoir units.
- The upper zone was mainly deposited during a major sea-level drop and consists mostly of dolomitic skeletal oolite.

Each of these intervals experienced a unique diagenetic history and has a distinct porosity distribution. For simplicity, we developed scenarios of porosity evolution for each zone separately on the basis of the diagenetic paragenesis.

- **Lower Interval**

On the basis of their original mineralogy, ooids were classified into two types in this interval: aragonitic and bimineralic. Each type of ooid has been altered through several diagenetic stages to produce distinct porosity values and types. The first stage of development of aragonitic ooids was direct precipitation of the oolitic grains with significant amounts of interparticle porosity. This was followed by precipitation of micrite envelopes, partial dissolution, marine cementation, partial/total dissolution of

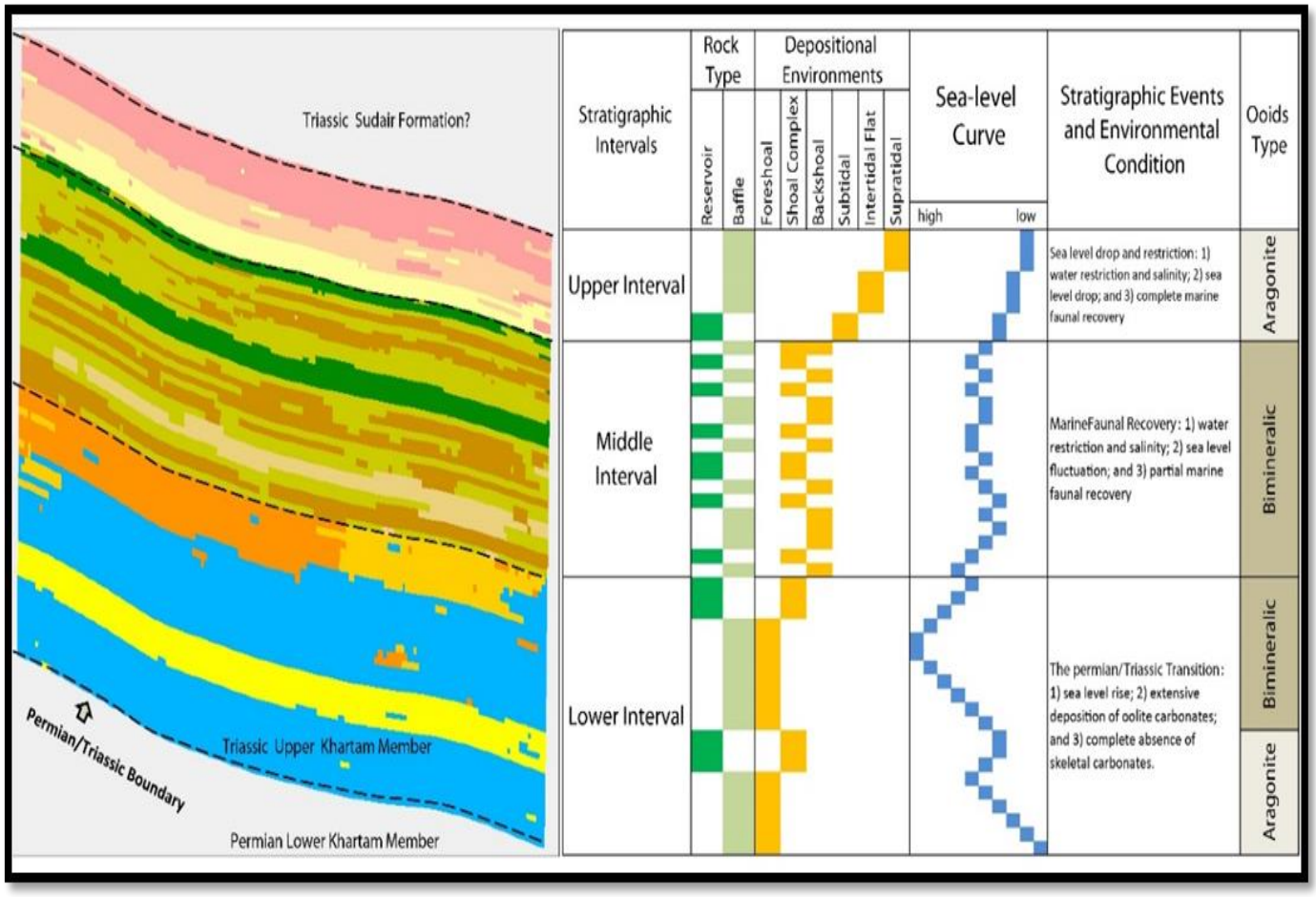


Figure 4.40: 2D slice of the 3D model show the stacking pattern of the outcrop sequences (left). Stratigraphic log based on outcrop observations show reservoir and baffle units, relative sea level curve and porosity values based on the six scenarios of porosity evolution.

oolitic grains in association with partial/total cementation in the intergranular space, and finally partial/total cementation of the moldic porosity. Figure 4.41 illustrates the diagenetic stages of the aragonitic and bimineralicooids with their estimated porosity values for each stage.

Bimineralic ooids are characterized by alternating layers of high–Mg calcite and aragonite (Lehrmann et al., 2012). This type of ooid was initially deposited with high interparticle porosity. In these ooids, the aragonitic layers always undergo similar stages of diagenesis to the aragoniticooids, while the calcitic layers have remained unaltered. In the lower interval, these two types of ooid occur in three stratigraphic positions. The top of Zone 1 contains aragonitic ooids in a stabilized shoal. Bimineralic ooids occur at the top of Zone 2 in both high-energy bars and the laterally equivalent rippled sand. Figure 4.42 shows six scenarios of porosity change with successive diagenetic stages. The six scenarios show high porosity in the first stages in all of the oolitic-dominated units. In the high-energy bar (bimineralic) oolitic unit, porosity gradually decreased as cementation increased, and all inter- and intra-particle pores were eventually occluded, leaving very low microporosity values. The rippled oolitic sand (bimineralic) unit shows similar stages of porosity reduction as the cementation rate increased. However, inter- and intra-particle porosities are still open in the outcrop stage, retaining average values of 15%. In the stabilized bar units (aragonitic), interparticle porosity decreased gradually until becoming completely occluded, and moldic porosity gradually increased to a maximum value (25%).

- **Middle Interval**

The middle interval consists of Zones 3 and 4. The reservoir units in Zone 3 are composed of a laterally continuous ooid-dominated unit (aragonitic) followed by highly cemented skeletal oolitic units (aragonitic). This interval is overlain by isolated, vertically connected and amalgamated ooid-dominated units (bimineralic). The uppermost beds are relatively thickly bedded (oomoldic unit). The aragonite and bimineralic ooids in this interval experienced the same diagenetic paragenesis as in the lower interval. The highly cemented skeletal oolite is aragonitic and underwent similar porosity evolution to the lower interval, with the difference that the pore space was completely filled by sparry calcite cement and moldic porosity was not preserved as in the stabilized shoal. The dolomitized ooids were initially aragonitic ooids that developed oomoldic pores, within which the oomoldic pores were later occluded by dolomite crystals with intercrystalline porosity. The paragenesis of reservoir units in Zone 3 and their estimated porosity is illustrated in figure 4.43. The reservoir units in Zone 4 are oolite-dominated and dolomitic oolite-dominated, and both could have had the same diagenetic paragenesis as Zone 3 (Figure 4.44). Because we do not have sufficient data about ooid morphology in this zone, we assume that the units developed originally as bimineralic. This assumption allows us to highlight more variability in the 3D porosity model.

The initial stages of the porosity models in both Zones 3 and 4 have high porosity, which then decreased gradually in both the skeletal oolitic and dolomitic oolitic units until reaching the lowest values in the outcrop stage. The pore space in the skeletal oolite decreased with the increase in calcite cementation, whereas the moldic pore spaces of the dolomitic ooids have been blocked by dolomite rhombs, leaving micropores.

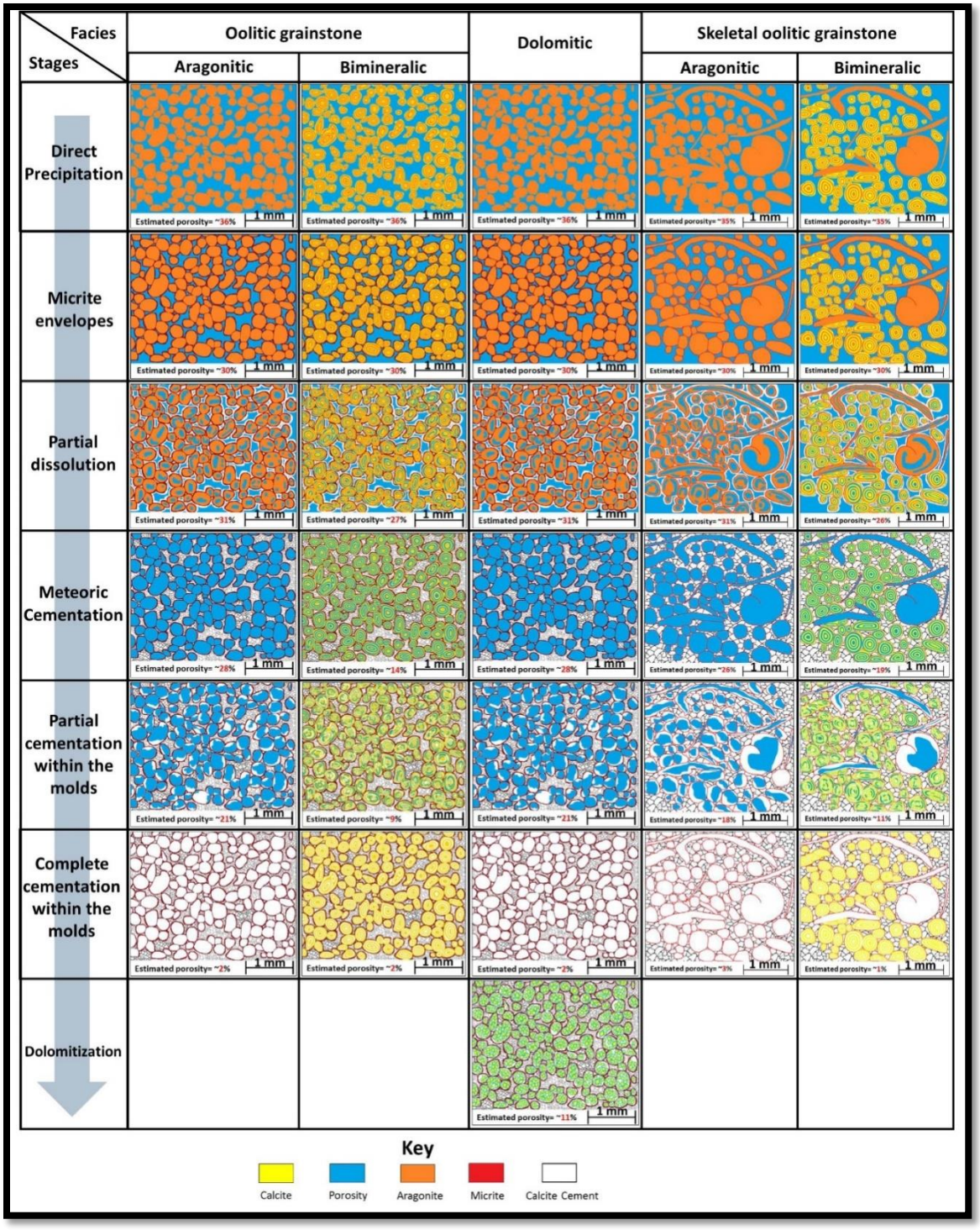


Figure 4.41: Proposed scenarios of qualitative and quantitative porosity evolution through time to outcrop stage.

- **Upper Interval**

The upper interval contains Zone 5 and has only one interval of reservoir unit, which is the dolomitic skeletal oolitic grainstone interval. Porosity types in this interval are interparticle, oomoldic, intraparticle, intraskeletal, and intercrystalline, with an average porosity value of 28% (Figure 4.45).

This interval is overlain by trace of dissolved evaporite layers and isolated collapsed breccia. The upper interval of this zone represent deposits of suppera tidal flat (thick algal mat with scattered ooids). The aragonite ooids in this interval is the dominated type of ooids and experienced the same diagenetic paragenesis as in the lower intervals. The highly dolomitized skeletal oolite is aragonitic and underwent similar porosity evolution to the lower interval, with further step of dolomitization, possibly due to the presence of successive evaporite layers.

The initial stages of the porosity models in both Zones 5 have high porosity, which then decreased gradually with the presence of anhydrite and calcite cements. Dolomitization produce intercrystalline porosity and redudse the intial pore system in the same time.

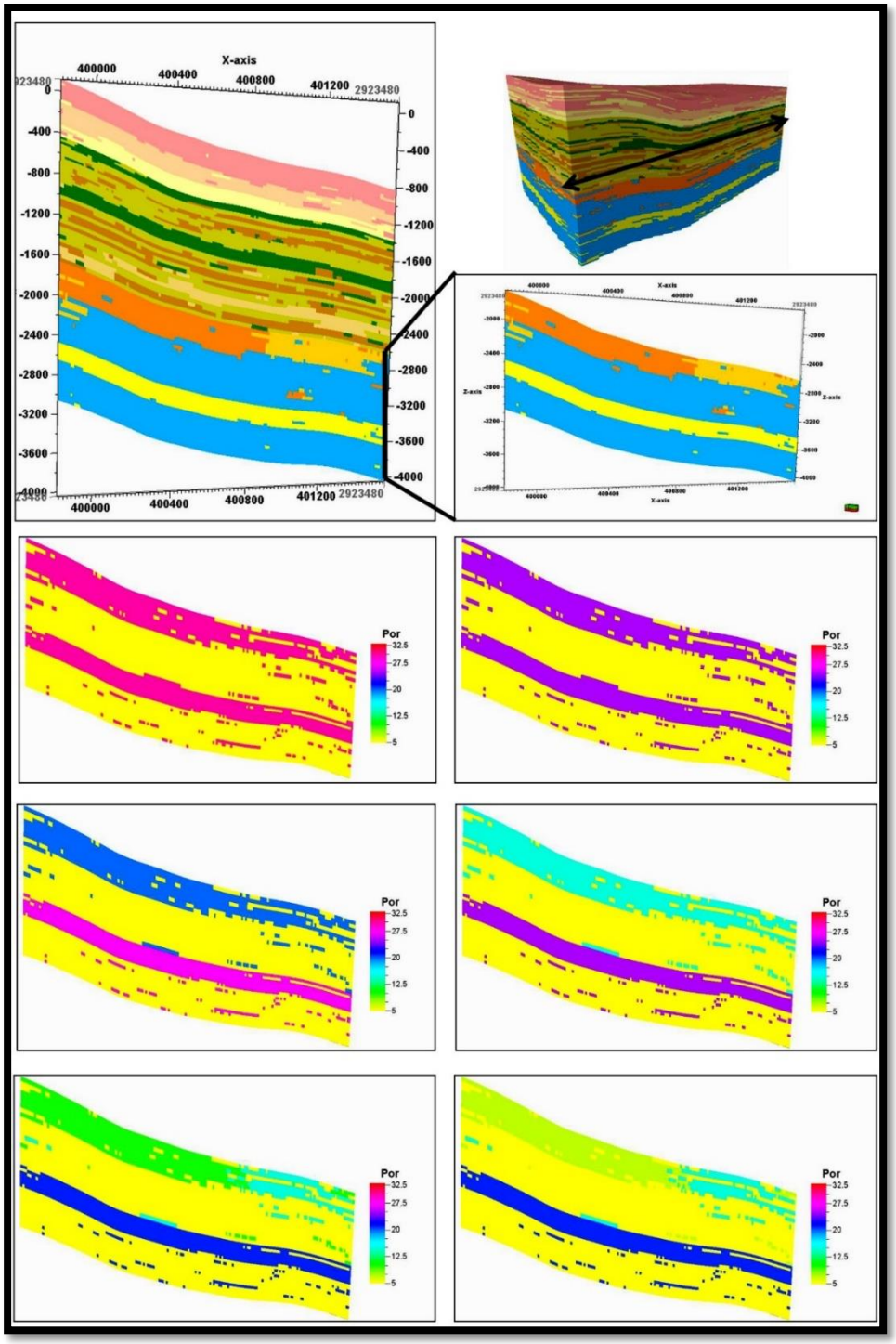


Figure 4.42: East-West traverse across the 3D outcrop model representing Zone 1 and 2 with the six proposed scenarios of porosity evolution through time to outcrop stage.

### 4.7.7 Implications for Subsurface Reservoirs

The systematic distribution of ooids with distinct original mineral compositions allows prediction of porosity distribution and occurrence within reservoirs. The ooids in the studied interval were originally aragonitic (lower interval), bimineralic (middle interval), and aragonitic again in the upper part. This observed pattern can be generalized to allow prediction of the types of porosity in analogous reservoirs.

Modeling of porosity evolution scenarios in a 3D framework highlights the ranges of variability in porosity distribution that may be observed in analogous reservoirs (Heydari, 1998). It is then necessary to consider which scenario would be the best analog for other oolite carbonate reservoirs. Comparison with previously published work indicates that all of these scenarios may potentially be applicable to other oolite carbonate reservoirs. For example, Ehrenberg et al. (2007) indicated that the Khuff reservoirs in the Gulf Area oilfields have average porosities of less than 12%. In contrast, Esrafili-Dizaji and Rahimpour-Bonab (2014) stated that the porosity of the Khuff Formation can exceed25%, with average porosities much higher than 12%. Although these porosity values are extremely different, both occur in the same reservoir in different regions. This difference is probably caused by local controls in each reservoir. These two scenarios of porosity variability are represented in the 3D porosity distribution of the outcrop models. Depending on the predicted porosity controls, it is possible to anticipate which porosity scenarios are the best analogs for other oolite carbonate reservoirs.

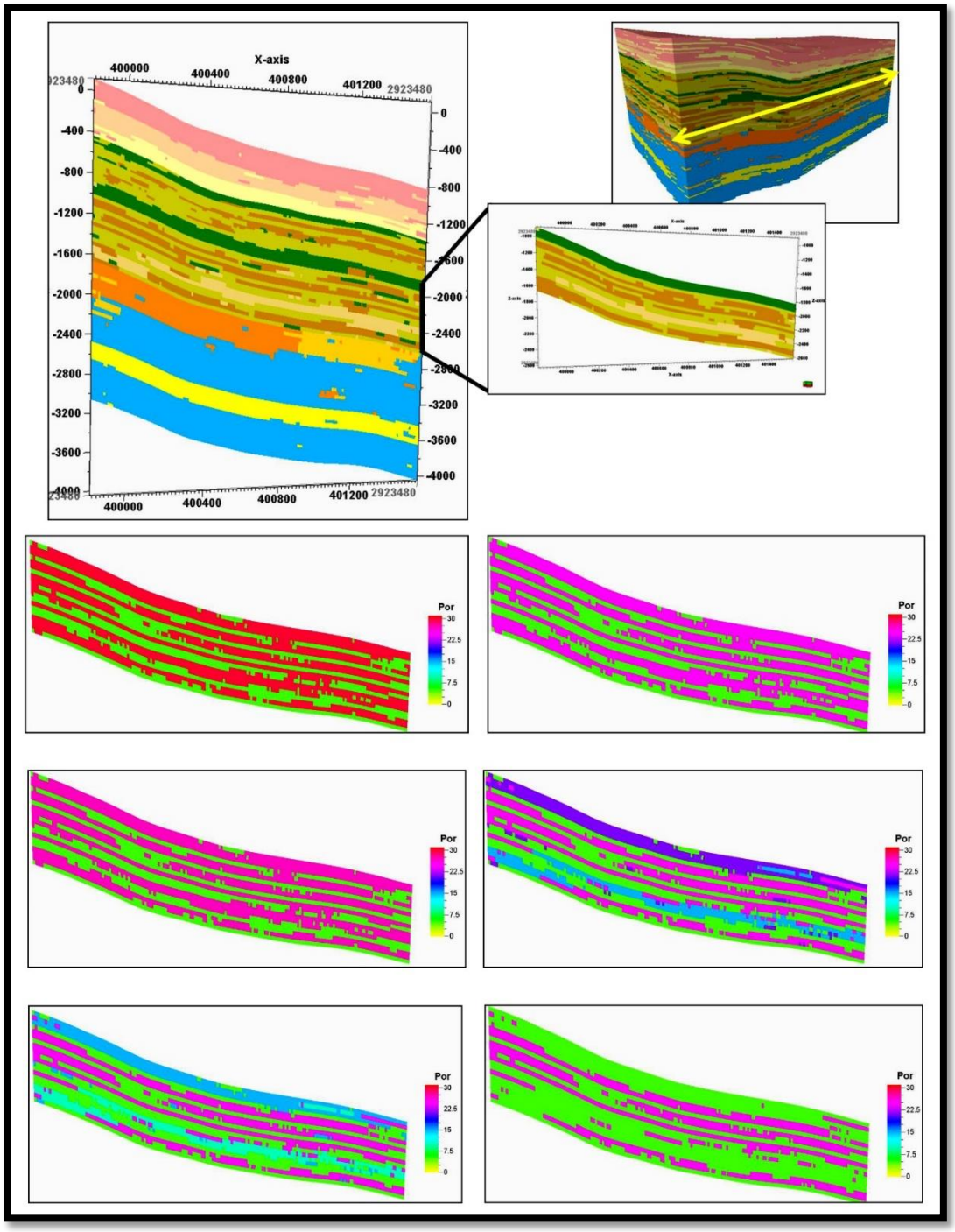


Figure 4.43: East-West traverse across the 3D outcrop model representing Zone 3 with the six proposed scenarios of porosity evolution through time to outcrop stage.

The high-resolution 3D outcrop models that incorporate porosity values from subsurface data can allow prediction of subsurface reservoirs in several ways. (1) The reservoir stacking pattern and architecture, e.g., the vertical relationship between mud-dominated units (baffles) and grain-dominated units (reservoirs), can be evaluated accurately using this outcrop model. Although the reservoir units in Zones 3, 4, and 5 are relatively thin and interbedded with baffle units, the units are occasionally interconnected in intervals in which lithofacies are amalgamated. This interconnection could provide vertical communication between different parts of a reservoir that appear compartmentalized. (2) The contrast in permeability in Zone 2 between the highly cemented oolitic grainstone (low porosity and permeability) and the juxtaposed rippled sand grainstone may cause lateral compartmentalization between these two reservoir units. (3) The calculation of the net growth of the reservoir units in the outcrop analog model may assist with estimation of the net growth of a reservoir in a subsurface analog.

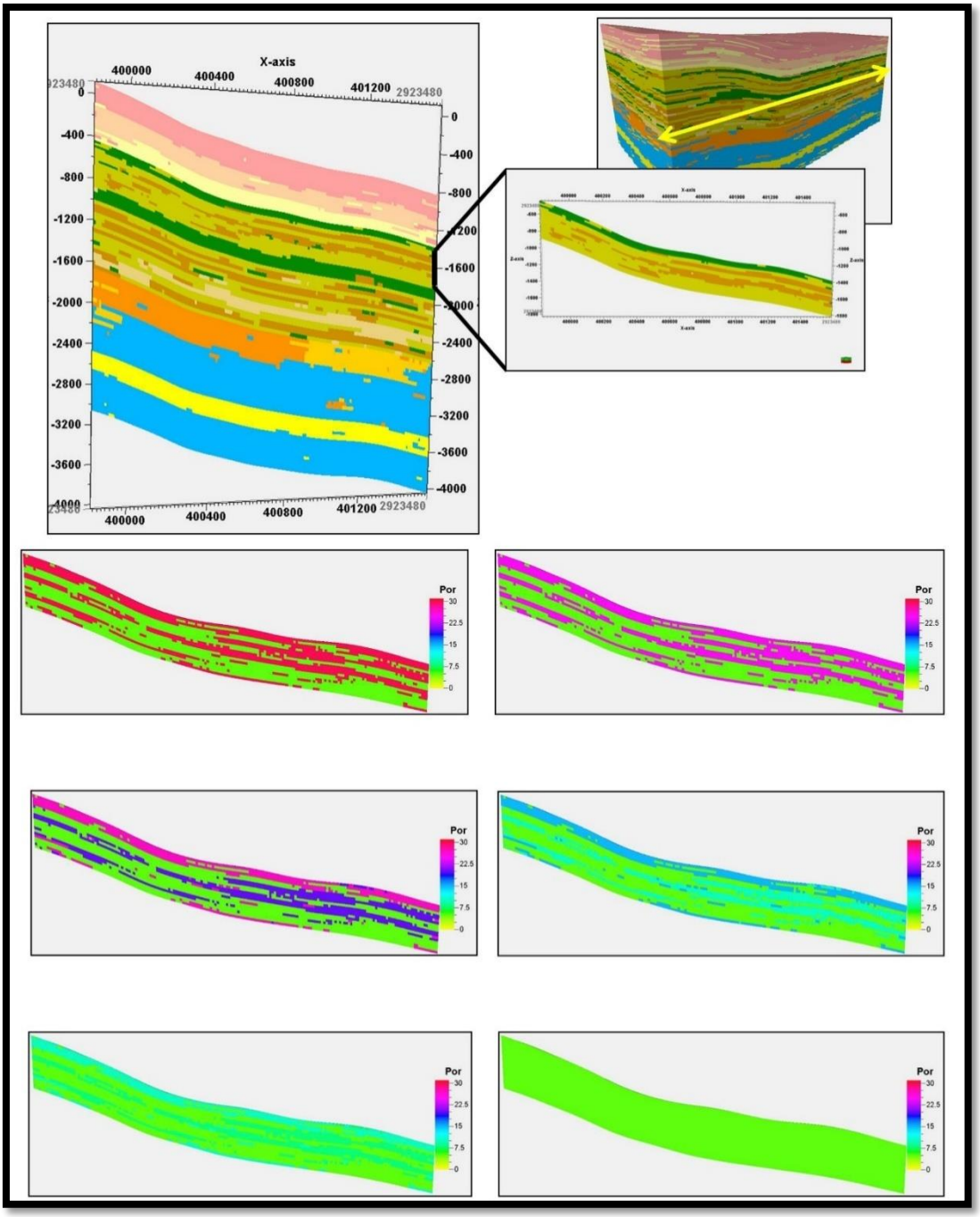


Figure 4.44: East-West traverse across the 3D outcrop model representing Zone 4 with the six proposed scenarios of porosity evolution through time to outcrop stage.

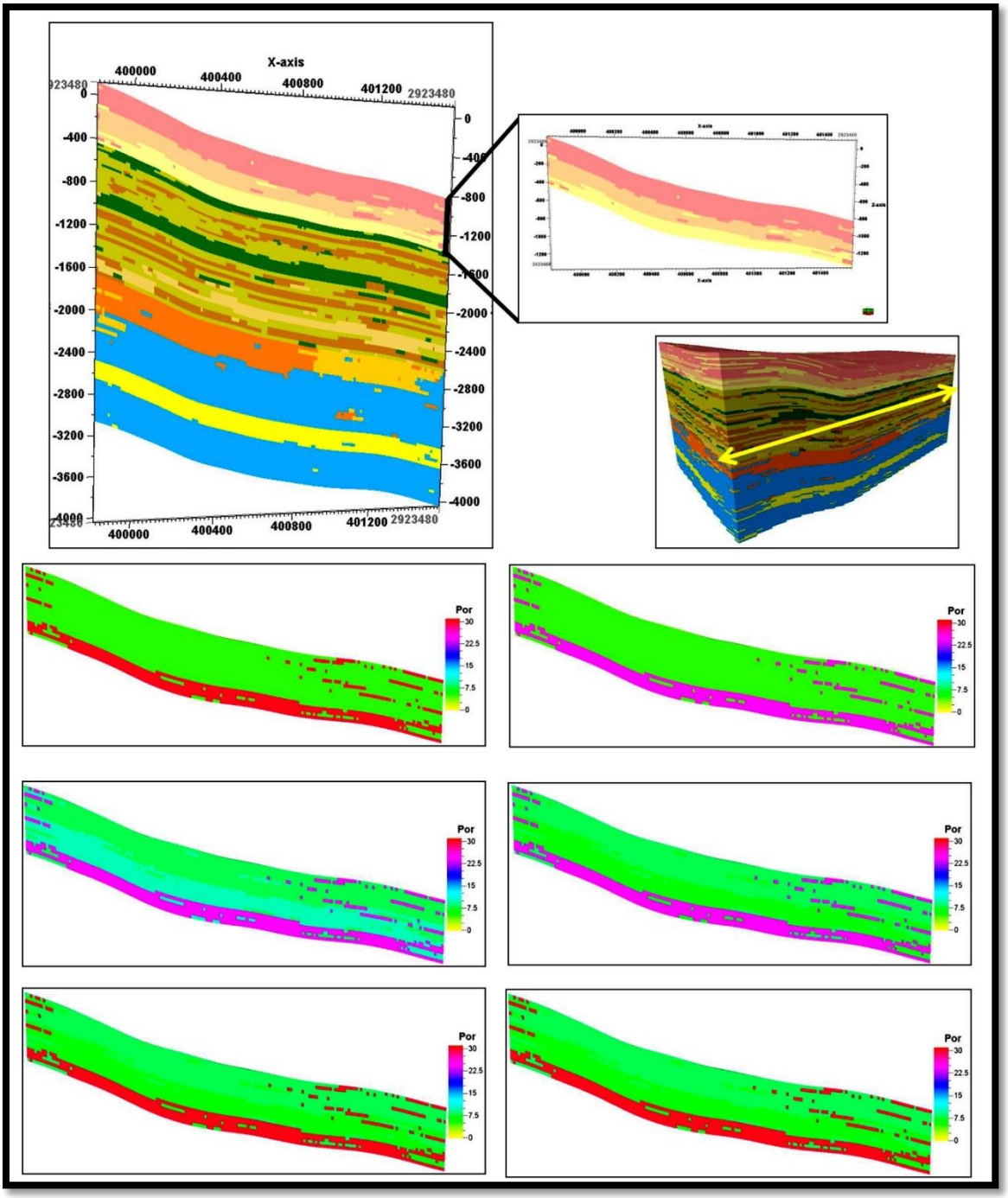


Figure 4.45: East-West traverse across the 3D outcrop model representing Zone 4 with the six proposed scenarios of porosity evolution through time to outcrop stage.

## 4.8 Model validation

The resultant models have been validated quantitativley and qualitatively as well. For the quantiative test, the percentage of the input data compared with the reproduced facies percentage of the model (Figure 4.46). Where, for the qualitative validation, high resolution photos of outcrop observations were used to control the resultant geocellular facies model (Figures 4.47, 4.48).

Several realizations were run to visualize the variability of the SIS and TGS models. The software functions allow averaging of any number of realizations of any property, including facies, in one model. To minimize the degree of uncertainity and getting closed to the reality, 30 realizations were generated using Sequential Indicator Simulation. Meanwhile, there is a need to validate the resultant models, so the stratigraphic correlation with trend of east-west compared with a slice from realization model which have the same orientation.

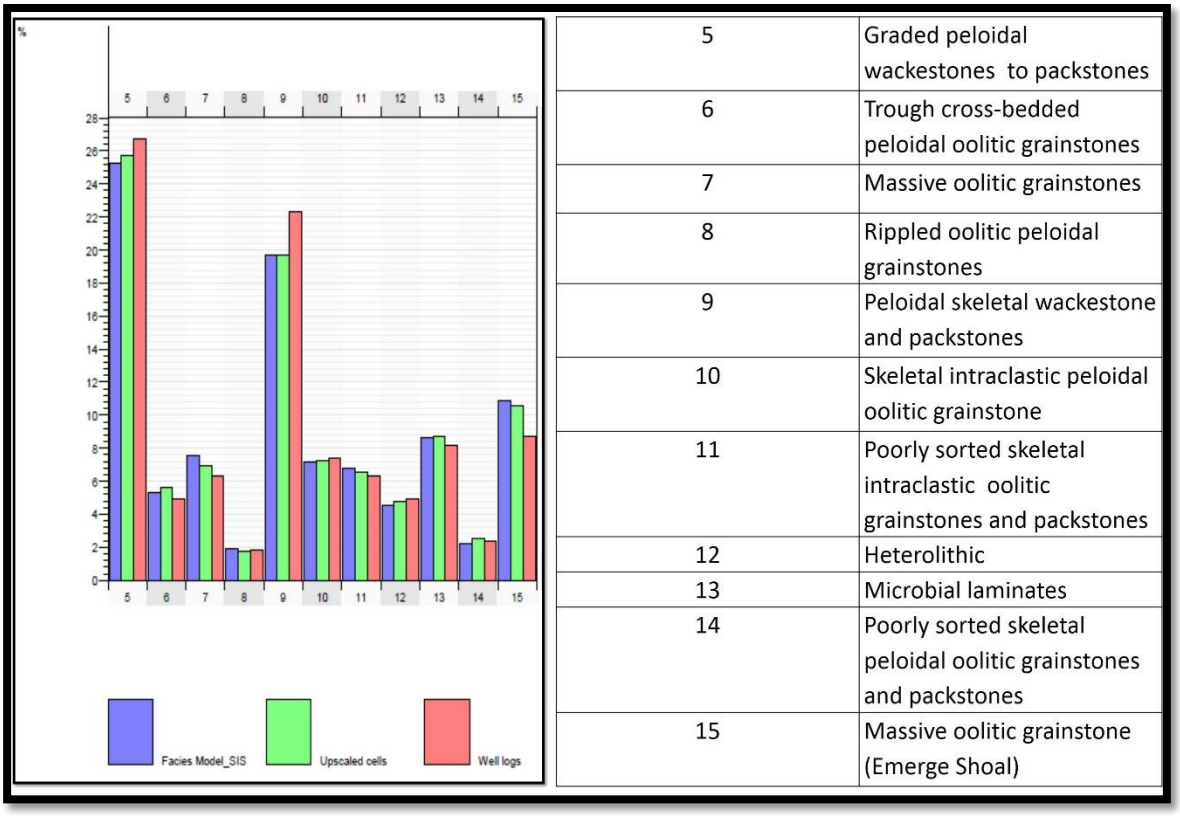


| | |
|---|---|
| 5 | Graded peloidal wackestones to packstones |
| 6 | Trough cross-bedded peloidal oolitic grainstones |
| 7 | Massive oolitic grainstones |
| 8 | Rippled oolitic peloidal grainstones |
| 9 | Peloidal skeletal wackestone and packstones |
| 10 | Skeletal intraclastic peloidal oolitic grainstone |
| 11 | Poorly sorted skeletal intraclastic oolitic grainstones and packstones |
| 12 | Heterolithic |
| 13 | Microbial laminates |
| 14 | Poorly sorted skeletal peloidal oolitic grainstones and packstones |
| 15 | Massive oolitic grainstone (Emerge Shoal) |

Figure 4.46: Shows the histogram of the facies model data, upscaled data and well logs.

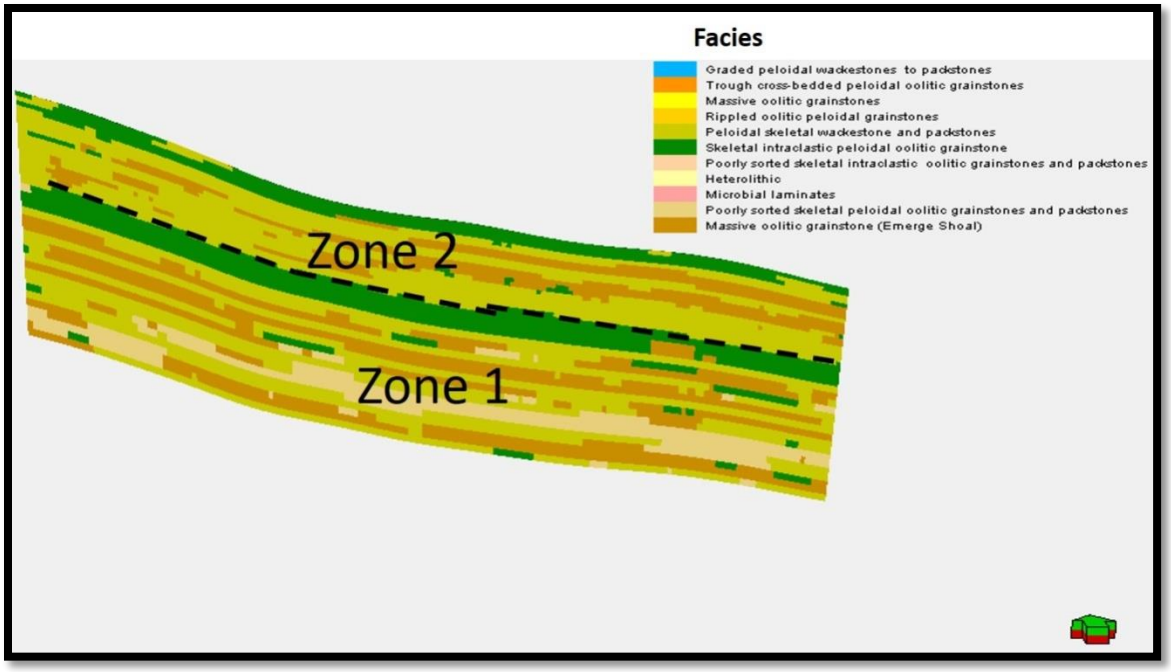


Figure 4.47: Visualizes slice across zone 2 and 3 of the 3D model.

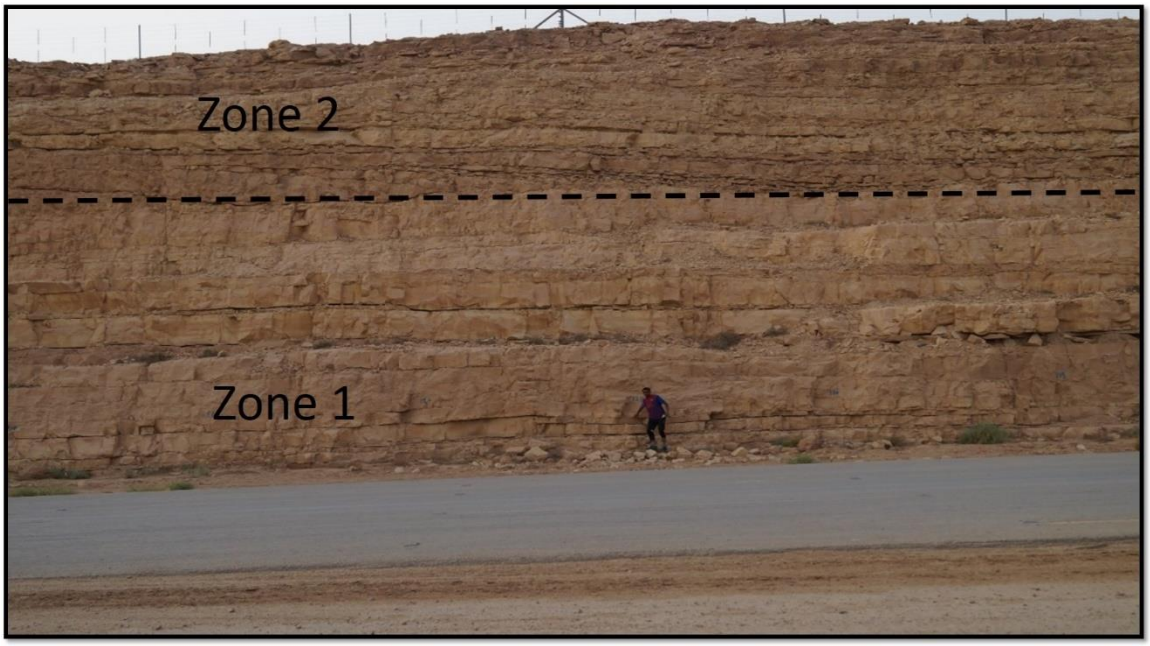


Figure 4.48: Shows outcrop wall and bed sets of zones 2 and 3.

# CHAPTER 5

# CONCLUSIONS

- The Upper Khartam Member was studied in area of 2 km long and 1 km wide. Thus the scale-dependent approach has been used for modelling scales range from large scale (3rd order) down to facies associations (4th order) and lithofacies types as the smallest scale. The stratigraphic hirarichy was similar to other eipiric carbonate ramps such as Upper Muschkalk Formation of Germany. Five medium scales of depositional cycles were identified and each cycle composed of 5th order cycles.
- Eleven lithofacies types were distinguised and listed into four groups; foreshoal, shoal complex, backshoal and tidal flat subenvironments.
- Porosity and permeability measurements were statisticaly analysed and their distributions checked base on the texture and the high frequency sequences as well. Both porosity and permeability datasets were log-normaly distributed when subdivided into three rock types according to the dominant texture. (grainy-, muddy-grainy-, muddy-dominated). Howevere the correlation of porosity versus permeability was enhanced by using texture of rock types as criteria for datasets analysis. The correlation factors for grainy-, muddy grainy- and muddy-dominated rock types equal; 0.6118, 0.3111 and 0.7348, respectively.
- The spatial variability of the facies was studied for the upper Khartam member through calculating variogram for each zone in**d**ividualy. The major directon of the variability was corrosponed to the direction of the deposition (NE).

- To visualize the lateral facies changes and their depositional sub-environments, 2D correlation of the outcrop logs was established. Then according to the correlated outcrop sections, six stratigraphic surfaces were constructed for the 3$^{rd}$ order sequence of Upper Khartam Member.
- To capture the lithofacies dimensions and morphology, 3D modelling techniques were properly chosen and applied. The lithofacies types were modelled deterministically (Indicator Kriging algorithm) and stochastically (Truncated Gaussian simulation and Sequential Indicator simulation algorithms) within the 3D grid cells.
- To improve our understanding of porosity evolution in Lower Triassic oolite reservoirs, we integrated small-scale geological heterogeneity (diagenetic phases of grainstones) and a large-scale 3D outcrop representation of Lower Triassic outcrops in central Saudi Arabia. Several lithofacies are present, which are interpreted as having been deposited in four broad depositional environments: (1) foreshoal, (2) shoal complex, (3) backshoal, and (4) tidal flat. A small-scale fifth-order cycle stack formed five fourth-order sequences (1 to 5). In turn, the fourth-order sequences are stacked vertically to form the Upper Khartam composite sequence (third-order sequence). The five sequences are bounded by abrupt, prominent surfaces that can be correlated over several kilometers in outcrop.
- Six major surfaces were constructed using fourth-order sequence boundaries selected from outcrop observations. On the basis of the depositional environments, these zones can be grouped as Zones 1 and 2 (foreshoal and shoal deposits), Zones 3 and 4 (shoal and backshoal deposits), and Zone 5 (tidal flat). Incorporation of

lithofacies in the 3D outcrop model was performed separately for each zone using a different geostatistical algorithm for each depositional environment. The resulting 3D outcrop model adequately illustrates the continuity of the beds and adequately represents the observed stacking pattern of the stratigraphic architecture in outcrop.

- Quantitative and qualitative characterization allows subdivision of the 3D outcrop model into three different intervals based on sea-level changes, porosity types, architecture, and facies. Each of these intervals experienced a unique process of porosity evolution. The five zones within the 3D volume of the reservoir units can be assigned to three sequence stratigraphic intervals. The lower interval (Zones 1 and 2) was deposited within a rapid sea-level rise at the Permian–Triassic boundary, and mainly consists of ooid-dominated units. The middle interval (Zones 3 and 4) was deposited within a rapid sea-level fluctuation and was characterized by the beginning of marine faunal recovery. The upper interval (Zone 5) was deposited during a fall in relative sea-level.
- Scenarios of porosity evolution were separately constructed for each zone. The systematic distribution of ooids with distinct original mineral compositions allows the prediction of porosity distribution and occurrence. The original mineralogy of ooids in the studied interval was aragonitic in the lower interval, bimineralic in the middle interval, and aragonitic again in the uppermost part.
- This study provides predictive scenarios of porosity evolution for both aragonite and bimineralicooids (calcite ooids were not detected in the study area). Similar oolitic reservoirs of different geological ages, such as the Upper Jurassic Smackover Formation, possess three types of ooid (aragonite, calcite, and

bimineralic). The degree of variability of porosity evolution if ooids with three different original compositions were present in a single reservoir is an issue to be addressed in future research.

# References


Abdulraziq, A., 2013. Porosity Classification and Reservoir Flow Units Ranking in the Khartam Member, Khuff Formation (Permo-Triassic): Outcrop Approach, Central Saudi Arabia. MSc thesis, King Fahd University of Petroleum and Minerals.

Al-Dukhayyil, R.K., and A.A. Al Tawil 2007. Reservoir architecture of the Triassic Khartam carbonate sequence, Khuff outcrop analogue in Al-Qasim, central Saudi Arabia. 7th Middle East Geosciences Conference, GEO 2006. GeoArabia, Abstract, v. 12, no. 3, p. 136

Al Dukhayyil, Raed K., 2007. High-resolution sequence stratigraphy of the Khuff A and B carbonates in the subsurface of Haradh area, Southern ghawar field, Saudi Arabia. M.Sc. thesis, King Fahd University of Petroleum and Minerals

Al-Khalifa, M. A. H. (2001). Data integration in 3-D geostatistical porosity modeling of Hanifa Reservoir in Berri field, Saudi Arabia (Doctoral dissertation, King Fahd University of Petroleum and Minerals)

Alsharhan, A. S. (2006). Sedimentological character and hydrocarbon parameters of the middle Permian to Early Triassic Khuff Formation, united Arab Emirates. GeoArabia, 11(3), 121-158.

Amour, F., Mutti, M., Christ, N., Immenhauser, A., Benson, G. S., Agar, S. M., &Kabiri, L. (2013). Outcrop analog for an oolitic carbonate ramp reservoir: A scale-dependent geologic modeling approach based on stratigraphic hierarchy.AAPG bulletin, 97(5), 845-871

Barbier, M., Hamon, Y., Callot, J. P., Floquet, M., & Daniel, J. M. (2012). Sedimentary and diagenetic controls on the multiscale fracturing pattern of a carbonate reservoir: The Madison Formation (Sheep Mountain, Wyoming, USA). Marine and Petroleum Geology, 29(1), 50-67

BENSON, G.S., FRANSEEN, E.K., GOLDSTEIN, R. H. and LI, Z., 2014. Workflows for incorporating stratigraphic and diagenetic relationships into a reservoir-analogue model from outcrops of Miocene carbonates in SE Spain. Petroleum Geoscience, 20(1), 55–78

Bohling, G. (2005). Introduction to geostatistics and variogram analysis. Kansas Geological Survey

Delfour, J., Dhellemmes, R., Elsass, P., Vaslet, D., Brosse, J., Le Nindre, Y. M. and Dottin, O. 1982. Explanatory notes to the geologic map of the Ad Dawadimi Quadrangle, Kingdom of Saudi Arabia. Geoscience Map GM-60C, scale 1:250,000, sheet 24G. Deputy Ministry for Mineral Resources, Ministry of Petroleum and Mineral Resources, Kingdom of Saudi Arabia.p. 36.

Deutsch, C. V. (1999). Reservoir modeling with publicly available software.Computers& Geosciences, 25(4), 355-363

Dunham, R.J. 1962. Classification of carbonate rocks according to depositional textures. American Association of Petroleum Geologists

EHRENBERG, S.N., NADEAU, P.H. and AQRAWI, A.A.M., 2007. A comparison of Khuff and Arab reservoir potential throughout the Middle East. American Association of Petroleum Geologists Bulletin, 91(3), 275-286

Eltom, H. A., Abdullatif, O. M., Babalola, L. O., Bashari, Osman, M. S., & Abdulraziq, A. M. (in press). Oolite-microbialite of the Lower Triassic Upper Khartam Member of the Khuff Formation, central Saudi Arabia: facies architecture, geochemical analysis, and ooidsgranulometrey Journal of Petroleum Geology.

Eltom, H. A., Abdullatif, O. M., Babalola, L. O., Bashari, M. A., Yassin, M., Osman, M. S., & Abdulraziq, A. M. (2016). GEOCHEMICAL CHARACTERIZATION OF THE PERMIAN–TRIASSIC TRANSITION AT OUTCROP, CENTRAL SAUDI ARABIA. Journal of Petroleum Geology, 39(1), 95-113

ELTOM, H., MAKKAWI, M., ABDULLATIF, O. and ALRAMADAN, K., 2012. High-resolution facies and porosity models of the upper Jurassic Arab-D carbonate reservoir using an outcrop analogue, central Saudi Arabia. Arabian Journal of Geosciences, 6(11), 4323–4335

ESRAFILI-DIZAJI, B. and RAHIMPOUR-BONAB, H., 2014. Generation and evolution of oolitic shoal reservoirs in the Permo-Triassic carbonates, the South Pars Field, Iran. Facies, 60(4), 921-940

Fabuel-Pe´rez, I. (2008). 3D Reservoir Modeling of Upper Triassic Continental Mixed Systems: Integration of Digital Outcrop Models (DOMs) and High Resolution Sedimentology.TheOukaimeden Sandstone Formation, Central High Atlas. Morocco. Unpublished PhD thesis, University of Manchester, 275 pp.

Falivene, O., Arbués, P., Howell, J., Muñoz, J. A., Fernández, O., &Marzo, M. (2006). Hierarchical geocellular facies modelling of a turbidite reservoir analogue from the Eocene of the Ainsa Basin, NE Spain. Marine and Petroleum Geology, 23(6), 679-701

FaliveneAldea, O., Cabrera, L., Muñoz, J. A., Arbués, P., Fernández, O., &Sáez, A. (2007). Statistical grid-based facies reconstruction and modelling for sedimentary bodies. Alluvial-palustrine and turbiditic examples. GeologicaActa, vol. 5, núm. 3, p. 199-230

Felletti, F. (2004). Statistical modelling and validation of correlation in turbidites: an example from the Tertiary Piedmont Basin (Castagnola Fm., Northern Italy). Marine and Petroleum Geology, 21(1), 23-39

Heydari, E. 1998. Paleoclimatic and paleoceanographic controls on deposition of organic-rich lime mudstones of the Upper Jurassic Smackover Formation, north-central U.S. Gulf Coast. Oceanography 1, p. 3-17

HUGHES, G.W., 2009. Micropaleontology and paleoenvironments of Saudi Arabian Upper Permian carbonates and reservoirs. In geologic problem solving with microfossils: A volume in honor of Garry D. Jones, society of economic paleontologists and mineralogists. Special Publication, 93, 111-126

INSALACO, E., VIRGONE, A., COURME, B., GAILLOT, J., KAMALI, M., MOALLEMI, A., LOTFPOUR, M. and MONIBI, S., 2006. Upper Dalan Member and Kangan Formation between the Zagros Mountains and offshore Fars, Iran: Depositional system, biostratigraphy and stratigraphic architecture. GeoArabia, 11(2), 75-176

KOEHRER, B., AIGNER, T., FORKE, H. and PÖPPELREITER, M., 2012. Middle to Upper Khuff (Sequences KS1 to KS4) outcrop-equivalents in the Oman Mountains: Grainstone architecture on a subregional scale. GeoArabia, 17(4), 59–104

KOEHRER, B., AIGNER, T. and POPPELREITER, M., 2011. Field-scale geometries of Upper Khuff reservoir geobodies in an outcrop analogue (Oman Mountains, Sultanate of Oman). Petroleum Geoscience, 17(1), 3–16

KOEHRER, B. S., HEYMANN, C., PROUSA, F. and AIGNER, T., 2010. Multiple-scale facies and reservoir quality variations within a dolomite body – Outcrop analog study from the Middle Triassic, SW German Basin. Marine and Petroleum Geology, 27(2), 386–411

KOEHRER, B., ZELLER, M., AIGNER, T., POEPPELREITER, M., MILROY, P., FORKE, H. and AL-KINDI, S., 2010. Facies and stratigraphic framework of a Khuff outcrop equivalent: Saiq and Mahil formations, Al Jabal al-Akhdar, Sultanate of Oman. GeoArabia, 15(2), 91–156

Kupfersberger, H., & Deutsch, C. V. (1999). Methodology for integrating analog geologic data in 3-D variogram modeling. AAPG bulletin, 83(8), 1262-1278

LEHRMANN, D.J., MINZONI, M., LI, X., YU, M., PAYNE, J.L., KELLEY, B.M., SCHAAL, E.K. and ENOS, P., 2012. Lower Triassic oolites of the Nanpanjiang Basin, south China: Facies architecture, giant ooids, and diagenesis—Implications for hydrocarbon reservoirs. American Association of Petroleum Geologists Bulletin, 96(8), 1389-1414

MANIVIT, J., VASLET, D., BERTHIAUX, A., LE STRAT, P. AND FOURNIGUET, J., 1986. Explanatory Notes of the Geological map of the Buraydah Quadrangle Sheet 26 G, kingdom of Saudi Arabia. Ministry of Petroleum and Mineral Resources. Deputy Ministry for Mineral Resources, 32

MAURER, F., MARTINI, R., RETTORI, R., HILLGARTNER, H. and CIRILLI, S., 2009. The geology of Khuff outcrop analogues in the Musandam Peninsula, United Arab Emirates and Oman. GeoArabia, 14(3), 125–158

Palermo, D., Aigner, T., Nardon, S., &Blendinger, W. (2010). Three-dimensional facies modeling of carbonate sand bodies: Outcrop analog study in an epicontinental basin (Triassic, southwest Germany). AAPG bulletin, 94(4), 475-512

POWERS, R.W., 1968. Saudi Arabia (excluding the Arabian Shield), LexiqueStratigraphique International, Paris, 3, Asie

Sahin, A., & Saner, S. (2001). Statistical distributions and correlations of petrophysical parameters in the Arab-D reservoir, Abqaiq oilfield, Eastern Saudi Arabia. Journal of Petroleum Geology, 24(1), 101-114

Saner, S., &Sahin, A. (1999). Lithological and zonal porosity-permeability distributions in the Arab-D reservoir, Uthmaniyah Field, Saudi Arabia. AAPG bulletin, 83(2), 230-243.

Sahin, A., Ghori, S. G., Ali, A. Z., El-Sahn, H. F., Hassan, H. M., & Al-Sanounah, A. (1998). Geological controls of variograms in a complex carbonate reservoir, Eastern Province, Saudi Arabia. Mathematical Geology, 30(3), 309-322

Sharland, P.R., E. Archer, D.M. Casey, R.B. Davies, S.H. Hall, A.P. Heward, A.D. Horbury and M.D. Simmons (2001). Arabian Plate Sequence Stratigraphy. GeoArabia, Special Publication 2, 369 p

Srinivasan, S., &Sen, M. K. (2009). Stochastic modeling of facies distribution in a carbonate reservoir in the Gulf of Mexico. Geohorizons, December, 54, 67

STEINEKE, M., BRAMKAMP, R.A. and SANDER, N.J., 1958. Stratigraphic relations of Arabian Jurassic Oil, habitat of oil. American Association of Petroleum Geologists Bulletin, 1294-1329

VASLET, D., NINDRE, Y. LE, VACHARD, D., BROUTIN, J., CRASQUIN-SOLEAU, S., BERTHELIN, M., GAILLOT, J., HALAWANI, M. and AL-HUSSEINI, M., 2005. The Permian-Triassic Khuff Formation of central Saudi Arabia. GeoArabia, 10(4), 77–134

WALZ, L., AIGNER, T. and KOEHRER, B., 2013. Khuff sequence KS5 outcrop equivalents in the Oman Mountains, Sultanate of Oman: Variations to the simple "layer-cake"stratigraphy. GeoArabia, 18(4), 179-218

White, C. D., Novakovic, D., Dutton, S. P., & Willis, B. J. (2003). A geostatistical model for calcite concretions in sandstone. Mathematical geology, 35(5), 549-575

ZIEGLER, P.A., 1990. Geological Atlas of Western and Central Europe, second ed. Shell International Petroleum, Maatschappij, 237 pp.

ZIEGLER, M. A., 2001. Late Permian to Holocene Paleofacies Evolution of the Arabian Plate and its Hydrocarbon Occurrences. GeoArabia, 6(3), 445–504

# Vitae


| | |
|---|---|
| Name | :Abdaseed Kubur Bokhari Kubur |
| Nationality | :Sudanese |
| Date of Birth | :2/19/1987 |
| Email | :kubur96@hotmail.com |
| Address | :Dhahran, Saudi Arabia |
| Academic Background | :Geology |